

CALCULATION OF CORE LOSSES OF A SIX-PHASE INDUCTION MOTOR WITH  
THIRD HARMONIC CURRENT INJECTION

A THESIS SUBMITTED TO  
THE GRADUATE SCHOOL OF NATURAL AND APPLIED SCIENCES  
OF  
THE MIDDLE EAST TECHNICAL UNIVERSITY

BY

AFŞİN BÜYÜKBAŞ

IN PARTIAL FULFILMENT OF THE REQUIREMENTS FOR THE DEGREE OF  
MASTER OF SCIENCE  
IN  
THE DEPARTMENT OF ELECTRICAL AND ELECTRONICS ENGINEERING

JANUARY 2004

Approval of the Graduate School of Natural and Applied Sciences

\_\_\_\_\_  
Prof. Dr. Canan ÖZGEN  
Director

I certify that this thesis satisfies all the requirements as a thesis for the degree of Master of Science.

\_\_\_\_\_  
Prof. Dr. Mübeccel DEMİREKLER  
Head of Department

This is to certify that we have read this thesis and that in our opinion it is fully adequate, in scope and quality, as a thesis for the degree of Master of Science

\_\_\_\_\_  
Prof. Dr. H. Bülent ERTAN  
Supervisor

Examining Committee Members

Prof. Dr. Muammer ERMİŞ

Prof. Dr. H. Bülent ERTAN

Prof Dr Yıldırım ÜÇTUĞ

Assist. Prof. Dr. Ahmet HAVA

M.Sc., Eng. Erdal BİZKEVELCİ

\_\_\_\_\_  
\_\_\_\_\_  
\_\_\_\_\_  
\_\_\_\_\_  
\_\_\_\_\_

## **ABSTRACT**

### **CALCULATION OF CORE LOSSES OF A SIX-PHASE INDUCTION MOTOR WITH THIRD HARMONIC CURRENT INJECTION**

BÜYÜKBAŞ, Afşin

M.S., Department of Electrical and Electronics Engineering

Supervisor: Prof. Dr. H. Bülent ERTAN

January 2004, 106 pages

The advantages of using a six-phase induction motor for industrial drives, over the conventional three-phase drive can be summarized as improved reliability, reduction on the power ratings for the static converters and harmonic reduction. A technique of injecting third harmonic zero sequence current components in the phase currents to improve the machine torque density was presented recently by another research study.

However, to meaningfully evaluate the performance of such machines and/or to be able to make good designs; it is necessary to obtain an accurate mathematical model for the loss calculation. The calculation of high frequency loss in this context presents a very difficult problem. In this thesis a modified version of a loss calculation model, which was developed in another MS thesis will be applied to a six-phase induction motor with third harmonic current injection.

Key words: Six-phase, harmonic injection, iron losses.

## ÖZ

### ÜÇÜNCÜ HARMONİK AKIM ENJEKTE EDİLEN ALTI FAZLI BİR ASENKRON MOTORUN ÇEKİRDEK KAYIPLARININ HESAPLANMASI

BÜYÜKBAŞ, Afşin

Yükek Lisans, Elektrik ve Elektronik Mühendisliği Bölümü

Tez Yöneticisi: Prof. Dr. H. Bülent ERTAN

Ocak 2004, 106 sayfa

Sanayi tipi sürücülerde altı fazlı asenkron motorların kullanılmasının faydaları, iyileştirilmiş güvenilirlik, statik dönüştürücülerin güç değerlerinde düşüş ve harmoniklerde oluşan düşüş olarak özetlenebilir. Geçtiğimiz yıllarda, makinenin tork yoğunluğunun iyileştirilmesi amacıyla faz akımlarına üçüncü harmonik akım bileşenlerinin enjekte edilmesine ilişkin bir yöntem ortaya atılmıştır.

Ne var ki, bu tip makinaların performansının doğru olarak değerlendirilebilmesi ve iyi tasarım yapılabilmesi için kayıpların hesabını doğru olarak yapabilen bir matematiksel modele de ihtiyaç vardır. Bu çerçevede yüksek frekans kayıplarının hesabı zor bir problem oluşturur. Bu çalışmada, başka bir tez çalışmasında geliştirilen çekirdek kayıpların bulunmasına ilişkin bir modelin değiştirilmiş bir hali, üçüncü harmonik akım enjeksiyonu ile çalışan asenkron motora uygulanmıştır.

Anahtar Kelimeler: Altı faz, harmonik enjeksiyonu, çekirdek kayıpları.

To My Family

## **ACKNOWLEDGEMENTS**

I would like to express my sincere appreciation to my supervisor, Prof. Dr. H. Bülent ERTAN for his guidance and insight throughout the research.

I owe special thanks to the members of the Intelligent Control Group of TÜBİTAK-ODTÜ BİLTEN for their support throughout my studies at METU.

Finally, my heartfelt thanks go to my family members, endless support of whom I felt throughout my studies.

## TABLE OF CONTENTS

ABSTRACT.....	iii
ÖZ.....	iv
DEDICATION.....	v
ACKNOWLEDGEMENTS.....	vi
TABLE OF CONTENTS.....	vii
LIST OF TABLES.....	x
LIST OF FIGURES.....	xi
1 INTRODUCTION.....	1
1.1 BASIS FOR THIS THESIS.....	1
1.2 PURPOSE AND ORGANIZATION.....	3
2 BACKGROUND.....	4
2.1 INTRODUCTION.....	4
2.2 MULTI-PHASE SYSTEMS.....	5
2.2.1 Split-phase electrical machines.....	5
2.2.2 Dual-stator electrical machines.....	5
2.3 A METHOD FOR TORQUE DENSITY IMPROVEMENT IN A SIX-PHASE MACHINE BY INJECTION OF THIRD HARMONIC CURRENT COMPONENTS.....	6
2.3.1 Three-phase induction machine.....	7
2.3.2 Six-phase induction machine.....	10
2.3.3 Six-phase induction machine winding diagram.....	12
2.3.4 MMF equation of six-phase winding with 1 <sup>st</sup> and 3 <sup>rd</sup> harmonic current components.....	18
2.3.5 Flux distribution on an asymmetric six-phase machine with 3 <sup>rd</sup> harmonic injection.....	27
2.3.6 Torque density increase with third harmonic injection.....	31

	2.3.7 Experimental setup.....	44
	2.3.8 Experimental evaluation of the six-phase system .....	46
	2.4 CONCLUSION .....	61
3	MACHINE LOSSES .....	64
	3.1 INTRODUCTION.....	64
	3.2 LOSSES OF INDUCTION MACHINES .....	64
	3.2.1 Friction and windage losses: .....	65
	3.2.2 Copper losses .....	65
	3.2.3 Stray load losses.....	65
	3.2.4 Core losses .....	65
	3.3 FINITE ELEMENT MODEL .....	67
	3.3.1 Creation of the finite element model.....	68
	3.3.2 Verification of the finite element model .....	75
4	CORE LOSS CALCULATION .....	80
	4.1 INTRODUCTION.....	80
	4.2 CALCULATION OF LOSSES.....	80
	4.2.1 Calculation of fundamental frequency losses of an induction motor .....	81
	4.2.2 Calculation of high frequency losses of an induction motor..	81
	4.2.3 Implementation of the calculation method of fundamental frequency core losses .....	85
	4.2.4 Implementation of the calculation method of high frequency core losses .....	86
5	RESULTS AND CONCLUSIONS .....	91
	5.1 INTRODUCTION.....	91
	5.2 THE RESULTS OF THE FUNDAMENTAL FREQUENCY CORE LOSS CALCULATIONS .....	91
	5.3 THE RESULTS OF THE HIGH FREQUENCY CORE LOSS CALCULATIONS .....	96
	5.4 COMPARISON WITH THE EXPERIMENTAL RESULTS .....	100
	5.5 KEY FINDINGS AND RECOMMENDATIONS.....	101
	5.6 AREAS FOR FURTHER RESEARCH.....	102



REFERENCES .....	103
APPENDIX	
CALCULATION OF PARAMETERS NEEDED AS INPUT FOR FLUX2D SOLUTIONS .....	105

## LIST OF TABLES

2.1	Baseline machine nameplate values.....	8
2.2	Stator geometrical dimensions.....	9
2.3	Rotor geometrical dimensions.....	9
2.4	Equivalent circuit parameters.....	10
3.1	Necessary calculated values for Flux2D.....	74
3.2	MMF Contribution of slots for $w_t = 86.4^\circ$ .....	77
4.3	Calculated skin depths of the harmonics, and the skin depth values used in the loss calculations.....	88
4.4	The calculated skin depth region coefficients.....	89
4.5	Skin depth regions and their $I_{av}$ and $\delta_i$ values.....	89
5.1	Microsoft Excel table used to calculate the fundamental freq. losses.....	95
5.2	Microsoft Excel table used to calculate the high frequency losses.....	99
5.3	Comparison of the measured and calculated core losses.....	100

## LIST OF FIGURES

2.1 Three-phase machine connection diagrams. ....	8
2.2 Stator teeth and rotor bar dimensions, in mm. ....	8
2.3 Measured magnetization curve. Solid line indicates measured values in the curve. ....	9
2.4 Six-phase machine diagrams. ....	11
2.5 Six-phase machine equivalent circuit for sinusoidal steady-state. ....	12
2.6 Winding diagram of each phase of the six-phase machine ....	15
2.7 Total winding ....	16
2.8 Phase axes of the six-phase machine winding. ....	17
2.9 Winding distribution of a three-phase concentrated winding induction machine and winding function for phase a. ....	18
2.10 Winding distribution of a three-phase distributed winding induction machine and winding function for phase a. ....	23
2.11 Winding distribution of asymmetric six-phase machine with concentrated windings. ....	24
2.12 Flux density distribution for the same peak air gap flux with and without third harmonic injection. ....	31
2.13 Induction machine steady-state per phase equivalent circuit. ....	32
2.14 Induction machine approximated steady-state per phase equivalent circuit. Negligible rotor leakage inductance. ....	32
2.15 Torque gain in an asymmetric six-phase machine with third harmonic injection considering reduction in the air gap flux to accommodate the core flux. ....	39
2.16 Flux density distribution for same peak core flux with and without third harmonic injection. ....	40
2.17 Simplified representation of stator slot and tooth. ....	40

2.18 Percentage variation on slot width as a function of initial tooth width for different tooth reduction factors.....	41
2.19 Torque gain in an asymmetric six-phase machine with third harmonic injection considering reduction in the air gap flux to accommodate the core flux and increase in the surface current density.....	43
2.20 Test setup.....	45
2.21 Power converter system used in the experiment.....	46
2.22 No-load operation of the six-phase machine without third harmonic injection. $f = 40$ Hz, $V_s = 84$ V, Trace A: Flux density distribution [0.788T/div]; Trace 3: Phase a current [3.125A/div]; Trace 4: Phase x current [3.125A/div].....	47
2.23 No-load operation of the six-phase machine with third harmonic injection. $f = 40$ Hz, $V_s = 84$ V, $V_{s3h} = 14$ V, Trace A: Flux density distribution [0.788T/div]; Trace 3: Phase a current [6.25A/div]; Trace 4: Phase x current [6.25A/div].....	48
2.24 No-load operation of the six-phase machine with third harmonic injection. $f = 40$ Hz, $V_s = 93$ V, $V_{s3h} = 14$ V, Trace A: Flux density distribution [0.788T/div]; Trace 3: Phase a current [6.25A/div]; Trace 4: Phase x current [6.25A/div].....	48
2.25 Operation of the six-phase machine without third harmonic injection. $T_1 = 5$ Nm, $f = 40$ Hz, $V_s = 80$ V, Trace A: Flux density distribution [0.788T/div]; Trace 3: Phase a current [6.25A/div]; Trace 4: Phase x current [6.25A/div].	49
2.26 Operation of the six-phase machine with third harmonic injection. $T_1 = 5$ Nm, $f = 40$ Hz, $V_s = 80$ V, $V_{s3h} = 14$ V, Trace A: Flux density distribution [0.788T/div]; Trace 3: Phase a current [6.25A/div]; Trace 4: Phase x current [6.25A/div].....	49
2.27 Operation of the six-phase machine with third harmonic injection. $T_1 = 5$ Nm, $f = 40$ Hz, $V_s = 89$ V, $V_{s3h} = 14$ V, Trace A: Flux density distribution [0.788T/div]; Trace 3: Phase a current [6.25A/div]; Trace 4: Phase x current [6.25A/div].....	50
2.28 Torque x speed characteristics for 3hp six-phase machine. Six-phase machine operating with and without third harmonic currents compared to the baseline three phase machine.....	51

2.29 Percentage torque gain, as a function of slip, for the 3hp six-phase machine compared to the baseline three-phase machine for operation with third harmonic current injection. ....	52
2.30 Magnetic losses at 20Hz. Comparison between the 3hp( $P_r=746$ W) six-phase machine with and without third harmonic injection and the baseline three-phase machine. ....	54
2.31 Magnetic losses at 30Hz. Comparison between the 3hp ( $P_r = 1,119$ W) six-phase machine with and without third harmonic injection and the baseline three-phase machine. ....	54
2.32 Magnetic losses at 40Hz. Comparison between the 3hp ( $P_r=1,492$ W) six-phase machine with and without third harmonic injection and the baseline three-phase machine. ....	55
2.33 Stator copper losses at 20 Hz. Comparison between the 3hp ( $P_r=746$ W) six-phase machine with and without third harmonic injection and the baseline three-phase machine. ....	56
2.34 Stator copper losses at 30 Hz. Comparison between the 3hp ( $P_r=1,119$ W) six-phase machine with and without third harmonic injection and the baseline three-phase machine. ....	56
2.35 Stator copper losses at 40 Hz. Comparison between the 3hp ( $P_r=1,492$ W) six-phase machine with and without third harmonic injection and the baseline three-phase machine. ....	57
2.36 Six-phase machine efficiency at 35Hz. Comparison between the three-phase machine and the six-phase machine with and without third harmonic current injection. ....	58
2.37 Six-phase machine efficiency at 45Hz. Comparison between the three-phase machine and the six-phase machine with and without third harmonic current injection. ....	58
2.38 Six-phase machine efficiency different frequencies with third harmonic current injection. ....	59
2.39 Six-phase machine efficiency different frequencies with third harmonic current injection. ....	65

2.40	Calculated and measured efficiency for the six-phase machine without third harmonic current injection for 45Hz. ....	60
2.41	Calculated and measured efficiency for the six-phase machine with third harmonic current injection for 45Hz. ....	60
3.1	Fundamental frequency loss versus peak flux density curves for different frequencies [21]. ....	66
3.2	The geometry drawn for the six phase machine. ....	70
3.3	The mesh created for the six phase machine. ....	71
3.4	Boundary conditions. ....	72
3.5	Iron BH curve used in the finite element analysis. ....	72
3.6	Stator circuit of the six phase machine. ....	74
3.7	MMF Waveform created by the currents in Table 3.1. ....	76
3.8	Bgap waveform for different time instants a) $t=0.1473$ b) $t=1.3473$ sec. c) $t=1.4973$ sec. ....	78
4.1	The current path the finite element analysis assumes in a rotor tooth pitch. ....	83
4.2	The current path considering the laminations. ....	84
4.3	The elements assumed to exist in one tooth pitch of the stator core. ....	85
4.4	Skin depth regions and average current path width values in a rotor tooth. ....	88
5.1	Flux density of the regions at the outermost part of a stator tooth pitch. ....	93
5.2	Flux density of regions at the slot ends in a stator tooth pitch. ....	93
5.3	Flux density of the regions in the middle of the tooth in a stator tooth pitch. ....	93
5.4	Flux density of the regions at the tooth tip in a stator tooth pitch. ....	93
5.5	Time variation and harmonic content of eddy currents in region R5 of the 4 <sup>th</sup> rotor tooth. ....	96
5.6	Time variation and harmonic content of eddy currents in region R11 of the 4 <sup>th</sup> rotor tooth. ....	96
5.7	Time variation and harmonic content of eddy currents in region R17 of the 4 <sup>th</sup> rotor tooth. ....	97

# **CHAPTER 1**

## **INTRODUCTION**

### **1.1 BASIS FOR THIS THESIS**

When high power levels are required, the use of six-phase machines is one of the alternatives in industry. For variable speed applications, power electronic converters are used to drive the machine and the power level of the converter has to match the machine and the load. Limitations on the power level of semiconductor devices establish a barrier to the increase of converter ratings. In order to get rid of this limitation, multilevel converters have been developed where switches of reduced rating are used to construct high power level converters.

Instead of multilevel converters, multi-phase machines can be used. By dividing the handled power between multiple phases, generally more than three, high power levels can be achieved even using limited rated power electronic converters.

There we face with a difficult choice between multi-phase machines and multilevel converters. The choice is dependent on the application. For example, a limitation on the insulation level allowed for the feeding cables, can make the use of high voltage systems prohibitive. So, to increase the power, more converters operating at lower voltage levels have to be applied, and hence, a multi-phase machine is chosen.

Multi-phase systems expand the universe for drive and control purposes. Having more phases means added degrees of freedom that can be explored in these systems.

In addition to using a multi-phase machine, there are some other ways to improve the machine output. Torque is proportional to the flux in the machine. Unfortunately the flux cannot be increased at will because of the saturation risk of iron and, as a result, a limitation in the flux level which should not be exceeded. However, if a third harmonic component is added to the flux of the machine, a square-like waveform is obtained for the air gap flux, and hence the fundamental component can be increased without making the peak flux too high. The reason why we do this in a six-phase machine but not a three-phase machine is that third harmonic currents in three-phase machines produce stationary, pulsating fields and therefore, by interaction with the fundamental field, pulsating torque.

In a six-phase machine, by injection of third harmonic currents, the fundamental component of the air gap flux can be increased without creating stationary fields. In addition to getting higher fundamental flux, the interaction between the two three-phase groups that composes the six-phase machine excited by third harmonic zero sequence currents, produces an additional rotating field.

Thus, the use of a six-phase machine with injection of third harmonic currents, increase the torque production by two different mechanisms. First, the fundamental flux is increased. Second, an additional rotating field, which rotates at the same frequency as the fundamental one, is created. If we neglect saturation, an improvement of up to 40% can be expected with this system [1].

However, it is important to map the machine losses in order to obtain the system overall efficiency more accurately. Obtaining a mathematical model especially for the core losses is an important tool in the machine design for correct calculation of losses of the machine. In [18] a method for calculating the core losses of induction machines are developed and in [19] this model is applied to several types of induction machines. This method is based on the finite element solution of the



motor. In this study, the core losses of the six-phase induction machine with third harmonic current injection, is calculated after creating the finite element model of the motor.

## **1.2 PURPOSE AND ORGANIZATION**

In this research work; a six-phase induction machine, which operates with third harmonic current injection and which was realized, analyzed without taking losses into consideration and tested experimentally by [1], will be explained by going into derivations, analyzed by using finite element method, and its core losses will be calculated by using a calculation method evaluated in [18].

This text is organized into five chapters as follows. Chapter 2 presents a brief review on multi-phase systems and their applications. The theory behind and the application of a method of injecting third harmonic currents for torque density improvement in a six-phase induction machine [1] is introduced and the derivations are clarified.

Chapter 3 is devoted firstly to the explanation of losses of an induction motor, and after an introduction of the finite element method, the process of creation of the finite element model of the motor will be presented.

In Chapter 4, the calculation method of core losses evaluated in [18], will be applied to the subject motor based on the finite element model of the motor in Chapter 3.

In Chapter 5, the results of the analysis and calculations done in Chapter 4 are shown. Then the discussions and final conclusions on this thesis and suggestions for future work are provided.

## **CHAPTER 2**

### **BACKGROUND**

#### **2.1 INTRODUCTION**

Three-phase induction machines have become a standard for industrial electrical drives. They have replaced the old dc drive systems because of the reasons like cost, reliability, robustness and maintenance free operation. As power electronics and signal processing systems developed, the issue of control which is the last disadvantage of such ac systems is eliminated. By using modern techniques of field oriented vector control, the variable speed control of induction machines is not a hot spot anymore.

At present, the ratings of power semiconductors, digital signal processing speed and control techniques to improve system performances are the new hot issues that limit the application of electrical machines in the most diverse areas and motivate the researchers. In order to increase system performance, many methods are being used.

In this chapter, some of the efforts conducted by researchers to achieve the main goals in industry applications: increase reliability and efficiency and reduce cost, are presented. The realization, analysis and experimentally testing of a six-phase induction machine operating with third harmonic current injection, by [1] is presented. The theory behind and the application of torque density improvement in the subject machine is introduced by making the derivations.

## **2.2 MULTI-PHASE SYSTEMS**

The limited power ratings of semiconductor devices forced the researchers to investigate new machines with higher number of phases in order to reach higher power levels. Here, a multi-phase system is assumed to be such a system that has more than the conventional three phases. If the number of phases is more than three, the machine output power can be divided into two or more solid state inverters within the same power limits. Moreover, additional phases to control bring additional degrees of freedom available for further improvements in the drive system. This section presents some of these efforts, outlining advantages and disadvantages.

### **2.2.1 Split-phase electrical machines**

Split-phase electrical machines consist of two similar stator windings sharing the same magnetic circuit. Such a construction made it possible to extend the power range of solid-state based drives by sharing the total power between two drives [2, 4]. Usually a split-phase machine is built by splitting the phase belt of a conventional three-phase machine into two equal parts with spatial phase separation of 30 electrical degrees. By using this arrangement, for the same air gap flux, the inverter dc bus voltage can be reduced by approximately a half, compared to a three-phase system, since the number of turns per phase is reduced [4]. Such structure has a disadvantage of the need for two or more inverters to drive the machine.

Another advantage of using this kind of winding arrangement is harmonic cancellation. The sixth harmonic torque pulsation, which is common in a six-step three-phase drive, can be eliminated by using split-phase arrangement, [5, 6].

### **2.2.2 Dual-stator electrical machines**

As in split-phase machines, the dual-stator machines consist basically of two independent stator windings sharing the same magnetic frame. Differently, a dual-stator machine does not necessarily have similar winding groups. For example, a

different voltage rating or a different number of phases could be used for each winding group.

For instance, two independent stator windings may be used for an induction generator system [3]. One set of windings may be responsible for the electromechanical power conversion (i.e. driving the load) while the second one is used for excitation purposes. This eliminates the need of a converter rated to full load power in a vector controlled induction generator [15]. The same idea can be used for power factor correction in induction motors. One of the two different sets of three-phase windings may be connected to the main power and carry the active power responsible for the torque production while the second winding carries the reactive power.

Using a dual-stator machine which is a particular case of a multi-phase machine, the power ratings may be extended without the need to use multi-level converters. Instead of increasing the power rating of a three-phase converter using multi-levels for the converter, additional phases are added and the current is shared by additional inverter legs [16].

### **2.3 A METHOD FOR TORQUE DENSITY IMPROVEMENT IN A SIX-PHASE MACHINE BY INJECTION OF THIRD HARMONIC CURRENT COMPONENTS**

This section presents a research study [1] which deals with torque density improvement of a six-phase induction motor by using third harmonic injection. It studies and characterizes a six-phase induction machine drive operating with third harmonic current injection. The performance of the system was measured in comparison with a standard three-phase machine system.

To achieve the objectives above, two machines were analyzed in [1]. To use the three-phase machine as a baseline for the analysis, the six-phase machine uses the same peak air gap flux density, similar winding configuration and same frame.

By comparing the operation of these two machines, the improvements were outlined. The machine was analyzed using mathematical models and finite element simulation.

A control system using PWM current control techniques was developed and implemented both in simulation and in the experimental setup. By controlling currents, instead of voltages, the rotor flux can be controlled and the effects of leakage inductances reduced. This is particularly important for the third harmonic injection since perfect alignment between fundamental and third harmonic is necessary. For a voltage fed system, the stator resistance and leakage inductance, as well as rotor leakage inductance, cause a phase shift between the two components that is a function of the machine parameters and operating conditions. This effect deteriorates the performance especially at low speeds.

To summarize, the contributions of [1] include: the development and analysis of a drive system that is able to operate with third harmonic injection at variable speed operation; the development of a current control system that enables the implementation of synchronous frame current regulators for both fundamental and third harmonic currents and therefore simplifies the design of the outer control loops; the implementation of a speed control loop using indirect flux orientation for the six-phase induction machine with third harmonic current injection, the simplification of the drive system by using six phases with unified windings for fundamental and third harmonic currents; the experimental evaluation of the iron losses in comparison with a three-phase machine operation; and the development of a machine model to be used for calculation of its operating conditions and evaluation of efficiency.

### **2.3.1 Three-phase induction machine**

A three-phase induction machine was used in [1] as baseline for the new machine design. Table 2.1 shows the nameplate values for the baseline machine. The connection diagrams for this machine are presented in Figure 2.1 for both parallel and series Y configurations, 230V and 460V connection respectively. Table 2.2

presents the stator dimensions and Table 2.3 presents the rotor geometrical data. Figure 2.2 shows stator tooth and the rotor bar dimensions.

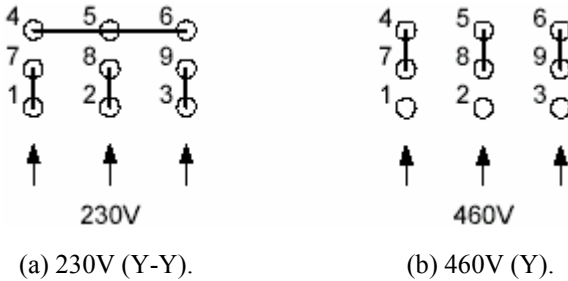


Figure 2.1 Three phase machine connection diagrams.

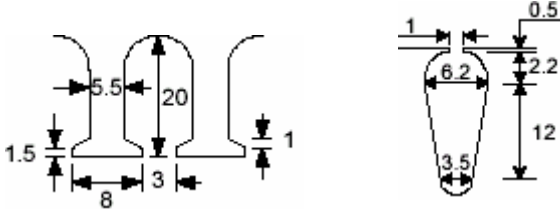


Figure 2.2 Stator teeth and rotor bar dimensions, in mm.

Table 2.1 Baseline machine nameplate values.

Model	5K182BC218A
HP	3
Service factor	1.15
Rating	Cont.
Voltage	230/460V
Current	9.0/4.5A
Phases	3
Frequency	60
NEMA Nominal Efficiency	82.5%
Insulation	Class B
Frame	182T
NEMA Design	B

Table 2.2 Stator geometrical dimensions.

Number of slots	36
Outer diameter	190mm
Inner diameter	120mm
Stack length	70.5mm

Table 2.3 Rotor geometrical dimensions.

Number of slots	28
Outer diameter	119.4mm
Inner diameter	32.0mm
Stack length	65.5mm
End connection	10.0mm
Tooth width	6.6mm
Bar depth	20.0mm
Shaft radius	16.0mm

The BH curve for the three-phase machine iron is shown in Figure 2.3. The solid line in Figure 2.3 corresponds to the portion measured and the dashed line is an extrapolation based on a standard grain oriented steel.

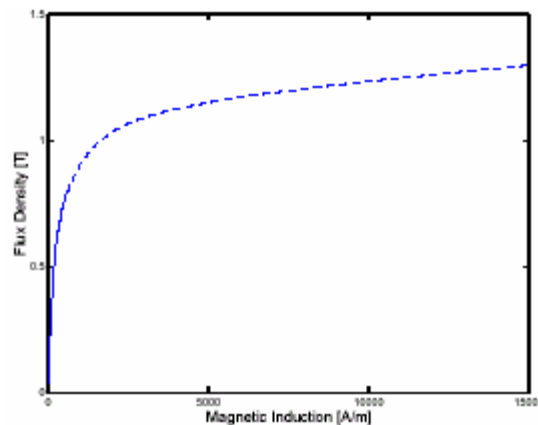


Figure 2.3 Measured magnetization curve. Solid line indicates measured values in the curve.

The three-phase machine uses a single layer concentric winding which distributes itself over 3 slots per pole per phase and has 98 conductors per slot. Using the Y connection (460V) there are 2 parallel circuits per phase, or in other perspective there is one circuit with two stranded wires. For the YY connection (230V) 4 parallel circuits, or 2 parallel circuits with two stranded wires, compose the windings per phase. The conductor diameter is 0.72mm corresponding to a 21 AWG wire.

The equivalent circuit parameters that were calculated by using no-load and locked-rotor tests are presented in Table 2.4.

*Table 2.4 Equivalent circuit parameters.*

$R_s$	0.85 $\Omega$
$L_s$	5.42 mH
$L_r$	5.42 mH
$L_m$	69.77 mH
$R_r$	0.55 $\Omega$

### **2.3.2 Six-phase induction machine**

The six-phase machine is a particular case of split-phase or dual-stator machine. It can be built by splitting a three-phase winding into two groups. These three-phase groups are shifted by thirty electrical degrees from each other. This composes an asymmetrical six-phase machine since the angular distance between phases is not the same. Figure 2.4 shows the representation of the machine stator windings for Y connection and a simplified construction diagram for a concentrated-winding two-pole six-phase machine.

A method which is similar to that of a three-phase machine can be adopted in analyzing a six-phase induction machine. In Figure 2.5, the steady-state equivalent circuit for sinusoidal excitation [7] which is similar to the one of a conventional three-phase machine with the addition of an extra stator circuit is shown.



We can reach to a result that, for steady-state operation the six-phase machine can be analyzed as two three-phase machines sharing the same magnetic circuit as well as rotor circuit. On the other hand, it should be noted that there can be currents flowing between the two three-phase stators that do not contribute to torque generation. This forces the designers to make direct control of stator currents for such systems.

Basically, the six-phase induction machine was introduced with two objectives. First, the opportunity to divide the output power into two three-phase groups allows the increase in the drive system power ratings. Secondly, for use with six-step inverters, the pulsating torque in a six-phase machine is lower than in a three-phase machine [6, 8, 9, 10]. Another reason for using six-phase systems is reliability. When a failure happens in one of the phases, in the machine or in the power converter, the system can still operate at a lower power rating since each three-phase group can be made independent from each other. In the case of losing one phase, the six-phase machine can be operated as a five-phase machine as described in [11].

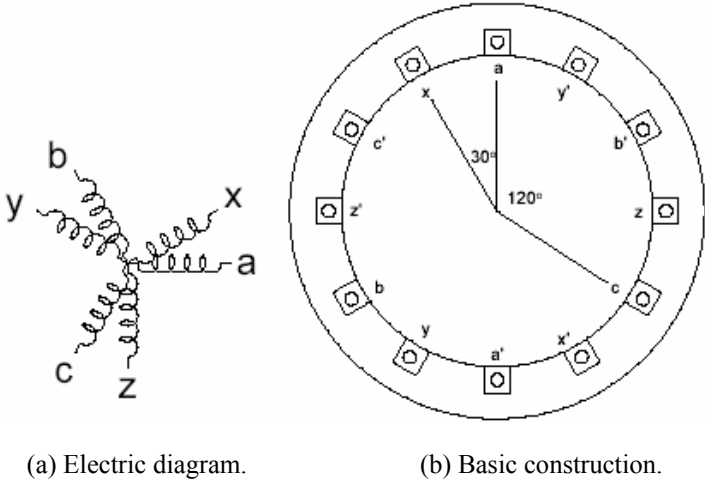


Figure 2.4 Six-phase machine diagrams.

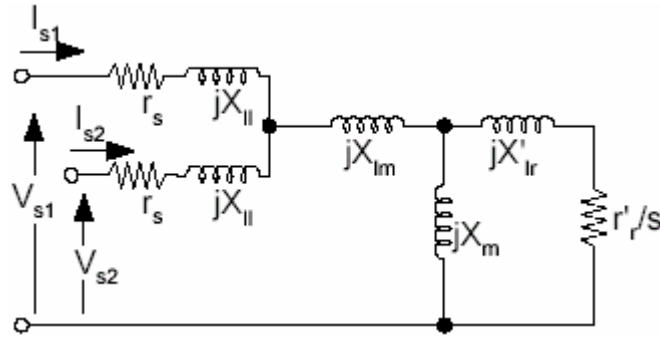


Figure 2.5 Six-phase machine equivalent circuit for sinusoidal steady-state.

### 2.3.3 Six-phase induction machine winding diagram

The six-phase machine in [1] uses the same magnetic frame with the baseline machine. We have the 4-pole machine with 36 stator slots. In order to keep the leakage distribution balanced, the phases are displaced among the two stator layers. The six-phases are constructed such that one three-phase group is displaced from the other one by 30 electrical degrees. Thus we have an asymmetrical six-phase machine where;

$$\theta_m = 2 \cdot \theta_e / p \quad (2.1)$$

$$\theta_m = 2 \cdot 30^\circ / 4 = 15^\circ \text{ mechanical} \quad (2.2)$$

$$\text{Slot pitch} = 360^\circ / 36 = 10^\circ \text{ mechanical} \quad (2.3)$$

Hence, the 30 electrical degrees displacement corresponds to  $15^\circ/10^\circ = 1,5$  slots. We cannot implement such a configuration and have to use an approximation. This is how it is done:

One of the three-phase groups has the same structure of the baseline machine with half of the circuits and winding distributed in 3 slots per pole per phase ( $q_A = 3$ ). The second group is distributed into 4 slots per pole per phase ( $q_X = 4$ ) but keeping the same number of conductors per pole per phase. The winding diagrams of each phase are shown in Figure 2.7. The total winding diagram is presented in Figure 2.6. The number of series connected conductors in each coil is given in the figure

and it is shown that to obtain the necessary 30 electrical degrees displacement between the two three-phase groups A and X, the outer side coils in the X group have reduced number of conductors.

In Figure 2.9, it can be seen that the difference between the axes of the phases  $a$  and  $x$ ,  $b$  and  $y$ ,  $c$  and  $z$  comes out to be 1.5 slot pitches.

As an example : Axis of phase  $a$  is at the middle point of slots 11 and 12

Axis of phase  $x$  is at the slot 13

So the difference between the axes of phases  $a$  and  $x$  is 1.5 slots.

Regarding the pitching of the windings;

Pole pitch = slot # / pole # =  $36 / 4 = 9$  slot pitches.

The first entrance of phase  $a$  is slot 6 and the first exit of phase  $a$  is slot 15

Coil pitch for Group A =  $15 - 6 = 9$  slot pitches → Group A is a full pitch winding.

The first entrance of phase  $x$  is slot 7 and the first exit of phase  $x$  is slot 16

Coil pitch for Group X =  $16 - 7 = 9$  slot pitches → Group X is a full pitch winding.

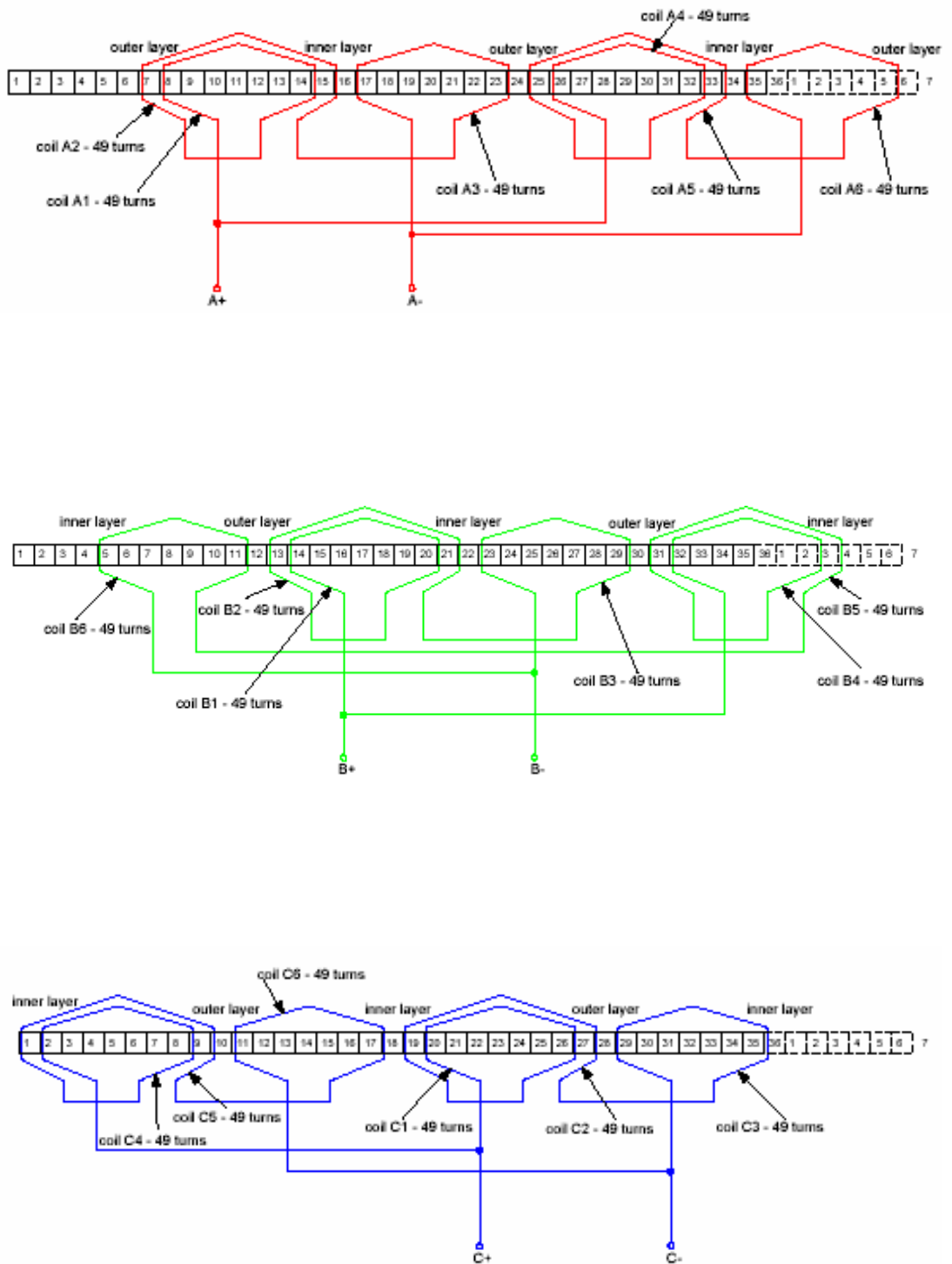


Figure 2.6 Winding diagram of each phase of the six-phase machine

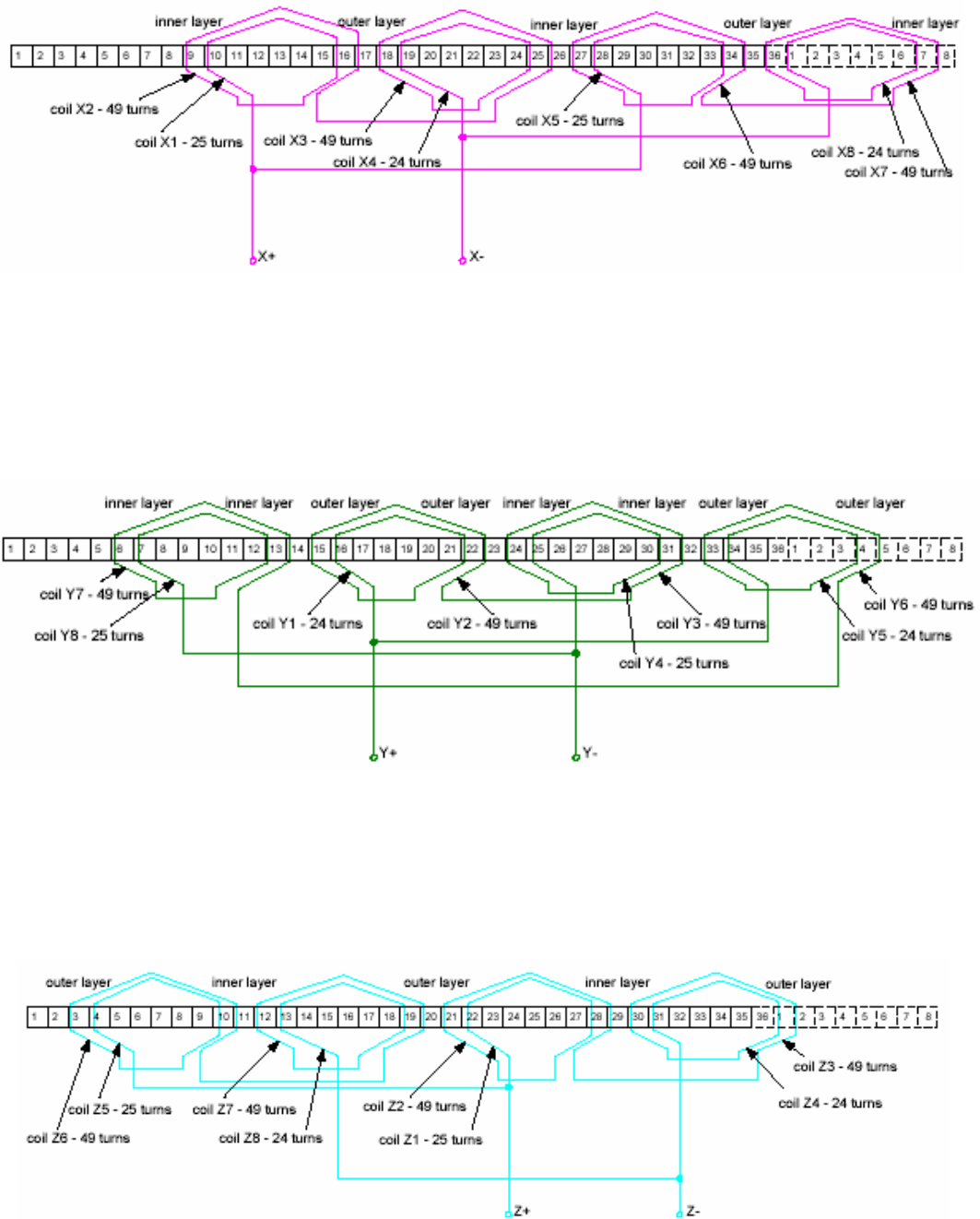


Figure 2.7 Winding diagram of each phase of the six-phase machine (cont.)

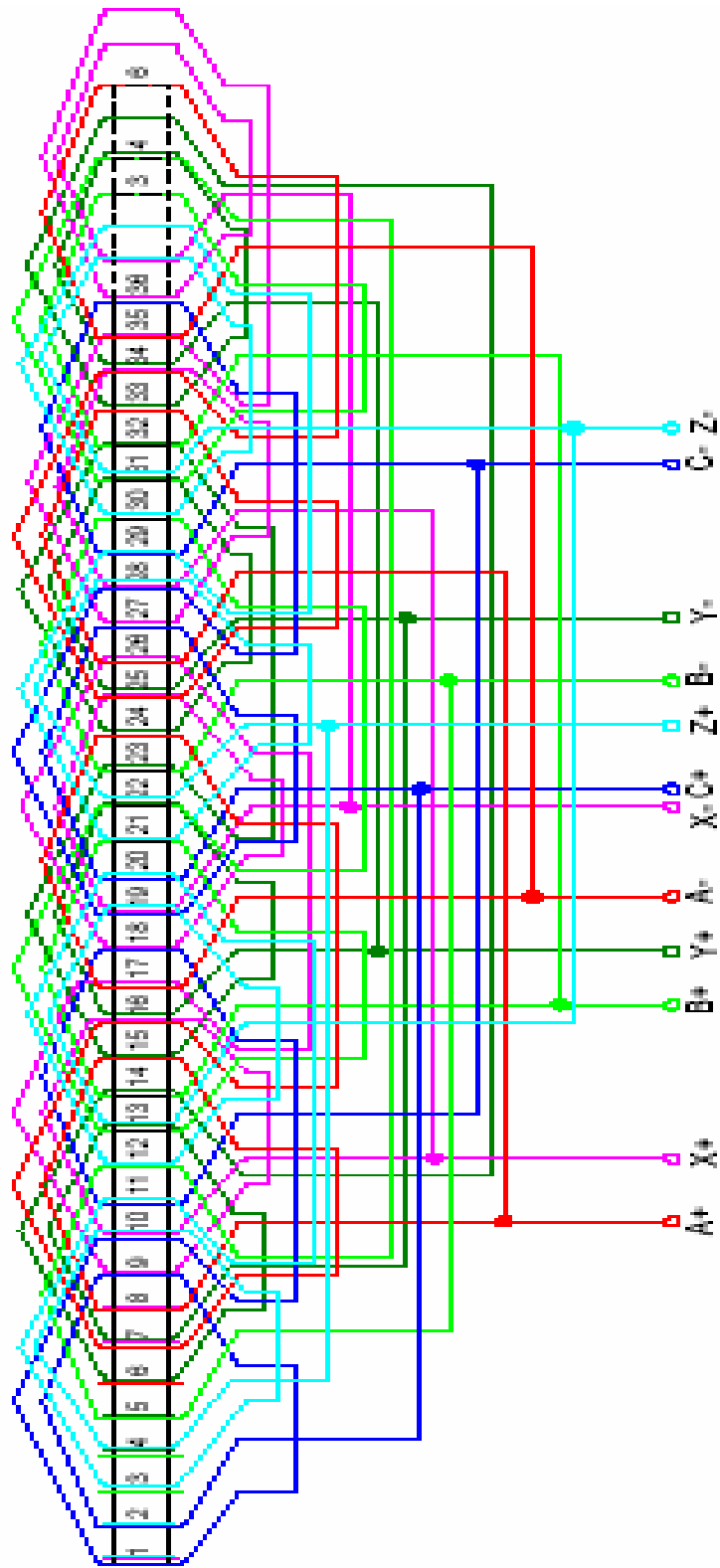


Figure 2.8 Total winding

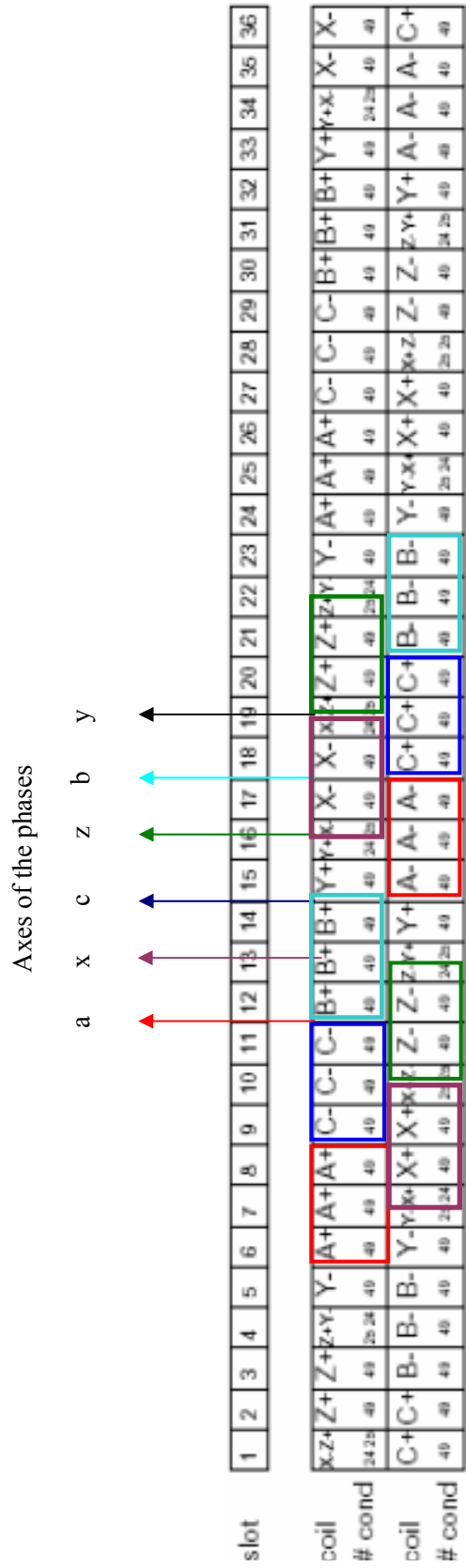


Figure 2.9 Phase axes of the six-phase machine winding.

### 2.3.4 MMF equation of six-phase winding with 1<sup>st</sup> and 3<sup>rd</sup> harmonic current components

Since the asymmetric six-phase machine is derived from a conventional three-phase induction machine, we can derive the *mmf* distribution of an asymmetric six-phase machine from a conventional three-phase induction machine in four steps.

i) First, the flux distribution on a concentrated winding three-phase machine is considered. Figure 2.10 shows the winding distribution for a simple two pole concentrated winding machine with one slot per pole per phase. The winding function for phase *a* is also shown in this figure.

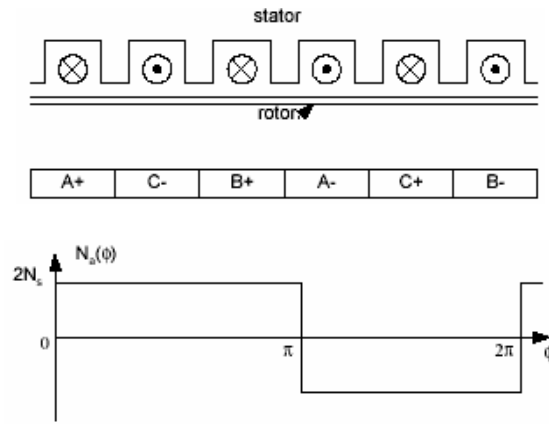


Figure 2.10 Winding distribution of a three-phase concentrated winding induction machine and winding function for phase *a*

Each of the coils is assumed to have  $4N_s$  turns and the *mmf* acting across the gap associated with stator currents is:

$$F = F_a + F_b + F_c = N_a(\Phi) i_a + N_b(\Phi) i_b + N_c(\Phi) i_c \quad (2.4)$$

where, the winding functions can be written as sum of odd harmonic components by Fourier representation as:

$$N_a(\Phi) = 4(2N_s)/\pi [\sin\Phi + (1/3)\sin3\Phi + (1/5)\sin5\Phi + (1/7)\sin7\Phi + \dots] \quad (2.5)$$

$$N_b(\Phi) = 4(2N_s)/\pi [\sin(\Phi-120^\circ) + (1/3)\sin3(\Phi-120^\circ) + (1/5)\sin5(\Phi-120^\circ) + (1/7)\sin7(\Phi-120^\circ) + \dots] \quad (2.6)$$



$$N_c(\Phi) = 4(2N_s)/\pi [\text{Sin}(\Phi+120^\circ) + (1/3) \text{Sin}3(\Phi+120^\circ) + (1/5) \text{Sin}5(\Phi+120^\circ) + (1/7) \text{Sin}7(\Phi+120^\circ) + \dots] \quad (2.7)$$

since the winding function is a typical odd function, even harmonics are zero and the currents can be written as:

$$i_a = I \text{Cos}\theta \quad (2.8)$$

$$i_b = I \text{Cos}(\theta-120^\circ) \quad (2.9)$$

$$i_c = I \text{Cos}(\theta+120^\circ) \quad (2.10)$$

$$\theta = \omega t \quad (2.11)$$

and the resulting *mmf* is obtained using the Fourier series representation,

$$F = \sum F_n = \sum [N_{an}(\Phi) i_a + N_{bn}(\Phi) i_b + N_{cn}(\Phi) i_c] \quad (2.12)$$

where  $n = 1, 2, 3, \dots, \infty$

Since  $N(\Phi) = 0$  for even values of  $n$ , even harmonics of  $F$  are also zero. Therefore the *mmf* can be given as,

$$F = F_1 + F_3 + F_5 + F_7 \quad (2.13)$$

For the fundamental component,

$$F_1 = N_{a1}(\Phi) i_a + N_{b1}(\Phi) i_b + N_{c1}(\Phi) i_c \quad (2.14)$$

$$\begin{aligned} F_1 &= 4(2N_s)/\pi \{ [\text{Sin}\Phi I \text{Cos}\theta] + [\text{Sin}(\Phi-120^\circ) I \text{Cos}(\theta-120^\circ)] \\ &\quad + [\text{Sin}(\Phi+120^\circ) I \text{Cos}(\theta+120^\circ)] \} \\ &= 8I N_s/\pi \{ [\text{Sin}\Phi \text{Cos}\theta] + [\text{Sin}(\Phi-120^\circ) \text{Cos}(\theta-120^\circ)] \\ &\quad + [\text{Sin}(\Phi+120^\circ) \text{Cos}(\theta+120^\circ)] \} \end{aligned} \quad (2.15)$$

Since,

$$\text{Sin}\Phi \text{Cos}\theta = \frac{1}{2} [\text{Sin}(\Phi-\theta) + \text{Sin}(\Phi+\theta)] \quad (2.16)$$

$$\begin{aligned} F_1 &= 8I N_s/\pi \{ \frac{1}{2} [\text{Sin}(\Phi-\theta) + \text{Sin}(\Phi+\theta)] + \frac{1}{2} [\text{Sin}(\Phi-\theta) + \text{Sin}(\Phi+\theta-240^\circ)] \\ &\quad + \frac{1}{2} [\text{Sin}(\Phi-\theta) + \text{Sin}(\Phi+\theta+240^\circ)] \} \end{aligned} \quad (2.17)$$

$$= 4I N_s / \pi \{ \sin(\Phi-\theta) [ 1 + (\sin(\Phi+\theta)/ \sin(\Phi-\theta)) + 1 + (\sin(\Phi+\theta-240^\circ)/ \sin(\Phi-\theta)) + 1 + (\sin(\Phi+\theta+240^\circ)/\sin(\Phi-\theta))] \} \quad (2.18)$$

$$F_1 = 12I N_s / \pi [ \sin(\Phi-\theta) ] \quad (2.19)$$

Also for the third harmonic component,

$$F_3 = N_{a3}(\Phi) i_a + N_{b3}(\Phi) i_b + N_{c3}(\Phi) i_c \quad (2.20)$$

$$\begin{aligned} F_3 &= 4(2N_s)/\pi \{ [(1/3)\sin 3\Phi \text{ICos}\theta ] + [ (1/3)\sin 3(\Phi-120^\circ) \text{ICos}(\theta-120^\circ)] \\ &\quad + [(1/3)\sin 3(\Phi+120^\circ) \text{ICos}(\theta+120^\circ) ] \} \\ &= 8IN_s/3\pi \{ [\sin 3\Phi \text{Cos}\theta ] + [ \sin 3(\Phi-120^\circ) \text{Cos}(\theta-120^\circ)] \\ &\quad + [\sin 3(\Phi+120^\circ) \text{Cos}(\theta+120^\circ)] \} \\ &= 8IN_s/3\pi \{ [ \sin 3\Phi \text{Cos}\theta ] + [ \sin 3\Phi \text{Cos}(\theta-120^\circ)] \\ &\quad + [\sin 3\Phi \text{Cos}(\theta+120^\circ)] \} \\ &= 8IN_s/3\pi \{ \sin 3\Phi [\text{Cos}\theta + \text{Cos}(\theta-120^\circ) + \text{Cos}(\theta+120^\circ)] \} = 0 \quad (2.21) \end{aligned}$$

$$F_3 = 0 \quad (2.22)$$

For the 5<sup>th</sup> harmonic component,

$$F_5 = N_{a5}(\Phi) i_a + N_{b5}(\Phi) i_b + N_{c5}(\Phi) i_c \quad (2.23)$$

$$\begin{aligned} F_5 &= 4(2N_s)/\pi \{ [(1/5)\sin 5\Phi \text{ICos}\theta ] + [ (1/5)\sin 5(\Phi-120^\circ) \text{ICos}(\theta-120^\circ)] \\ &\quad + [(1/5)\sin 5(\Phi+120^\circ) \text{ICos}(\theta+120^\circ) ] \} \\ &= 8IN_s/5\pi \{ [\sin 5\Phi \text{Cos}\theta ] + [ \sin 5(\Phi-120^\circ) \text{Cos}(\theta-120^\circ)] \\ &\quad + [ \sin 5(\Phi+120^\circ) \text{Cos}(\theta+120^\circ)] \} \\ &= 8IN_s/5\pi \{ [ \sin 5\Phi \text{Cos}\theta ] + [ \sin(5\Phi+120^\circ) \text{Cos}(\theta-120^\circ)] \\ &\quad + [ \sin(5\Phi-120^\circ) \text{Cos}(\theta+120^\circ)] \} \quad (2.24) \end{aligned}$$

Since,

$$\sin\Phi \text{Cos}\theta = \frac{1}{2} [\sin(\Phi-\theta) + \sin(\Phi+\theta)] \quad (2.25)$$

$$\begin{aligned} F_5 &= 4I N_s / 5\pi \{ [\sin(5\Phi-\theta) + \sin(5\Phi+\theta)] + [\sin(5\Phi-\theta+240^\circ) + \sin(5\Phi+\theta)] \\ &\quad + [\sin(5\Phi-\theta-240^\circ) + \sin(5\Phi+\theta)] \} \end{aligned}$$

$$\begin{aligned}
&= 4I N_s/5\pi \{ \text{Sin}(5\Phi+\theta) [ 1 + (\text{Sin}(5\Phi-\theta)/\text{Sin}(5\Phi+\theta)) \\
&\quad + 1 + (\text{Sin}(5\Phi-\theta+240^\circ)/\text{Sin}(5\Phi+\theta)) \\
&\quad + 1 + (\text{Sin}(5\Phi-\theta-240^\circ)/\text{Sin}(5\Phi+\theta)) ] \} \quad (2.26)
\end{aligned}$$

$$F_5 = 12I N_s/5\pi [\text{Sin}(5\Phi+\theta)] \quad (2.27)$$

For the 7<sup>th</sup> harmonic component,

$$F_7 = N_{a7}(\Phi) i_a + N_{b7}(\Phi) i_b + N_{c7}(\Phi) i_c \quad (2.28)$$

$$\begin{aligned}
F_7 &= 4(2N_s)/\pi \{ [(1/7)\text{Sin}7\Phi \text{ICos}\theta ] + [ (1/7)\text{Sin}7(\Phi-120^\circ) \text{ICos}(\theta-120^\circ)] \\
&\quad + [(1/7)\text{Sin}7(\Phi+120^\circ) \text{ICos}(\theta+120^\circ) ] \} \\
&= 8I N_s/7\pi \{ [\text{Sin}7\Phi \text{Cos}\theta ] + [ \text{Sin}7(\Phi-120^\circ) \text{Cos}(\theta-120^\circ)] \\
&\quad + [ \text{Sin}7(\Phi+120^\circ) \text{Cos}(\theta+120^\circ)] \} \\
&= 8I N_s/7\pi \{ [ \text{Sin}7\Phi \text{Cos}\theta ] + [ \text{Sin}(7\Phi-120^\circ) \text{Cos}(\theta-120^\circ)] \\
&\quad + [ \text{Sin}(7\Phi+120^\circ) \text{Cos}(\theta+120^\circ)] \} \quad (2.29)
\end{aligned}$$

Since,

$$\text{Sin}\Phi \text{Cos}\theta = \frac{1}{2} [\text{Sin}(\Phi-\theta) + \text{Sin}(\Phi+\theta)] \quad (2.30)$$

$$\begin{aligned}
F_7 &= 4I N_s/7\pi \{ [ \text{Sin}(7\Phi-\theta) + \text{Sin}(7\Phi+\theta) ] + [\text{Sin}(7\Phi-\theta) + \text{Sin}(7\Phi+\theta-240^\circ)] \\
&\quad + [\text{Sin}(7\Phi-\theta) + \text{Sin}(7\Phi+\theta+240^\circ)] \} \\
&= 4I N_s/7\pi \{ \text{Sin}(7\Phi-\theta) [ 1 + (\text{Sin}(7\Phi+\theta)/\text{Sin}(7\Phi-\theta)) \\
&\quad + 1 + (\text{Sin}(7\Phi+\theta-240)/\text{Sin}(7\Phi-\theta)) \\
&\quad + 1 + (\text{Sin}(7\Phi+\theta+240^\circ)/\text{Sin}(7\Phi-\theta))] \} \quad (2.31)
\end{aligned}$$

$$F_7 = 12I N_s/7\pi [\text{Sin}(7\Phi-\theta)] \quad (2.32)$$

We see that, for a three-phase concentrated winding machine, since  $F_3$  is zero,  $F = F_1 + F_5 + F_7$ . A point of maximum amplitude of the fundamental component is found by setting the argument equal to  $90^\circ$ . The rotational speed of this point is found by taking the time derivative.

For  $F_1$  ;

$$(\Phi - \theta) = 90^\circ \quad (2.33)$$

$$d/dt [ (\Phi - \theta) ] = 0 \quad (2.34)$$

$$d/dt [(\Phi - \omega t)] = 0 \quad (2.35)$$

$$d\Phi/dt - \omega = 0 \quad (2.36)$$

$$d\Phi/dt = \omega \quad (2.37)$$

Thus, the peak of the fundamental component rotates in the direction of increasing  $\Phi$  with angular speed

For  $F_5$  ;

$$(5\Phi + \theta) = 90^\circ \quad (2.37)$$

$$d/dt [ (5\Phi + \theta) ] = 0 \quad (2.38)$$

$$d/dt [(5\Phi + \omega t)] = 0 \quad (2.39)$$

$$5 d\Phi/dt + \omega = 0 \quad (2.40)$$

$$d\Phi/dt = -\omega/5 \quad (2.41)$$

The fifth harmonic component rotates in the direction of decreasing  $\Phi$  at 1/5 the speed of the fundamental component. This is then a negative sequence component that produces negative average torque (braking).

For  $F_7$  ;

$$(7\Phi - \theta) = 90^\circ \quad (2.42)$$

$$d/dt [ (7\Phi - \theta) ] = 0 \quad (2.43)$$

$$d/dt [(7\Phi - \omega t)] = 0 \quad (2.44)$$

$$7 d\Phi/dt - \omega = 0 \quad (2.45)$$

$$d\Phi/dt = \omega/7 \quad (2.46)$$

The seventh harmonic rotates in the direction of increasing  $\Phi$  at 1/7 the speed of the fundamental component and therefore is a positive sequence component. While positively rotating, its synchronous speed is only 1/7 that of the fundamental and only produces desirable positive torque when the rotor is between 0 and 1/7 of the synchronous speed corresponding to the fundamental component.

When excited at variable frequency, the motor operates continuously at low slip frequency. Hence, in this case, the fifth and seventh spatial harmonics always produce undesirable braking torque and both should be minimized.

ii) To minimize the fifth and seventh harmonics we consider the phase winding distribution over two slots, or two slots per pole per phase. The new winding distribution and winding function for phase  $a$  are shown in Figure 2.11. Here the machine could be analyzed as a three-phase machine with distributed windings over two slots per pole per phase, or, if each winding is treated separately, this configuration corresponds to an asymmetric six-phase machine with 30 degrees separation between the two three-phase groups. Thus, the six-phase machine is composed by two three-phase groups spatially shifted by 30 degrees with respect to each other.

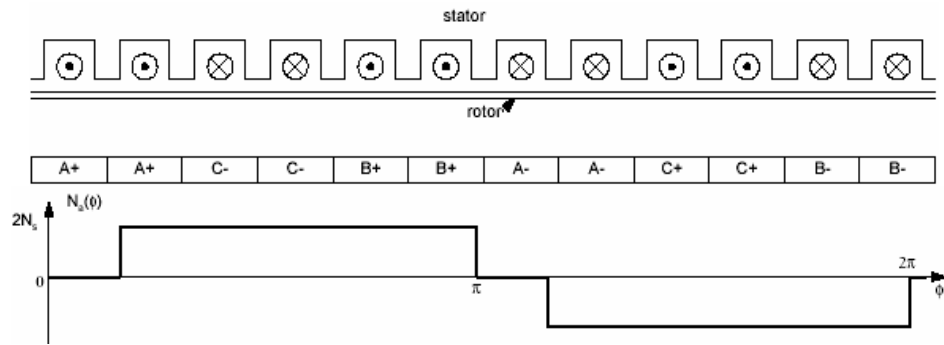


Figure 2.11 Winding distribution of a three-phase distributed winding induction machine and winding function for phase  $a$

The fundamental component of the rotating  $mmf$  can be considered as the sum of two components produced by the two stator groups with the same total number of turns which are phase shifted spatially by 30 electrical degrees. Thus,

If we substitute  $\Phi$  by  $(\Phi-30^\circ)$  in the expressions added to the equations (2.19,27,32) for the  $30^\circ$  shifted group and take half of the initial turn number for each group:

$$F_1 = 6I N_s/\pi [ \text{Sin}(\Phi-\theta) + \text{Sin}(\Phi-30^\circ-\theta) ] \quad (2.47)$$

$$F_5 = 6I N_s/5\pi [ \text{Sin}(5\Phi+\theta) + \text{Sin}(5\Phi-150^\circ-\theta) ] \quad (2.48)$$

$$F_7 = 6I N_s/7\pi [ \text{Sin}(7\Phi-\theta) + \text{Sin}(7\Phi+210^\circ-\theta) ] \quad (2.49)$$

iii) Thirdly, we consider phase shifting one of the stator winding groups spatially by 30 electrical degrees but also shifting the currents in each group by 30 degrees in time. In effect this configuration becomes a dual three-phase, or asymmetrical six-phase machine. The winding diagram for this case is shown in Figure 2.12.

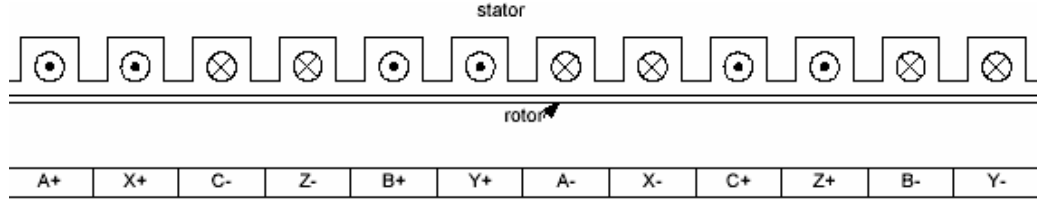


Figure 2.12 Winding distribution of asymmetric six-phase machine with concentrated windings.

Three additional currents  $i_x$ ,  $i_y$ , and  $i_z$  are defined to correspond to a three-phase set of currents which are phase shifted with respect to currents  $i_a$ ,  $i_b$  and  $i_c$  by 30 electrical degrees.

$$i_x = I \cos(\theta - 30^\circ) \quad (2.50)$$

$$i_y = I \cos(\theta - 150^\circ) \quad (2.51)$$

$$i_z = I \cos(\theta + 90^\circ) \quad (2.52)$$

The total  $mmf$  can again be found by taking the sum of two  $mmf$ 's that are now phase shifted in space and time:

If we substitute  $\theta$  by  $(\theta - 30^\circ)$  in the second terms of the equations (2.47,48,49),

$$\begin{aligned} F_1 &= 6I N_s / \pi [ \sin(\Phi - \theta) + \sin((\Phi - 30^\circ) - (\theta - 30^\circ)) ] \\ &= 12I N_s / \pi [ \sin(\Phi - \theta) ] \end{aligned} \quad (2.53)$$

$$\begin{aligned} F_5 &= 6I N_s / 5\pi [ \sin(5\Phi + \theta) + \sin(5(\Phi - 30^\circ) + (\theta - 30^\circ)) ] \\ &= 6I N_s / 5\pi [ \sin(5\Phi + \theta) + \sin(5\Phi + \theta - 180^\circ) ] = 0 \end{aligned} \quad (2.54)$$

$$\begin{aligned} F_7 &= 6I N_s / 7\pi [ \sin(7\Phi - \theta) + \sin(7(\Phi - 30^\circ) + (\theta - 30^\circ)) ] \\ &= 6I N_s / 7\pi [ \sin(7\Phi - \theta) + \sin(7\Phi - \theta - 180^\circ) ] = 0 \end{aligned} \quad (2.55)$$

So, use of an asymmetrical six-phase machine by shifting one of the stator winding groups spatially by 30 electrical degrees and also shifting the currents in each group by 30 degrees in time, produces as much fundamental flux in the air gap as a full pitched concentrated coil winding while at the same time reducing the 5<sup>th</sup> and 7<sup>th</sup> spatial harmonics to zero.

iv) Finally, a zero sequence third harmonic component could be injected in the phase currents if the neutral connection is present. For the three-phase machine, this component produces nothing more than a stationary or standing wave which produces only braking and pulsating torques. For the asymmetrical six-phase machine however, a particular choice of the zero sequence components produces rotating waves at the same angular speed as the fundamental and therefore contributes for the final machine torque.

The zero sequence component must be handled separately and it is assumed that the stator currents are made up of two components:

$$i_a = I \cos\theta + I_0 \quad (2.56)$$

$$i_b = I \cos(\theta-120^\circ) + I_0 \quad (2.57)$$

$$i_c = I \cos(\theta+120^\circ) + I_0 \quad (2.58)$$

$$\theta = \omega t \quad (2.59)$$

$$\begin{aligned} i_a + i_b + i_c &= [I \cos\theta + I_0] + [I \cos(\theta-120^\circ) + I_0] + [I \cos(\theta+120^\circ) + I_0] \\ &= 3 I_0 + I [\cos\theta + \cos(\theta-120^\circ) + \cos(\theta+120^\circ)] \\ &= 3 I_0 \end{aligned} \quad (2.60)$$

Hence,

$$I_0 = [i_a + i_b + i_c] / 3 \quad (2.61)$$

We inject the zero sequence third harmonic current components as:

$$I_{0A} = I_3 \cos(3\theta) \quad (2.62)$$

$$I_{0X} = I_3 \sin(3\theta) \quad (2.63)$$

To analyze the influence of the zero sequence current component it is necessary to represent the winding functions in a  $dq0$  frame. The winding functions can undergo a  $dq0$  transformation in much the same manner as voltages and currents. So in a  $dq0$  stationary frame the zero sequence components of the winding functions of the two shifted stator winding groups are derived as follows:

The winding functions were:

$$N_a(\Phi) = 4(2N_s)/\pi [ \text{Sin}\Phi + (1/3)\text{Sin}3\Phi + (1/5) \text{Sin}5\Phi + (1/7) \text{Sin}7\Phi + \dots ] \quad (2.64)$$

$$N_b(\Phi) = 4(2N_s)/\pi [ \text{Sin}(\Phi-120^\circ) + (1/3)\text{Sin}3(\Phi-120^\circ) + (1/5) \text{Sin}5(\Phi-120^\circ) + (1/7) \text{Sin}7(\Phi-120^\circ) + \dots ] \quad (2.65)$$

$$N_c(\Phi) = 4(2N_s)/\pi [ \text{Sin}(\Phi+120^\circ) + (1/3) \text{Sin}3(\Phi+120^\circ) + (1/5) \text{Sin}5(\Phi+120^\circ) + (1/7) \text{Sin}7(\Phi+120^\circ) + \dots ] \quad (2.66)$$

Hence we derive the zero sequence components of the winding functions as:

$$\begin{aligned} N_{0A} &= [ N_a(\Phi) + N_b(\Phi) + N_c(\Phi) ] / 3 \\ &= 4N_s/\pi [1/3 \text{ Sin}3\Phi] \end{aligned} \quad (2.67)$$

$$\begin{aligned} N_{0X} &= [ N_x(\Phi) + N_y(\Phi) + N_z(\Phi) ] / 3 \\ &= 4N_s/\pi [1/3 \text{ Sin}3(\Phi-30^\circ)] \\ &= - 4N_s/\pi [1/3 \text{ Cos}3\Phi] \end{aligned} \quad (2.68)$$

Therefore the zero sequence  $mmf$  for the third harmonic can be considered as the sum of two components, one for each of the shifted stator winding groups. The third harmonic  $mmf$  is in this case,

$$F_3 = F_{3A} + F_{3X} = N_{0A}(\Phi) I_{0A} + N_{0X}(\Phi) I_{0X} \quad (2.69)$$

$$\begin{aligned} F_3 &= 4N_s/\pi [1/3 \text{ Sin}3\Phi] \cdot I_3 \text{ Cos}(3\theta) - 4N_s/\pi [1/3 \text{ Cos}3\Phi] \cdot I_3 \text{ Sin}(3\theta) \\ &= 4N_s I_3/3\pi [ \text{Sin}3\Phi \text{ Cos}(3\theta) - \text{Cos}3\Phi \text{ Sin}(3\theta) ] \end{aligned} \quad (2.70)$$

$$F_3 = 4N_s I_3/3\pi [ \text{Sin}3(\Phi - \theta) ] \quad (2.71)$$



Therefore, the zero sequence component can be now used to produce a second positively rotating component. The angular speed of this wave is calculated as:

$$3(\Phi - \theta) = \pi \quad (2.72)$$

$$d/dt [3(\Phi - \theta)] = 0 \quad (2.73)$$

$$d/dt [3(\Phi - \omega t)] = 0 \quad (2.74)$$

$$3 d\Phi/dt - \omega = 0 \quad (2.75)$$

$$d\Phi/dt = \omega/3 \quad (2.76)$$

As a result, the total *mmf* is the sum of the equations (2.53) and (2.71),

$$\begin{aligned} F_1 + F_3 &= 12I N_s/\pi [\text{Sin}(\Phi-\theta)] + 4N_s I_3/3\pi [\text{Sin}3(\Phi - \theta)] \\ &= 4N_s/\pi [3I \text{Sin}(\Phi-\theta) + I_3/3 \text{Sin}3(\Phi - \theta)] \end{aligned} \quad (2.77)$$

### 2.3.5 Flux distribution on an asymmetric six-phase machine with 3<sup>rd</sup> harmonic injection

As known, the maximum modulation depth of a regular sampled PWM system could be increased by including a common mode third harmonic term into the target reference waveform of each phase leg of an inverter. This third harmonic component does not affect the line to line fundamental output voltages, since the common mode voltages cancel between the phase legs, but it does reduce the peak envelope of each phase leg voltage, and thus allows the modulation depth *M* to be increased beyond 1 without the modulation strategy becoming overmodulated (i.e. when the reference waveform magnitude exceeds the carrier peak during the fundamental cycle). The same principle can be used to increase the fundamental component of flux density in the six-phase machine. It will be assumed that because of saturation issues, the peak value of flux density in the stator teeth is limited to the value resulting from the *mmf* imposed by the basic concentrated full pitch winding.

The below equation defines the appropriate sinusoidal target reference waveform which is extended from a sine wave to include the third harmonic component.

$$B_g(\Phi) = B_1 \text{Sin}\Phi + B_3 \text{Sin}3\Phi \quad (2.78)$$

By dividing through by  $B_1$ , can be written in the per unit form,

$$\mathbf{b} = \text{Sin}\Phi + \mathbf{a} \cdot \text{Sin}3\Phi \quad (2.79)$$

where,

$$\mathbf{b} = B_g / B_1 \quad (2.80)$$

$$\mathbf{a} = B_3 / B_1 \quad (2.81)$$

For  $\mathbf{b}$  to be maximum ( $\mathbf{b}_{\max}$ ),

$$\begin{aligned} d\mathbf{b}/dt &= d/dt \cdot [\text{Sin}\Phi + \mathbf{a} \cdot \text{Sin}3\Phi] = 0 \\ &= d\Phi/dt \cdot \text{Cos}\Phi + \mathbf{a} \cdot d\Phi/dt \cdot 3 \cdot \text{Cos}3\Phi = 0 \\ &= d\Phi/dt \cdot [\text{Cos}\Phi + \mathbf{a} \cdot 3 \cdot \text{Cos}3\Phi] = 0 \end{aligned} \quad (2.82)$$

$$0 = [\text{Cos}\Phi + 3 \mathbf{a} \cdot \text{Cos}3\Phi] \quad (2.83)$$

On the other hand by using the trigonometric equations :

$$\text{Cos}3\Phi = \text{Cos}2\Phi \cdot \text{Cos}\Phi - \text{Sin}2\Phi \cdot \text{Sin}\Phi \quad (2.84)$$

$$\text{Cos}2\Phi = \text{Cos}\Phi \cdot \text{Cos}\Phi - \text{Sin}\Phi \cdot \text{Sin}\Phi \quad (2.85)$$

$$\text{Sin}2\Phi = \text{Sin}\Phi \cdot \text{Cos}\Phi + \text{Cos}\Phi \cdot \text{Sin}\Phi. \quad (2.86)$$

we obtain,

$$\begin{aligned} \text{Cos}3\Phi &= \text{Cos}^3\Phi - \text{Sin}^2\Phi \cdot \text{Cos}\Phi - \text{Sin}^2\Phi \cdot \text{Cos}\Phi - \text{Sin}^2\Phi \cdot \text{Cos}\Phi \\ \text{Cos}3\Phi &= \text{Cos}^3\Phi - 3 \cdot \text{Sin}^2\Phi \cdot \text{Cos}\Phi \end{aligned} \quad (2.87)$$

If we substitute (2.87) in (2.83)

$$\begin{aligned} \text{Cos}\Phi + 3 \mathbf{a} \cdot (\text{Cos}^3\Phi - 3 \cdot \text{Sin}^2\Phi \cdot \text{Cos}\Phi) &= 0 \\ \text{Cos}\Phi \cdot [1 + 3 \mathbf{a} \cdot (\text{Cos}^2\Phi - 3 \cdot \text{Sin}^2\Phi)] &= 0 \\ [1 + 3 \mathbf{a} \cdot (\text{Cos}^2\Phi - 3 \cdot \text{Sin}^2\Phi)] &= 0 \end{aligned} \quad (2.88)$$

and since,

$$\text{Sin}^2\Phi = 1 - \text{Cos}^2\Phi, \quad (2.89)$$

$$[1 + 3 \mathbf{a} \cdot (\text{Cos}^2\Phi - 3 + 3 \cdot \text{Cos}^2\Phi)] = 0$$

$$[1 + 3 \mathbf{a} \cdot (4 \cdot \text{Cos}^2\Phi - 3)] = 0$$

$$3 - 1/3\mathbf{a} = 4 \cdot \text{Cos}^2\Phi$$

$$\text{Cos}\Phi_{\max} = [(9\mathbf{a} - 1) / 12\mathbf{a}]^{1/2} \quad (2.90)$$

$$\begin{aligned} \text{Sin}\Phi_{\max} &= \{ 1 - [(9\mathbf{a} - 1) / 12\mathbf{a}] \}^{1/2} \\ &= [(3 \cdot \mathbf{a} + 1) / 12 \cdot \mathbf{a}]^{1/2} \end{aligned} \quad (2.91)$$

where  $\Phi_{\max}$  is the angle value when  $\mathbf{b} = \mathbf{b}_{\max}$

Also by using the equations (2.85,86,89) and,

$$\text{Sin}3\Phi = \text{Sin}2\Phi \cdot \text{Cos}\Phi + \text{Cos}2\Phi \cdot \text{Sin}\Phi \quad (2.92)$$

we obtain,

$$\begin{aligned} \text{Sin}3\Phi &= 2 \cdot \text{Cos}^2\Phi \cdot \text{Sin}\Phi + \text{Cos}^2\Phi \cdot \text{Sin}\Phi - \text{Sin}\Phi \text{Cos}2\Phi - \text{Sin}\Phi + \text{Cos}^2\Phi \cdot \text{Sin}\Phi \\ &= 2 \cdot (1 - \text{Sin}^2\Phi) \cdot \text{Sin}\Phi + (2 \cdot \text{Cos}^2\Phi - 1) \cdot \text{Sin}\Phi \\ &= 2 \cdot \text{Sin}\Phi - 2 \text{Sin}^3\Phi + 2 \cdot \text{Sin}\Phi - 2 \text{Sin}^3\Phi - \text{Sin}\Phi \\ &= 3 \cdot \text{Sin}\Phi - 4 \cdot \text{Sin}^3\Phi \end{aligned} \quad (2.93)$$

If we substitute (2.91) in (2.93), we obtain,

$$\begin{aligned} \text{Sin}3\Phi_{\max} &= 3 \cdot [(3 \cdot \mathbf{a} + 1) / 12 \cdot \mathbf{a}]^{1/2} - 4 \cdot [(3 \cdot \mathbf{a} + 1) / 12 \cdot \mathbf{a}]^{3/2} \\ &= [(3 \cdot \mathbf{a} + 1) / 12 \cdot \mathbf{a}]^{1/2} \cdot \{ 3 - 4 \cdot (3 \cdot \mathbf{a} + 1) / 12 \cdot \mathbf{a} \} \\ &= [(3 \cdot \mathbf{a} + 1) / 3 \cdot \mathbf{a}]^{1/2} \cdot (6 \cdot \mathbf{a} - 1) / 6 \cdot \mathbf{a} \end{aligned} \quad (2.94)$$

If we put (2.94) in (2.79) which was  $\mathbf{b} = \text{Sin}\Phi + \mathbf{a} \cdot \text{Sin}3\Phi$ , we get,

$$\begin{aligned} \mathbf{b}_{\max} &= [(3 \cdot \mathbf{a} + 1) / 12 \cdot \mathbf{a}]^{1/2} + \mathbf{a} \cdot \{ [(3 \cdot \mathbf{a} + 1) / 3 \cdot \mathbf{a}]^{1/2} \cdot (6 \cdot \mathbf{a} - 1) / 6 \cdot \mathbf{a} \} \\ &= [(3 \cdot \mathbf{a} + 1) / 3 \cdot \mathbf{a}]^{1/2} \cdot [1/2 + (6 \cdot \mathbf{a} - 1) / 6] \\ &= [(3 \cdot \mathbf{a} + 1) / 3 \cdot \mathbf{a}]^{1/2} \cdot (3 \cdot \mathbf{a} + 1) / 3 \end{aligned} \quad (2.95)$$

To determine the amount of 3<sup>rd</sup> harmonic to be injected, we should deal with,

$$\mathbf{a} = \mathbf{B}_3 / \mathbf{B}_1$$

To find the value of  $\mathbf{a}$  for  $\mathbf{b} = \mathbf{b}_{\max}$ ,  $\rightarrow d\mathbf{b}_{\max}/d\mathbf{a} = 0$

$$\begin{aligned} d\mathbf{b}_{\max}/d\mathbf{a} &= [(3 \cdot \mathbf{a} + 1) / 3 \cdot \mathbf{a}]^{1/2} - (3 \cdot \mathbf{a} + 1) / 3 \cdot [(3 \cdot \mathbf{a} + 1) / 3 \cdot \mathbf{a}]^{-1/2} \cdot 1/6\mathbf{a}^2 = 0 \\ d\mathbf{b}_{\max}/d\mathbf{a} &= [(3 \cdot \mathbf{a} + 1) / 3 \cdot \mathbf{a}]^{-1/2} \cdot \{ [(3 \cdot \mathbf{a} + 1) / 3 \cdot \mathbf{a}] - (3 \cdot \mathbf{a} + 1) / 3 \cdot 1/6\mathbf{a}^2 \} = 0 \end{aligned} \quad (2.96)$$

$$\begin{aligned}
& [(3 \cdot \mathbf{a} + 1) / 3 \cdot \mathbf{a}] - (3 \cdot \mathbf{a} + 1) / 18 \mathbf{a}^2 = 0 \\
& (18 \mathbf{a}^2 + 6 \mathbf{a} - 3 \mathbf{a} - 1) / 18 \mathbf{a}^2 = 0 \\
& 18 \mathbf{a}^2 + 6 \mathbf{a} - 3 \mathbf{a} - 1 = 0
\end{aligned} \tag{2.97}$$

$$\mathbf{a} = -1/3 \text{ and } \mathbf{a} = 1/6 \tag{2.98}$$

If we put these values in (2.95), we get,

$$\mathbf{a} = -1/3 \rightarrow \mathbf{b} = 0 \tag{2.99}$$

$$\mathbf{a} = 1/6 \rightarrow \mathbf{b} = 0.866 \tag{2.100}$$

Hence,

$$\mathbf{b}_{\max} = 0.866 = B_g / B_1 \tag{2.101}$$

This means  $B_{g_{\max}}$  decreases to 0.866 times its initial value ( $B_1$ ) when 3<sup>rd</sup> harmonic component is added. After the addition of 3<sup>rd</sup> harmonic component  $B_3$ , we can increase  $B_1$  by,

$$1 / 0.866 = 1.1547 \tag{2.102}$$

factor in order to keep the same  $B_{g_{\max}}$  value. Since  $\mathbf{a} = B_3 / B_1$ , when we increase  $B_1$ , then  $B_3$  also increases.

$$\mathbf{a} = B_3 / B_1$$

$$1/6 = B_3 / 1.1547 \cdot B_{g_{\max}}$$

$$B_3 = 0.1925 \cdot B_{g_{\max}} \tag{2.103}$$

When we substitute the values above in (2.78),  $B_g(\Phi) = B_1 \sin \Phi + B_3 \sin 3\Phi$ , we get,

$$B_g = 1,1547 B_{g_{\max}} \left( \sin \Phi + \frac{1}{6} \sin 3\Phi \right) \tag{2.104}$$

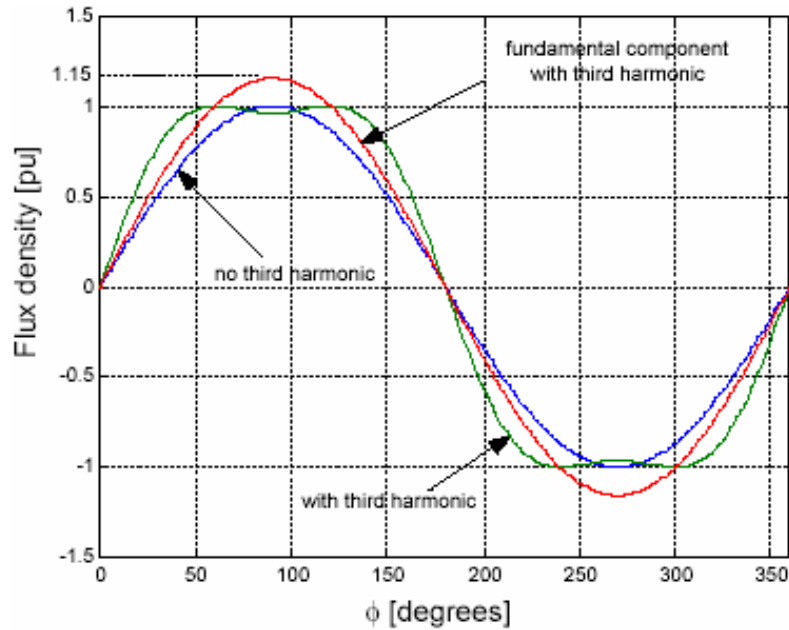


Figure 2.13 Flux density distribution for the same peak air gap flux with and without third harmonic injection.

In conclusion, harmonic currents may be injected in multi-phase systems to create an air gap flux that resembles the winding functions of the machine. Adding a voltage harmonic reference would force harmonic currents to flow in the machine. However, for a three-phase induction drive without neutral connection, the third harmonic current cannot flow and therefore the fundamental voltage in the machine is increased without the penalty of harmonic voltage and current distortion. Connecting the neutral in a three-phase machine causes third harmonic currents to flow and torque pulsations to appear. In a six-phase machine, third harmonic zero sequence currents are used to increase the fundamental flux and to generate extra torque. These results are only obtained if the currents, not voltages, in the machine can be correctly controlled.

### 2.3.6 Torque density increase with third harmonic injection

The contribution of using the third harmonic component in the improvement of the torque density is now investigated. Torque production in any induction machine can be best analyzed by utilizing the usual per phase equivalent circuit shown in Figure 2.14.

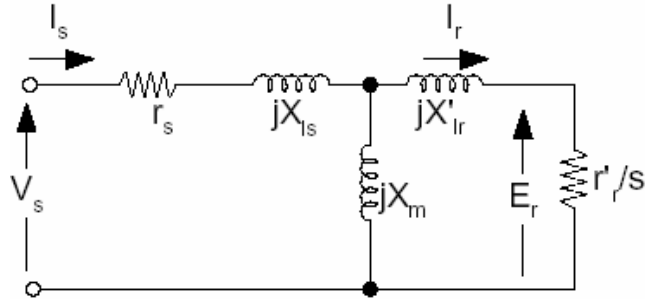


Figure 2.14 Induction machine steady-state per phase equivalent circuit.

From [12], assuming peak values for the variables, the torque can be calculated as,

$$T = \frac{(3/2) P}{2} I_r^2 r'_r / s \omega_e \quad (2.105)$$

If we substitute  $E_r = I_r r'_r / s$

$$T = \frac{(3/2) P}{2} I_r E_r / \omega_e \quad (2.106)$$

In order to analyze the benefit of increased flux in torque production, it is necessary to express torque as a function of the machine back *emf*. In Figure 2.15, an approximated equivalent circuit can be obtained by neglecting rotor leakage reactance. In this circuit, the rotor current is determined by a modified back *emf* voltage that corresponds to the rotor flux instead of the air gap flux. This suggests that the rotor flux is the one to be controlled in order to increase the torque density.

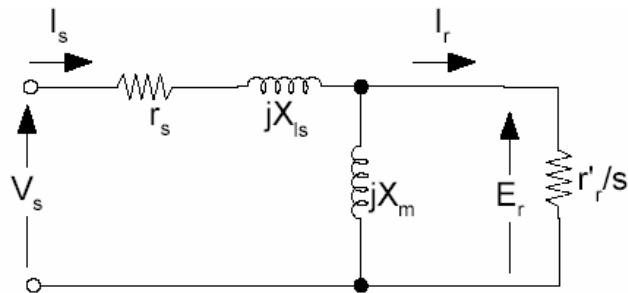


Figure 2.15 Induction machine approximated steady-state per phase equivalent circuit. Negligible rotor leakage inductance.

Rotor current can be calculated, for the approximated equivalent circuit as,

$$I_r = E_r s / r_r' \quad (2.107)$$

and the torque is,

$$T = (3/2) \frac{P}{2} E_r^2 s / r_r' \cdot \omega_e \quad (2.108)$$

The peak voltage is proportional to the peak air gap flux density by :

$$E_r = \omega_e \cdot (2/\pi) \cdot B_{\max} \cdot A_{\text{pole}} \cdot N_s \quad (2.109)$$

where  $B_{\max}$  is the peak flux density allowable for the full pitch, concentrated coil three-phase machine  $A_{\text{pole}}$  is the area of one magnetic pole and  $N_s$  is the number of series connected turns. The factor  $2/\pi$  express the average value of B in terms of the peak value.

In the case of the asymmetric six-phase machine, the maximum allowable fundamental flux density can be increased by 1,1547 as shown in the equation (2.104).

T is proportional to  $E_r^2$ , and  $E_r$  is directly proportional to B. Since all other parameters of torque equation remain the same for this machine, the increase in torque obtained by raising the fundamental component of flux density, while keeping the same peak tooth and air gap flux density is:

$$T_{6\text{-phase fund}} / T_{3\text{-phase}} = (1,1547)^2 = 1,33 \quad (2.110)$$

Thus, there is an addition of 33% in the torque production for the six-phase machine with third harmonic injection due to the increase in the fundamental flux. In addition to that, the contribution of the third harmonic component must be considered. Since the third harmonic circuit is a two-phase system (X0 and A0 zero sequence components) rather than a three-phase system, the factor 3/2 in the torque expression is absent.

However, the third harmonic component has three times the number of poles so that the factor 3 must be reintroduced. The torque produced by the third harmonic currents in the six-phase machine is:

$$T_{6\text{-phase}, 3h} = \frac{3P}{2} E_{r3h}^2 s_{3h} / r'_{r3h} \cdot 3\omega_e \quad (2.111)$$

The third harmonic voltage can be computed as:

$$E_{r3h} = 3\omega_e \cdot (2/\pi) \cdot B_3 \cdot \frac{A_{\text{pole}}}{3} \cdot \frac{3N_s}{3} = \omega_e \cdot (2/\pi) \cdot B_3 \cdot A_{\text{pole}} \cdot N_s \quad (2.112)$$

The additional factor of 3 is necessary since all of the three third harmonic poles having  $N_s/3$  turns each are, necessarily, connected in series so that the total number of series connected turns is again  $N_s$ . The third harmonic flux density is related to the fundamental component by

$$B_3 = 1,1547 \cdot \frac{1}{6} B_{\text{max}} \quad (2.113)$$

If we put this in (2.112), we get,

$$E_{r3h} = \frac{1,1547}{6} \cdot \omega_e \cdot (2/\pi) \cdot B_{\text{max}} \cdot A_{\text{pole}} \cdot N_s \quad (2.114)$$

The slip for the third harmonic which is identical to the slip corresponding to the fundamental spatial component is:

$$\begin{aligned} s_{3h} &= [3\omega_e - \frac{3P}{2} \omega_{rm}] / 3\omega_e \\ &= [\omega_e - \frac{P}{2} \omega_{rm}] / \omega_e \\ &= [\omega_e - \omega_{re}] / \omega_e \end{aligned} \quad (2.115)$$

where  $\omega_{rm}$  is the actual rotor mechanical speed,  $\omega_{re}$  is the electrical rotor speed and  $3P/2$  is the number of pole pairs of the third harmonic.



Finally, the rotor resistance as seen by the third harmonic of *mmf* must be computed. Rather than work out this expression from basic principles, it is easier to assume that the relationship will not be far different from the classical expressions for a squirrel cage machine.

In an induction machine, it can be assumed that the *mmfs* of the two sides of the equivalent circuit are equal if the magnetic permeance is taken as infinite [17]. That is,

$$F_1 = F_2 \quad (2.116)$$

$$\frac{0.9}{p} q_1 k_{w1} N_1 i_1' = \frac{0.9}{p} q_2 k_{w2} N_2 i_2'' \quad (2.117)$$

where  $q_1$  and  $q_2$  are number of phases,  $k_{w1}$  and  $k_{w2}$  are the winding factors,  $N_1$  and  $N_2$  are the turn numbers of the stator and rotor side respectively, and  $i_1'$  and  $i_2''$  are the currents transferred to the stator side.

If  $k_w$ s of the stator and rotor are taken as equal,

$$i_2'' = q_1 N_1 i_1' / q_2 N_2 \quad (2.118)$$

It can be assumed that the rotor consists of a winding with  $S_r / p$  phases and  $p/2$  turns [17]. When we substitute these values,

$$i_2'' = i_b = q_1 N_1 i_1' / [(S_r / p) (p/2)] \quad (2.119)$$

$$i_b / i_1' = 2 q_1 N_1 / S_r \quad (2.120)$$

where  $i_b$  is the current of a bar,  $S_r$  is the number of rotor slots and  $p$  is the number of magnetic poles.

On the other hand, the rotor copper loss of a  $q$  phase induction machine can be calculated from,

$$P_{r-Cu} = q \cdot i_1'^2 \cdot r_r' = S_r i_b^2 \cdot r_{be} \quad (2.121)$$

where  $r_{be}$  is the resistance of the rotor bar taking into account the effect of the end ring and  $r_r'$  is the rotor resistance transferred to the stator side.

$$r'_r = S_r i_b^2 \cdot r_{be} / q_1 \cdot i_1^2 \quad (2.122)$$

If we substitute equation (2.120) in (2.122),

$$r'_r = [2 q_1 N_1 / S_r]^2 \cdot S_r \cdot r_{be} / q_1 \quad (2.123)$$

$$r'_r = 4 q_1 N_1^2 r_{be} / S_r \quad (2.124)$$

Then for a three phase machine the secondary resistance for the fundamental component is,

$$r'_r = 12 N_1^2 r_{be} / S_r \quad (2.125)$$

and for the third harmonic component,

$$r'_{r3h} = \frac{3 \cdot 12 (N_s/3)^2 r_{be}}{S_r} \quad (2.126)$$

where  $N_s/3$  is the number of series connected turns of one of the three pairs of poles of the third harmonic. The factor of 3 is used since the three pole pairs of the third harmonic are connected in series. Inserting these expressions in (2.111),

$$\begin{aligned} T_{6\text{-phase, 3h}} &= \frac{3P}{2} \frac{[\omega_e \cdot (2/\pi) \cdot B_3 \cdot A_{\text{pole}} \cdot N_s]^2}{\omega_e^2 \cdot 12 \cdot N_s^2 \cdot r_{be}/S_r} \times [\omega_e - (P/2) \omega_{rm}] / \omega_e \\ &= \frac{3P}{2} \frac{[(1,1547/6) \cdot (2/\pi) \cdot B_{\text{max}} \cdot A_{\text{pole}}]^2}{12 \cdot r_{be}/S_r} \times [\omega_e - (P/2) \omega_{rm}] \quad (2.127) \end{aligned}$$

The corresponding torque expression for the baseline machine is:

$$\begin{aligned} T_{3\text{-phase}} &= \frac{3P}{2 \cdot 2} \frac{[\omega_e \cdot (2/\pi) \cdot B_{\text{max}} \cdot A_{\text{pole}} \cdot N_s]^2}{\omega_e^2 \cdot 12 \cdot N_s^2 \cdot r_{be}/S_r} \times [\omega_e - (P/2) \omega_{rm}] \\ &= \frac{3P}{2 \cdot 2} \frac{[(2/\pi) \cdot B_{\text{max}} \cdot A_{\text{pole}}]^2}{12 \cdot r_{be}/S_r} \times [\omega_e - (P/2) \omega_{rm}] \quad (2.128) \end{aligned}$$

Taking the ratio (2.127) / (2.128),

$$\frac{T_{6\text{-phase, 3h}}}{T_{3\text{phase}}} = \frac{(1,1547/6)}{\frac{1}{2}} = 0.0741 \quad (2.129)$$

Hence, the contribution of the third harmonic is 7.4% of the value produced by the baseline machine. The total torque improvement is thus from (2.110) and (2.129),

$$\frac{T_{6\text{-phase, fund}} + T_{6\text{-phase, 3h}} - T_{3\text{-phase}}}{T_{3\text{-phase}}} 100\% = 0,33 + 0,0741 = 40,7 \% \quad (2.130)$$

Therefore, a 40% torque improvement is obtained in the six-phase induction machine with 3<sup>rd</sup> harmonic injection compared to the three-phase machine.

The ground rule for this analysis was the air gap flux density, and consequently the tooth flux density, should be held constant. Nothing has been said about the core flux density. The flux in the core is essentially the integral of the flux in the air gap so that,

$$A_{\text{core}} \cdot B_{\text{core}} = A_g \int B_g d\Phi \quad (2.131)$$

If we substitute the value of  $B_g$  from (2.104),

$$\begin{aligned} B_{\text{core}} &= \frac{A_g}{A_{\text{core}}} \int 1,1547 \cdot B_{\text{max}} \left[ \sin\Phi + \frac{1}{6} \sin 3\Phi \right] d\Phi \\ &= - \frac{A_g}{A_{\text{core}}} 1,1547 \cdot B_{\text{max}} \left[ \cos\Phi + \frac{1}{18} \cos 3\Phi \right] \end{aligned} \quad (2.132)$$

The maximum function is clearly the point  $\Phi = 0$  at which

$$B_{\text{core, max}} = - \frac{A_g}{A_{\text{core}}} 1,1547 \cdot B_{\text{max}} \frac{19}{18} \quad (2.133)$$

For the baseline machine, the air gap flux is:

$$B_{g \text{ 3-phase}} = B_{\text{max}} \sin\Phi \quad (2.134)$$

and, with the similar analysis, the core flux is:

$$B_{\text{core, 3-phase}} = - \frac{A_g}{A_{\text{core}}} \cdot B_{\text{max}} \cos\Phi \quad (2.135)$$

that gives for maximum,

$$B_{\text{core, 3-phase max}} = - \frac{A_g}{A_{\text{core}}} \cdot B_{\text{max}} \quad (2.136)$$

The core flux increase with the third harmonic injection is, then

$$\frac{B_{\text{core, max}} - B_{\text{core, 3-phase max}}}{B_{\text{core, 3-phase max}}} 100\% = 22\% \quad (2.137)$$

To accommodate the additional flux in the core, if no saturation is not acceptable, the core cross section area have to be increased what could be impossible in some applications. Alternatively, the core peak flux can be reduced by reducing the peak air gap flux. However, doing that causes the gain in torque to reduce accordingly and it is important to quantify this reduction. Assuming a reduction in the peak air gap by a factor  $k$ , equations (2.110) and (2.129) are corrected to be,

$$\frac{T_{6\text{-phase fund}}}{T_{3\text{-phase}}} = (k \cdot 1,1547)^2 = 1,33 k^2 \quad (2.138)$$

$$\frac{T_{6\text{-phase, 3h}}}{T_{3\text{-phase}}} = 0,0741 \cdot k^2 \quad (2.139)$$

Therefore the total torque gain is now a function of  $k$

$$\frac{T_{6\text{-phase.fund}} + T_{6\text{-phase.3h}} - T_{3\text{-phase}}}{T_{3\text{-phase}}} 100\% = (1,407 \cdot k^2 - 1) 100\% \quad (2.140)$$

The torque gain for third harmonic injection considering the air gap flux reduction for accommodating the core flux is plotted in Figure 2.16. It is clear that for  $k < 0,845$  the torque is indeed reduced with the third harmonic application. Therefore a trade-off between the core cross-section and the reduction in the air gap flux must be obtained to guarantee the increase in the machine torque.

If no flux increase in the core is acceptable, the peak air gap flux density has to be set to a value that keeps the core peak flux in equation (2.133) equal to the core peak flux for the three-phase machine in equation (2.136). Therefore the peak fundamental flux has to be reduced by a factor of

$$\mathbf{k}_\Phi = \frac{18}{19 \times 1,1547} = 0,8204 \quad (2.141)$$

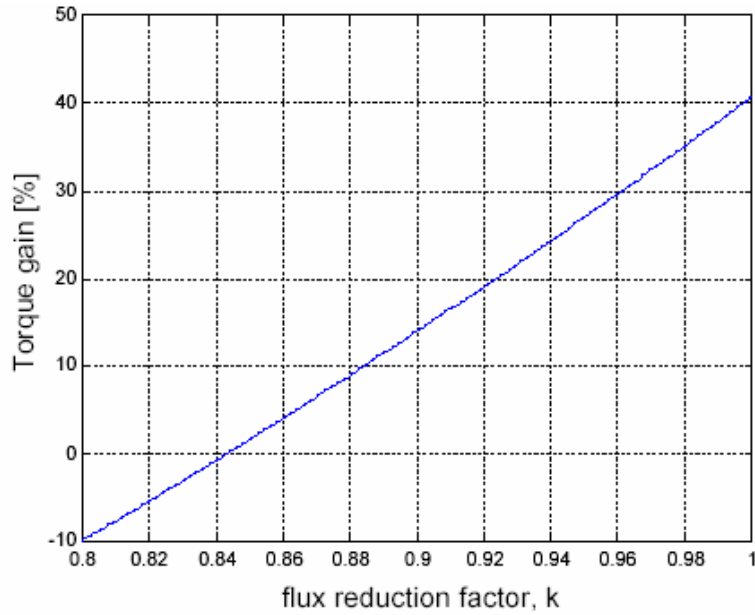


Figure 2.16 Torque gain in an asymmetric six-phase machine with third harmonic injection considering reduction in the air gap flux to accommodate the core flux.

The air gap flux is obtained using (2.104) and applying the reduction factor  $\mathbf{k}_\Phi$  to be,

$$B_g = \mathbf{k}_\Phi \cdot 1,1547 \cdot B_{g\max} \left( \sin\Phi + \frac{1}{6} \sin 3\Phi \right) \quad (2.142)$$

$$B_g = \frac{18}{19} \cdot B_{g\max} \left( \sin\Phi + \frac{1}{6} \sin 3\Phi \right) \quad (2.143)$$

Note that the ratio between fundamental and third harmonic is the same as in the previous case since the optimization is not a function of  $B_{\max}$ . Figure 2.17 shows the new airgap flux distribution. Both air gap peak flux and fundamental peak flux decrease as a result of a fixed core peak flux. From Equation (2.140) with  $\mathbf{k} = \mathbf{k}_\Phi = 0.8204$  and the total gain is - 5.26 %. Therefore, there is in fact a reduction in the torque production if the core flux has to be limited to the corresponding three-phase machine value.

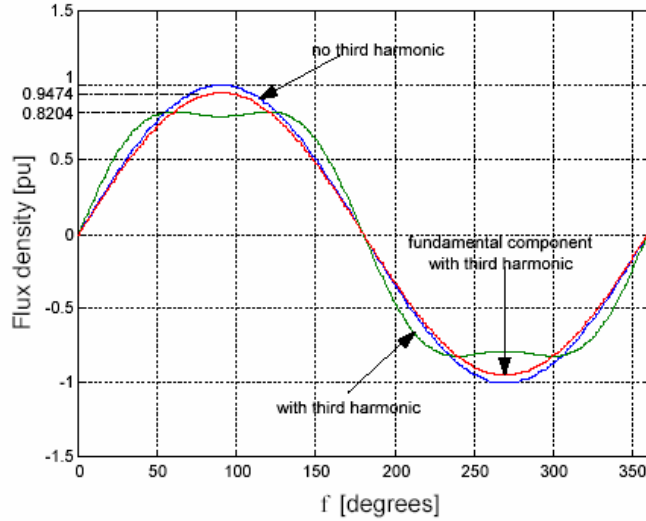


Figure 2.17 Flux density distribution for same peak core flux with and without third harmonic injection.

On the other hand, since the peak air gap flux decreases, there is an additional opportunity for torque density increase. With this lower flux density, the stator tooth width can be made accordingly smaller still preserving the iron flux levels. Therefore, stator slots can be made bigger and would accommodate more copper making the current density to increase. Torque improvement is obtained from the increase in the current density for a similar air gap flux. For a flux reduction factor  $k$ , the stator tooth width is reduced by the same factor. The increase in the stator slot width is a function of the initial relation between stator tooth and slot widths. Figure 2.18 shows a simplified representation of a stator tooth and slot where  $\tau_s$  is the slot pitch,  $t_0$  is the tooth width and  $b_0$  is the slot width.

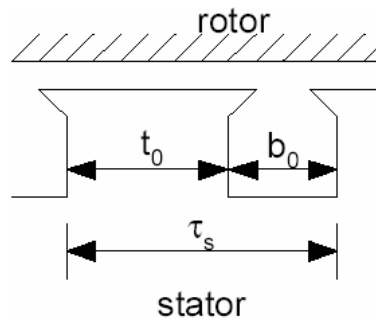


Figure 2.18 Simplified representation of stator slot and tooth.

The tooth width and the slot width are related to the slot pitch by

$$t_0 = \gamma \tau_s \text{ and } b_0 = (1 - \gamma) \tau_s \quad (2.144)$$

such that,

$$t_0 + b_0 = \tau_s \quad (2.145)$$

and  $\gamma$  is a coefficient that could assume any value between 0 and 1. For a constant slot pitch, when a reduction factor  $k$  is applied to the stator tooth the slot pitch is given by,

$$\tau_s = \tau_0' + b_0' = k \gamma \tau_s + b_0' \quad (2.146)$$

and substituting  $\tau_s$  the new value for the slot width as a function of the reduction factor  $k$ , the tooth width factor  $\gamma$  and the previous slot width is,

$$b_0' = \frac{1 - k\gamma}{1 - \gamma} b_0 \quad (2.147)$$

Using the values  $\gamma = 0,5$  and  $k = 0,8204$  there is an increase of 18% in the slot width. In Figure 2.19, a graphical representation of slot width increase where the variation of the percentage increase in the slot width is plotted as a function of the initial tooth width coefficient for different tooth reduction factors  $k$ . The bigger the initial tooth width, the bigger the impact on the slot increase for a fixed reduction factor.

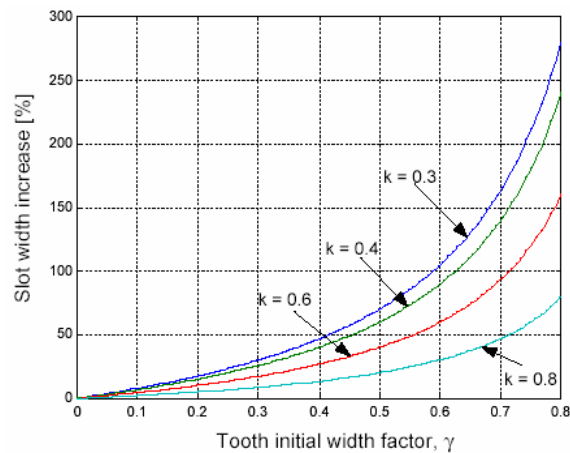


Figure 2.19 Percentage variation on slot width as a function of initial tooth width for different tooth reduction factors.

From [13], the output torque for an ac machine can be expressed as,

$$T_{3\text{-phase}} = \frac{\sqrt{2} \pi^2 k_1 (D_{is}^2 L_s) B_{g1} J_{s,rms} \eta_{gap} \cos(\Phi_{gap})}{120} \quad (2.148)$$

where  $k_1$  is the winding factor,  $D_{is}$  is the stator inner diameter,  $L_s$  is the stator length,  $B_{g1}$  is the peak fundamental air gap flux density,  $J_{s,rms}$  is the rms current per unit length of the stator circumference or surface current density,  $\eta_{gap}$  is the efficiency as seen from the air gap that includes rotor iron and copper loss and stray losses, and  $\Phi_{gap}$  is the power factor at the gap of the machine.

The increase in the slot width  $b_0'$  allows the increase on the surface current density  $J_{s,rms}$  by the same factor. Considering the reduction on the fundamental flux density caused by the necessity of keeping the peak core flux equal as the baseline machine, the torque for the six-phase machine when the tooth reduction is applied is given by,

$$T_{6\text{-phase,slot}} = \frac{\sqrt{2} \pi^2 k_1 (D_{is}^2 l_s)}{120} \frac{18 B_{g1}}{19} \frac{1-k\gamma}{1-\gamma} J_{s,rms} \eta_{gap} \cos(\Phi_{gap}) \quad (2.149)$$

so the torque increase is given by,

$$\frac{T_{6\text{-phase, slot}}}{T_{3\text{-phase}}} = \frac{18}{19} \frac{1-k\gamma}{1-\gamma} \quad (2.150)$$

Again for  $\gamma = 0,5$  and  $k = 0,8204$  the torque improvement due to the increase in the surface current density is 12%. Including all effects, for the six-phase machine with third harmonic injection, the torque gain is given as a function of the flux reduction factor  $k$  as,

$$\%Gain = [(1,407 \times k^2 - 1) + \frac{18}{19} \frac{1-k\gamma}{1-\gamma} - 1] 100\% \quad (2.151)$$

The percentage torque gain as a function of the flux reduction factor for different initial tooth factors  $\gamma$ , is shown in Figure 2.20. The bigger the initial tooth factor, the bigger the increase in the torque density. For keeping the peak core flux as the baseline machine, the flux reduction factor has to be kept as  $k = 0,8204$ . As an example, with this value for  $k$  and for  $\gamma = 0,6$  a torque improvement of 15% can be achieved.



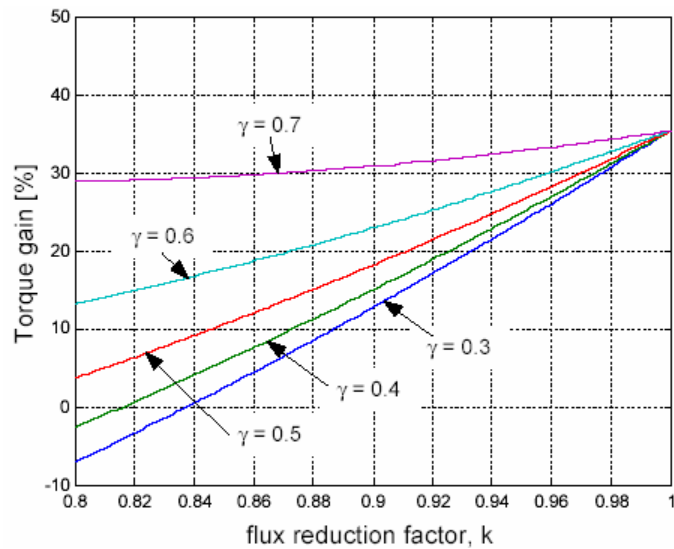


Figure 2.20 Torque gain in an asymmetric six-phase machine with third harmonic injection considering reduction in the air gap flux to accommodate the core flux and increase in the surface current density.

As a result, the use of third harmonic current injection in an asymmetric six-phase machine can contribute to an increase of up to 40% in the torque production. This is a very significant improvement and it is proper to add up the pros, cons and restrictions of this approach.

To begin with, the machine efficiency is not expected to be significantly affected since a corresponding increase in the stator and rotor current must accompany the increased fundamental component of flux density plus the third harmonic.

The main disadvantage of this type of connection is the number of cables. A six-phase stator must be fed by seven cables, six phases plus neutral, compared to three for the three-phase machine. The amount of copper in the seven cables will equal the amount in the four three-phase cables but, more insulation will be needed and so that the overall weight of the cables will increase. This must be traded-off versus the 40% weight reduction that will be possible by the asymmetrical six-phase design.

The zero rotor leakage inductance assumption is convenient since it allowed the voltage impressed across the air gap, produced by the air gap flux, to be equated to the voltage across the rotor resistor. The derivation simplified considerably by using this assumption. If the secondary leakage is considerably high, the voltage across the leakage inductance has to be calculated. A voltage drop across this leakage inductance would mean that the voltage across the rotor resistor would be reduced, decreasing the 40% gain that has been cited.

Lastly, the maximum core flux is shown to increase by 22%. If no saturation is acceptable then the air gap flux density has to be reduced by 22% which reduces the torque below the three-phase machine. Instead, the core area cross section can be increased by 22% to accommodate the increase in core flux. A trade-off between air gap flux and core cross section area must be done to obtain the optimum machine design for each particular application. An analysis of stator core losses has to be conducted to evaluate the actual impact of the increased core peak flux. Although peak flux increases, the distribution has a peaked up waveform and only a portion of the core will be under higher flux densities. If no flux increase in the core is acceptable, the peak air gap flux has to be reduced and with this, stator teeth are made thinner without increasing the iron losses. Therefore additional copper is used to increase the torque density. Torque improvement of 15%, without compromising core flux levels, can be expected with this technique.

### **2.3.7 Experimental setup**

This subsection describes the experimental setup that was built in [1] to test the proposed technique for increasing the torque density in the induction machine.

Figure 2.21 shows the machine test setup composed of the machine under test, a six-phase induction machine, a torque and speed transducer, a permanent magnet machine used as load or driving unit, and a digital encoder. The PM machine was connected in the generator mode through a diode bridge to an adjustable resistive load that guarantees evenly distribution of load currents in its windings. In the motor mode, a commercial voltage inverter was used to drive the PM machine.

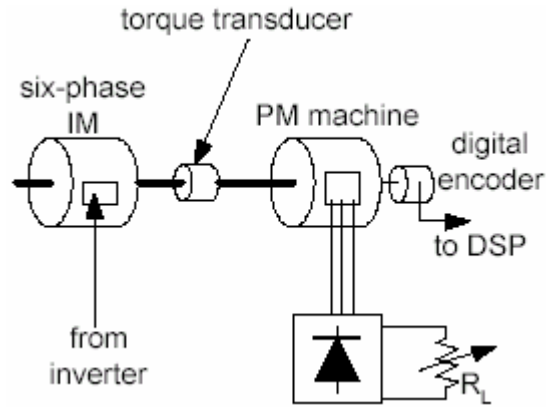


Figure 2.21 Test setup.

The operation in motor mode for the PM machine is necessary when testing the induction machine at no load, where the rotor has to be spun at synchronous speed.

A digital encoder was used for speed measurement. The control was implemented in a Digital Signal Processing board.

Two machines were tested in the experiments, the six-phase machine and the three-phase baseline machine. Since a standard three-phase machine frame was used in the new machine design, an equally rated three-phase machine was used as a baseline for comparing the results obtained and to validate the expected improvement. Two different rotors were used, the standard squirrel cage rotor and a specially prepared rotor without the rotor bar ending connections that was used in no-load tests and magnetic losses evaluation.

The airgap flux was measured using a search coil installed in the machine. The objective of the flux measurement in this system was to demonstrate the reshape of the air gap flux by injecting third harmonic currents and to determine the ratio between the fundamental and third harmonic flux components.

Torque was measured using a torque sensor connected directly to the machine shaft. The torque sensor is composed of a strain gage torquemeter and a transducer amplifier.

A six-phase power inverter using IGBT switches was built to test the six-phase machine. Figure 2.22 shows the diagram of the power system. The dc bus was fed directly from the ac mains through a variac and a diode bridge. A middle point connection was provided in the dc bus to return the neutral connection of the machine.

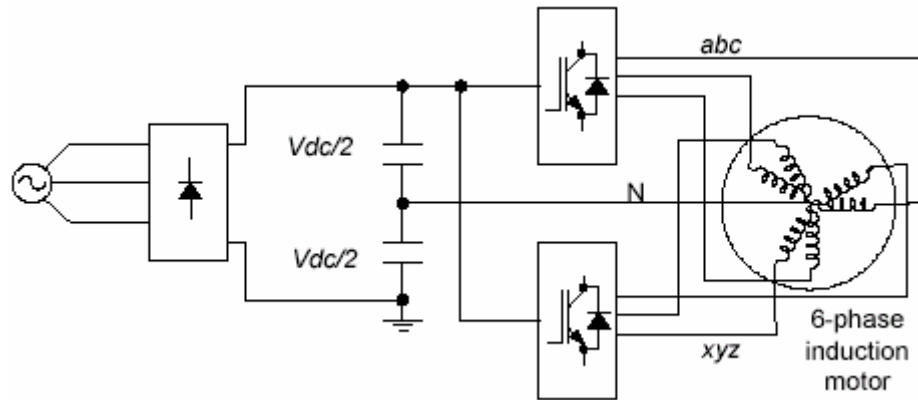


Figure 2.22 Power converter system used in the experiment.

### 2.3.8 Experimental evaluation of the six-phase system

In [1], the system described in the previous subsection was tested to verify the improvement in the torque production and to address the necessary operating conditions for both machine and power converter.

The basic operation was tested using an open loop voltage source inverter with the ability of adjusting both phase delay between the two three-phase groups A and X, and fundamental to third harmonic phase relation. As expected for the three-phase machine under balanced operation, the air gap flux was mainly composed of a fundamental component with all harmonics negligible. At this condition the machine operates with a peak flux density of  $B_{gpeak} = 0.84$  T.

To obtain the proposed torque improvement in the six-phase motor system, it is important to keep the correct phase relation between fundamental and third harmonic flux distributions. Failure to do so could cause misshaping of the magnetic flux and therefore unwanted iron saturation.

Regarding the third harmonic currents, the six-phase machine behaves like a two-phase machine with each three-phase group being one of the phases of the third harmonic machine. At no-load, the machine can be driven only by applying the third harmonic currents. However, the flux level in the machine with only third harmonic currents remains quite low, what causes high currents to flow.

For no-load, the process of increasing the fundamental flux of the machine is demonstrated in Figure 2.23, Figure 2.24, Figure 2.25. First operating without third harmonic at  $f = 40$  Hz and  $V_s = 84$  V the peak air gap flux density is  $B_{gpeak} = 0.84$  T (Figure 2.23). It can be seen that groups A and X currents are 30 degrees phase shifted from each other as necessary for the proposed machine operation.

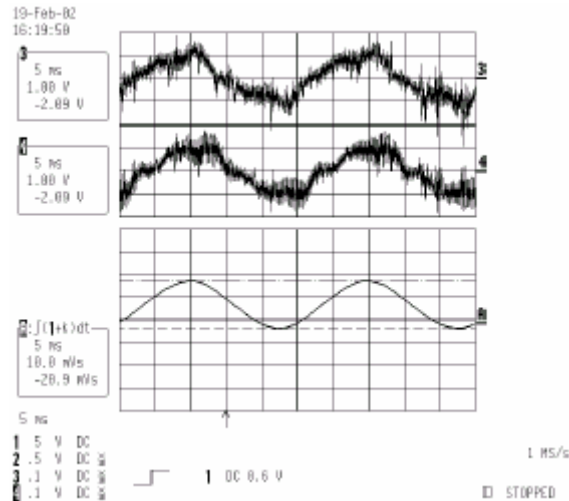


Figure 2.23 No-load operation of the six-phase machine without third harmonic injection.  $f = 40$  Hz,  $V_s = 84$  V, Trace A: Flux density distribution [0.788T/div]; Trace 3: Phase a current [3.125A/div]; Trace 4: Phase x current [3.125A/div].

Adding third harmonic currents causes the peak flux density to decrease as seen in Figure 2.24 where a third harmonic voltage of  $V_{s3h} = 14$  V was added and the peak flux density reduces to  $B_{gpeak} = 0.74$  T. This corresponds to a sub-utilization of the machine iron when compared to the previous case.

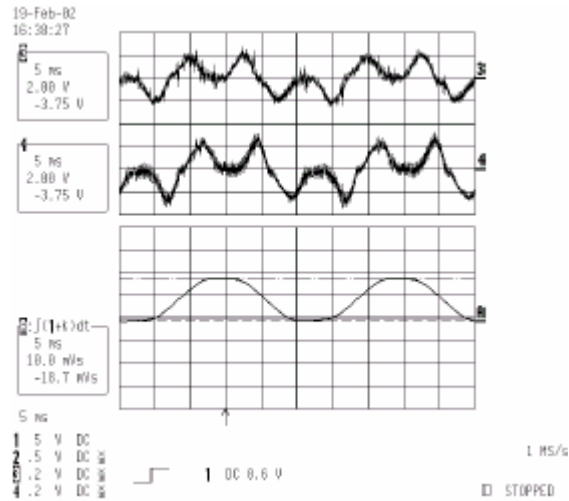


Figure 2.24 No-load operation of the six-phase machine with third harmonic injection.  $f = 40$  Hz,  $V_s = 84$  V,  $V_{s3h} = 14$  V, Trace A: Flux density distribution [0.788T/div]; Trace 3: Phase a current [6.25A/div]; Trace 4: Phase x current [6.25A/div].

In order to raise the peak flux again, the fundamental voltage could be increased until the previous level of flux was reached. This is shown in Figure 2.25 where for the same third harmonic voltage, the fundamental voltage was raised to  $V_s = 93$  V and the peak flux density is again  $B_{gpeak} = 0.82$  T.

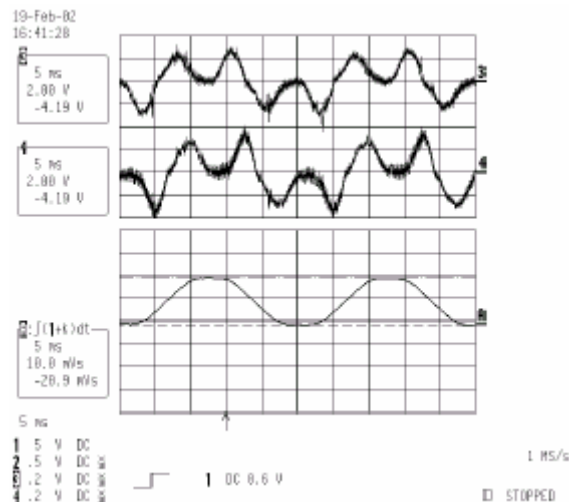


Figure 2.25 No-load operation of the six-phase machine with third harmonic injection.  $f = 40$  Hz,  $V_s = 93$  V,  $V_{s3h} = 14$  V, Trace A: Flux density distribution [0.788T/div]; Trace 3: Phase a current [6.25A/div]; Trace 4: Phase x current [6.25A/div].

For loaded case a similar operation can be seen as in Figure 2.26, Figure 2.27, Figure 2.28. For a load with  $T_l = 5\text{Nm}$ ; with no third harmonic injection, phase voltages are  $V_s = 80\text{ V}$ . A third harmonic voltage of  $V_{s3h} = 14\text{ V}$  was then added. Finally, the fundamental voltage component was raised to  $V_s = 89\text{ V}$ .

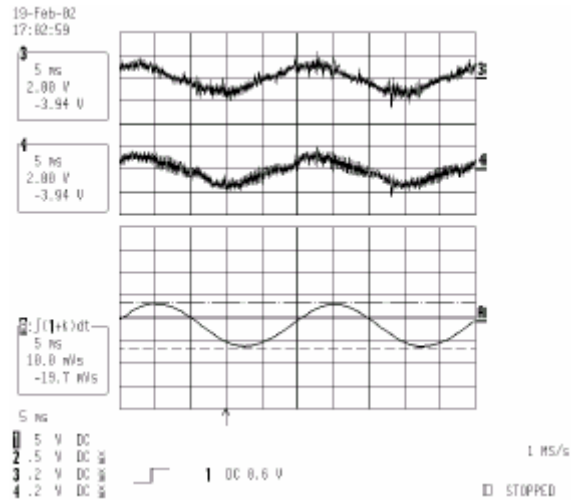


Figure 2.26 Operation of the six-phase machine without third harmonic injection.  $T_l = 5\text{ Nm}$ ,  $f = 40\text{ Hz}$ ,  $V_s = 80\text{ V}$ , Trace A: Flux density distribution [0.788T/div]; Trace 3: Phase a current [6.25A/div]; Trace 4: Phase x current [6.25A/div].

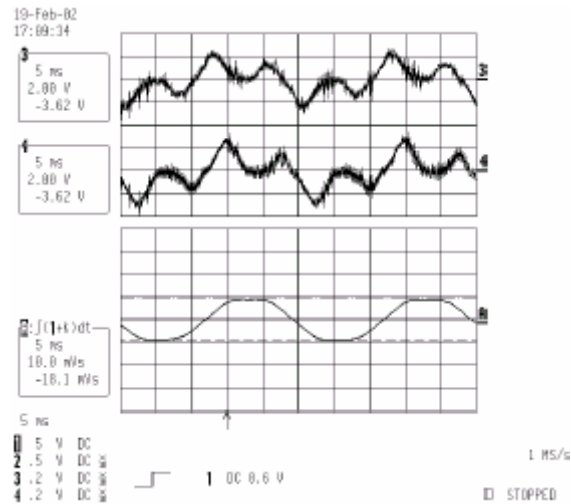


Figure 2.27 Operation of the six-phase machine with third harmonic injection.  $T_l = 5\text{ Nm}$ ,  $f = 40\text{ Hz}$ ,  $V_s = 80\text{ V}$ ,  $V_{s3h} = 14\text{ V}$ , Trace A: Flux density distribution [0.788T/div]; Trace 3: Phase a current [6.25A/div]; Trace 4: Phase x current [6.25A/div].

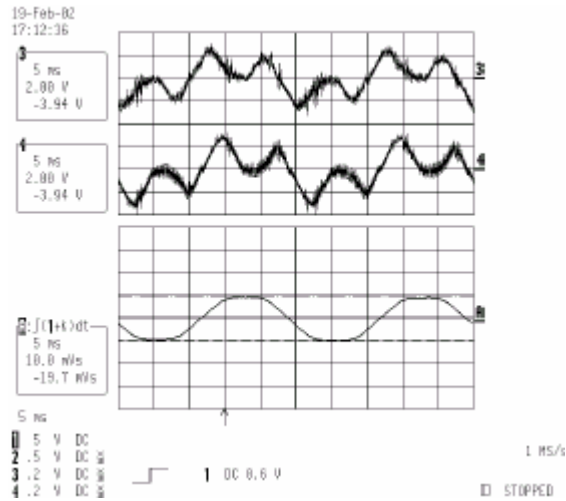
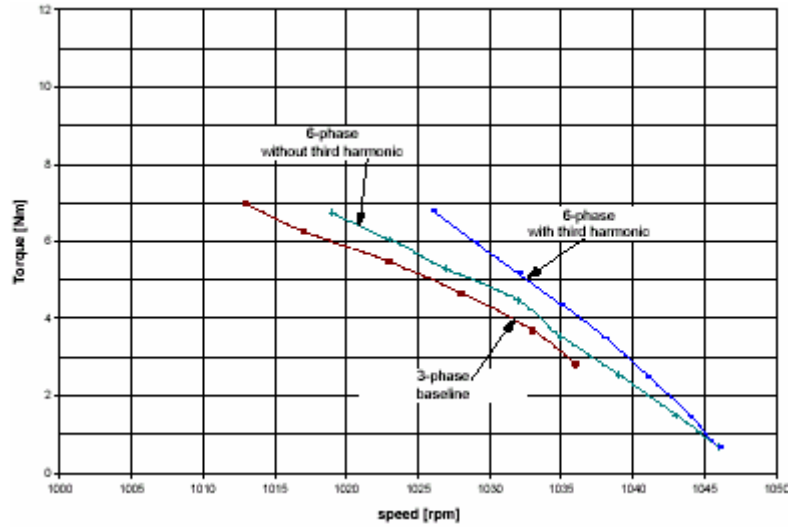


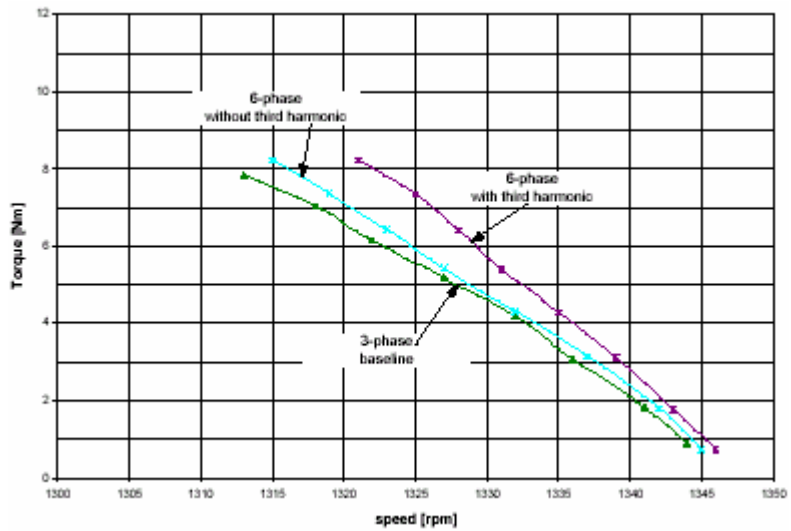
Figure 2.28 Operation of the six-phase machine with third harmonic injection.  $T_l = 5 \text{ Nm}$ ,  $f = 40 \text{ Hz}$ ,  $V_s = 89 \text{ V}$ ,  $V_{s3h} = 14 \text{ V}$ , Trace A: Flux density distribution [0.788T/div]; Trace 3: Phase a current [6.25A/div]; Trace 4: Phase x current [6.25A/div].

The torque x speed characteristics for the six-phase machine was measured experimentally and compared to the three-phase machine. Two cases were analyzed, the machine was tested with and without injection of third harmonic currents. The test was done for three different operating frequencies keeping the peak flux density constant. Figure 2.29 shows the torque x speed curves for 45 Hz and 35 Hz. The increase in the torque production for the same size machine can be seen clearly. At different operating frequencies, the six-phase machine presents better torque production noted by a lower speed variation for the mechanical torque application.





(a) 35 Hz.



(b) 45 Hz.

Figure 2.29 Torque x speed characteristics for 3hp six-phase machine. Six-phase machine operating with and without third harmonic currents compared to the baseline three phase machine.

Figure 2.30 shows the percentage torque improvement when compared to the three-phase baseline machine torque at a particular value of slip. Since the amount of third harmonic currents injected as well as the increase in the fundamental component was not similar in the tests for the two frequencies, the improvement was different. However, in both cases, the torque improvement when compared to the three-phase baseline machine is clear. At very low slip, close to no-load operation, the results for torque increase are not reliable since torque measurement at very low values is not accurate. Therefore, to quantify the percentage torque gain, one should take the value at slip close to the rated value. This does not mean that there was no improvement at low load conditions, but states a limitation on the torque measurement system.

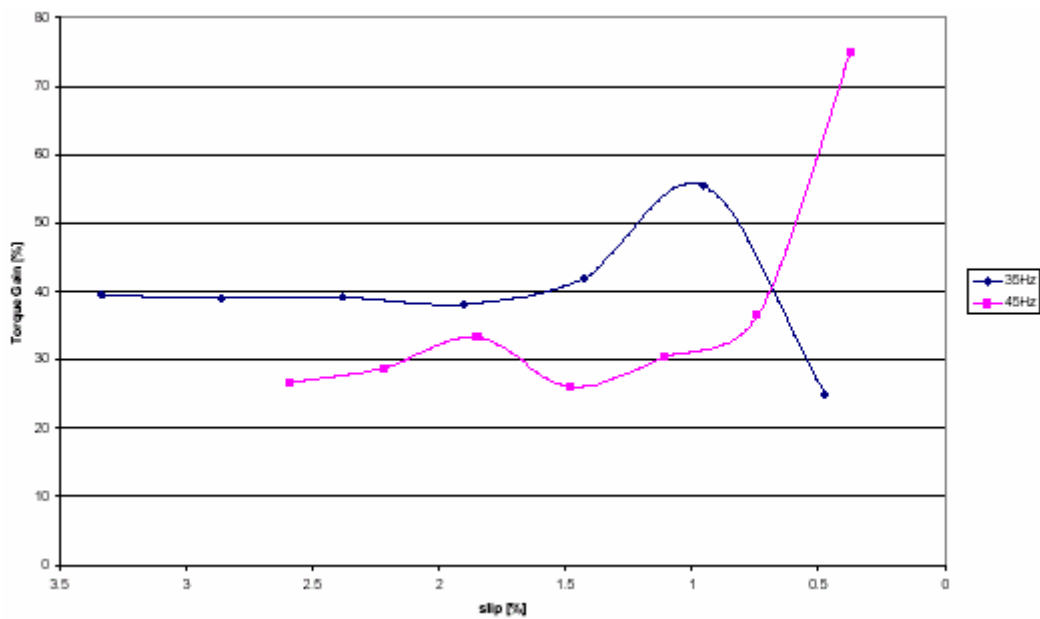


*Figure 2.30 Percentage torque gain, as a function of slip, for the 3hp six-phase machine compared to the baseline three-phase machine for operation with third harmonic current injection.*

Iron and copper losses were addressed through the measurement at different operating frequencies. Improvement in the torque production in the six-phase induction machine with third-harmonic current injection was obtained by increasing the fundamental flux without increasing the peak flux in the machine.

The extra output power comes from an increase in the stator current and the reshaping of the magnetic flux distribution. These two factors have an important impact in the machine magnetic and copper losses and an assessment of those losses is important in validating the proposed drive system.

Both iron and copper losses were measured experimentally for no-load operation and the results were compared to the measurement in the baseline three-phase machine.

Iron losses were measured in the machine operating at no-load and at different frequencies. For a better measurement of the magnetic losses, the machine has to be driven at synchronous speed and therefore zero slip. This guarantees that no currents flow in the rotor circuit for the fundamental component. However, due to the presence of harmonics in the real machine, simply driving the machine at its synchronous speed does not guarantee zero currents in the rotor circuit.

By cutting the rotor end windings and therefore increasing the rotor resistance a drastic reduction in the rotor currents was obtained. The same machine, now with a rotor lacking of end windings, was driven mechanically at synchronous speed and the input power is measured. Magnetic power losses are obtained by subtracting the stator copper losses from the measured power.

Iron losses as a function of the peak air gap flux density were measured at 20, 30 and 40Hz and Figure 2.31, Figure 2.32, Figure 2.33 show the results obtained. For the three operating frequencies, the magnetic losses for the six-phase machine do not increase significantly when compared to the baseline three-phase machine up to approximately 0.8T peak flux density. Since the machine is designed to operate under this value, no great impact in the iron losses is expected.

The small increase in the iron losses for the six-phase machine is caused by the increase in the  $dB/dt$  of the flux density distribution. However, when comparing the operation of the six-phase machine to the three-phase one, one have to keep in mind that the six-phase machine operates with lower peak flux density than the three-phase one and therefore, the iron loss remains approximately equal.

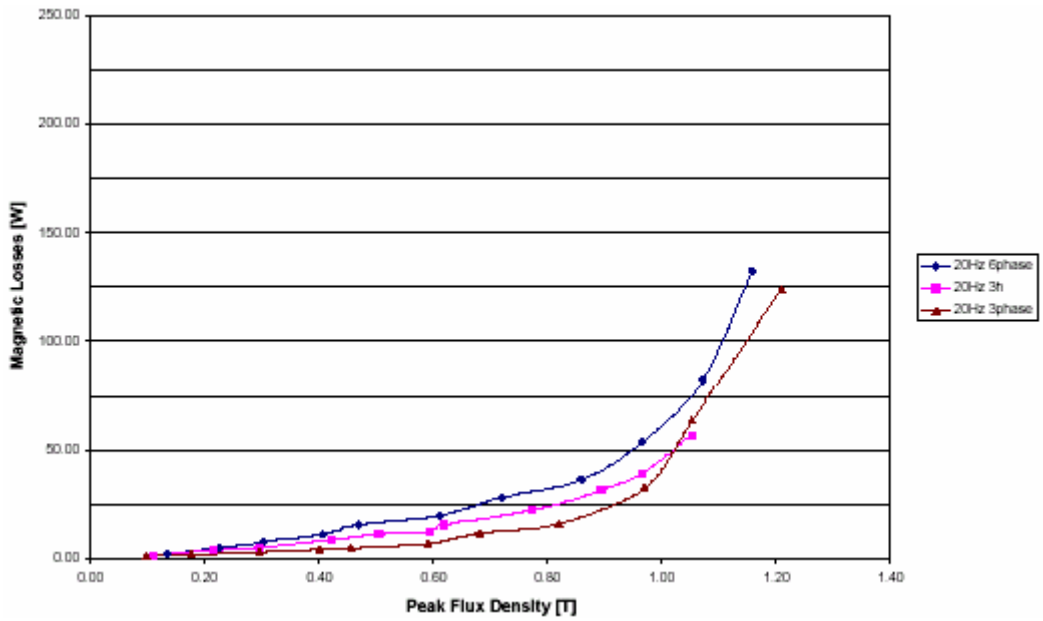


Figure 2.31 Magnetic losses at 20Hz. Comparison between the 3hp( $P_r=746\text{ W}$ ) six-phase machine with and without third harmonic injection and the baseline three-phase machine.

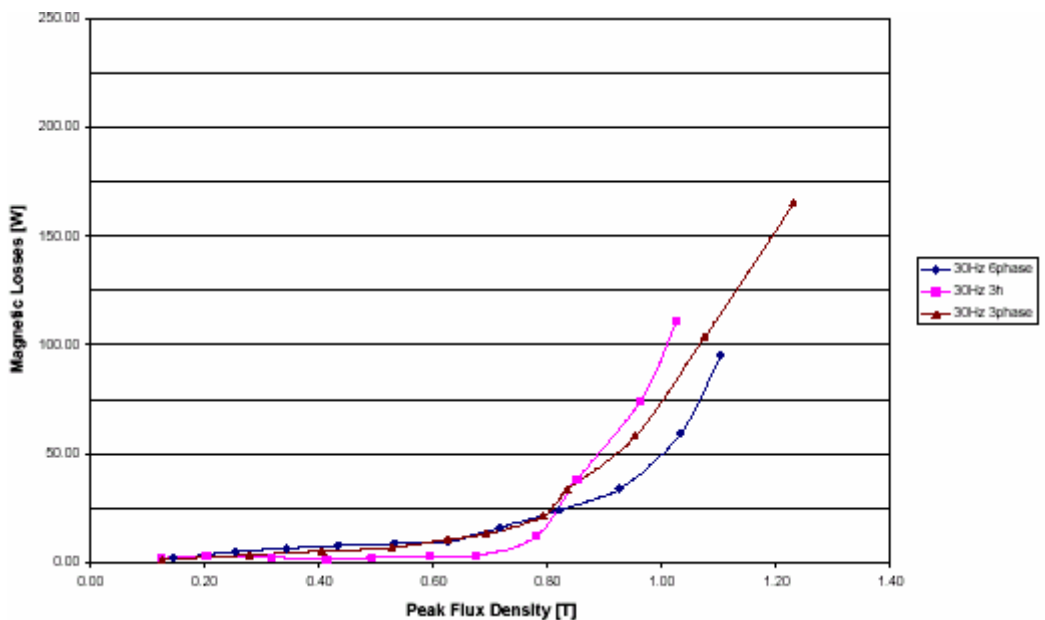


Figure 2.32 Magnetic losses at 30Hz. Comparison between the 3hp ( $P_r = 1,119\text{ W}$ ) six-phase machine with and without third harmonic injection and the baseline three-phase machine.

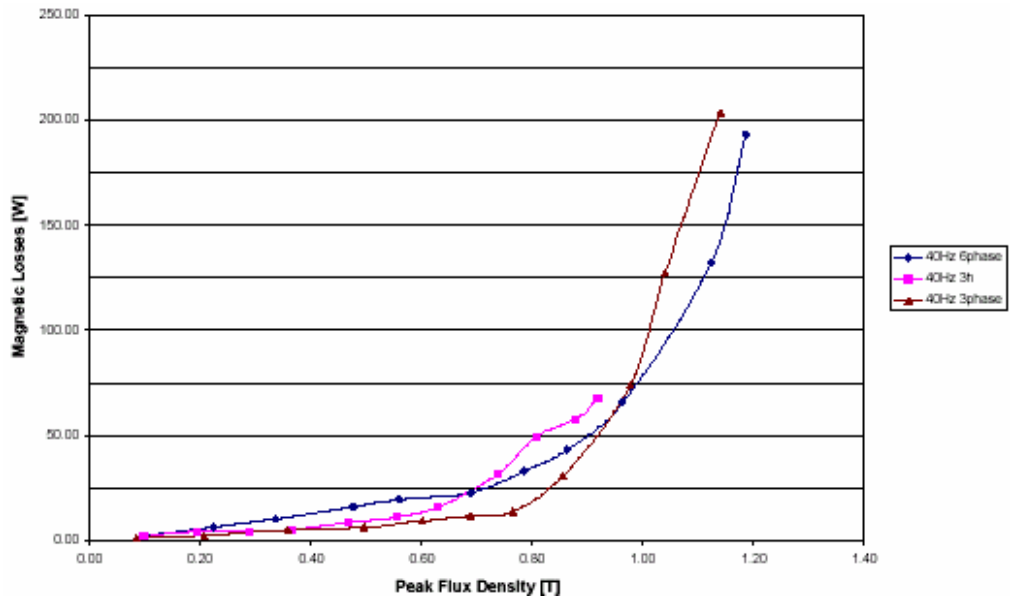


Figure 2.33 Magnetic losses at 40Hz. Comparison between the 3hp ( $P_r=1,492\text{ W}$ ) six-phase machine with and without third harmonic injection and the baseline three-phase machine.

Another important class of power loss is copper losses. They are basically composed by stator and rotor resistive losses. At no-load, only the stator copper losses were measured and compared to the baseline three-phase machine. This is not a problem since both machines use the same rotor structure and are rated at the same power level. Therefore, the rotor losses are expected to be similar for the two machines being the stator losses the one that differentiate their operation.

Stator copper losses as a function of the peak air gap flux density were measured for no-load at different operating frequencies. Figure 2.34, Figure 2.35, Figure 2.36 show the comparison of stator copper losses with the baseline three-phase machine for operation at 20, 30 and 40Hz respectively. The six-phase machine operating without third harmonic current injection behaves similarly to the three-phase machine. With the injection of third harmonic currents, the copper losses increase in the three frequencies. However, for peak flux levels up to 0.8T, there is not a significant increase in the losses. It is important to remember that these measurements were performed in a 3hp machine. Since the higher the rated power, the lower the stator resistance, the increase in the copper losses for a high power level induction machine presents no significant problem.

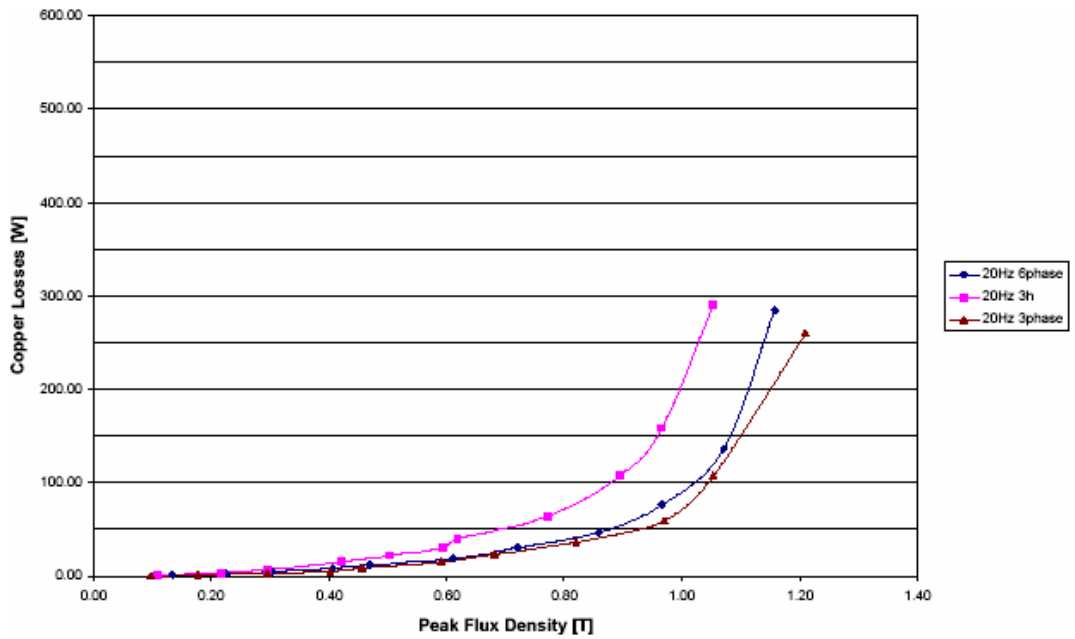


Figure 2.34 Stator copper losses at 20 Hz. Comparison between the 3hp ( $P_r=746$  W) six-phase machine with and without third harmonic injection and the baseline three-phase machine.

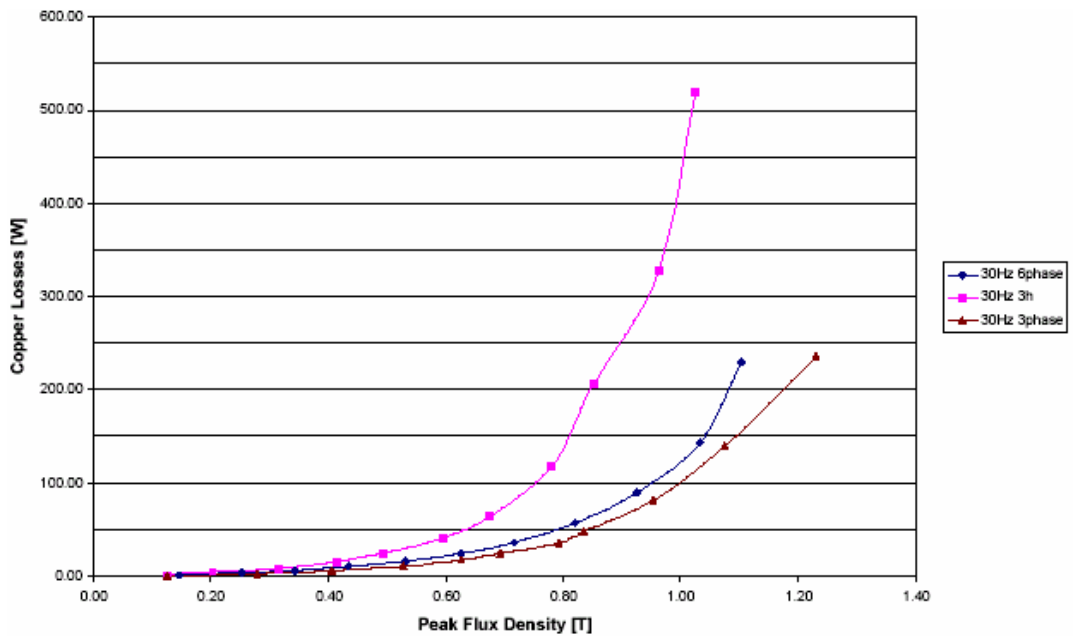


Figure 2.35 Stator copper losses at 30 Hz. Comparison between the 3hp ( $P_r=1,119$  W) six-phase machine with and without third harmonic injection and the baseline three-phase machine.

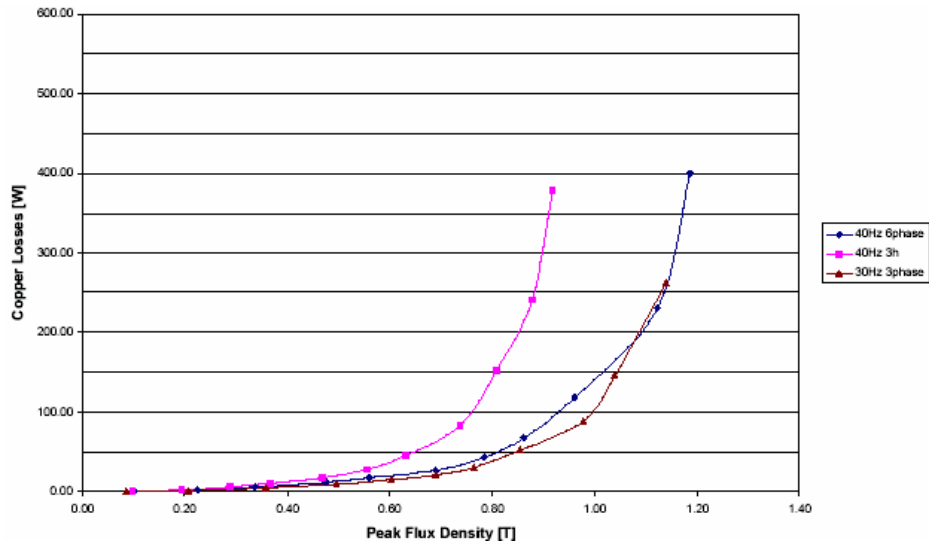


Figure 2.36 Stator copper losses at 40 Hz. Comparison between the 3hp ( $P_r=1,492$  W) six-phase machine with and without third harmonic injection and the baseline three-phase machine.

The basic effect of the increased copper losses is a reduction on the machine efficiency. For a fixed frequency, the efficiency of the machine is measured for different load conditions. Efficiency of the three-phase machine, as the relation between input electrical power and output mechanical power, was tested at different frequencies. The efficiency seem to increase with the electric frequency, as expected since the baseline machine is designed to operate at 60Hz. The six-phase machine efficiency was measured for both cases, without and with third harmonic injection. For 35 Hz voltage supply frequency, Figure 2.37 shows the comparison between the six-phase machine efficiency and the baseline machine. Without third harmonic injection, the six-phase machine presents an efficiency close to the baseline machine.

On the other hand, the efficiency drops considerably when third harmonic currents were injected for light load condition. This occurs at any supply frequency as can be seen in Figure 2.38 where a similar test was done for 45Hz power supply. For higher mechanical load, the efficiency of the six-phase machine with the third harmonic current injection is comparable to the baseline machine, getting eventually better as the load torque increases beyond rated value and the efficiency of the baseline machine drops.

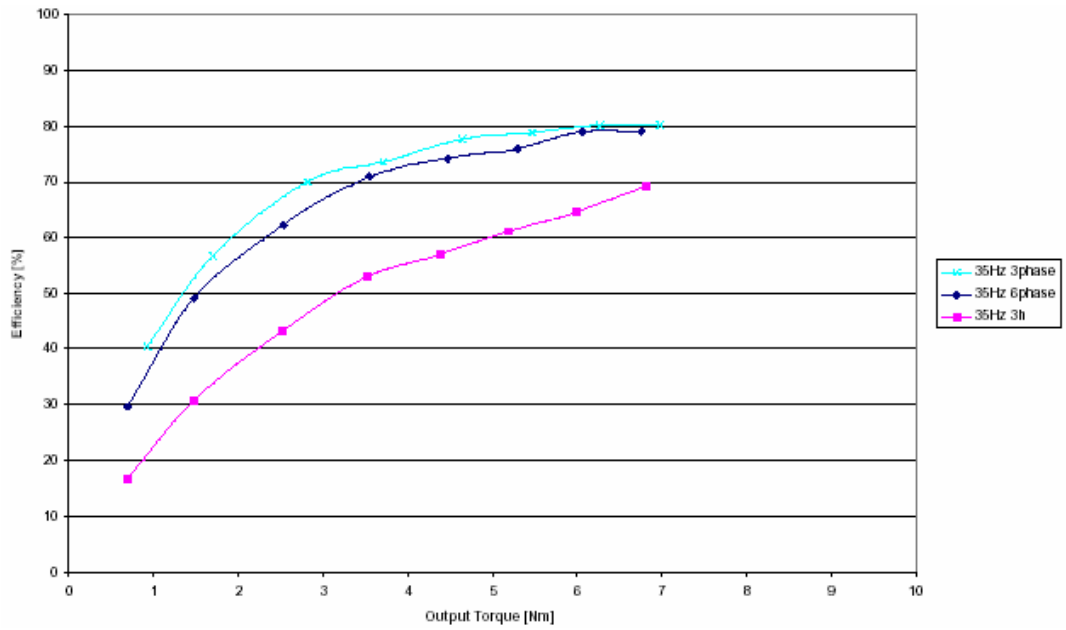


Figure 2.37 Six-phase machine efficiency at 35Hz. Comparison between the three-phase machine and the six-phase machine with and without third harmonic current injection.

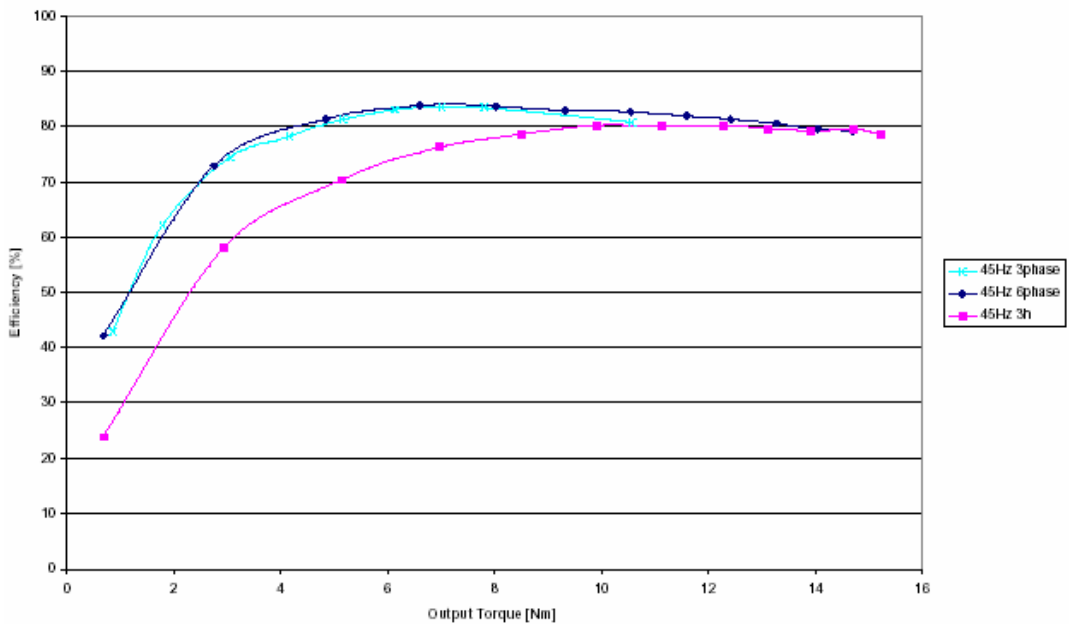
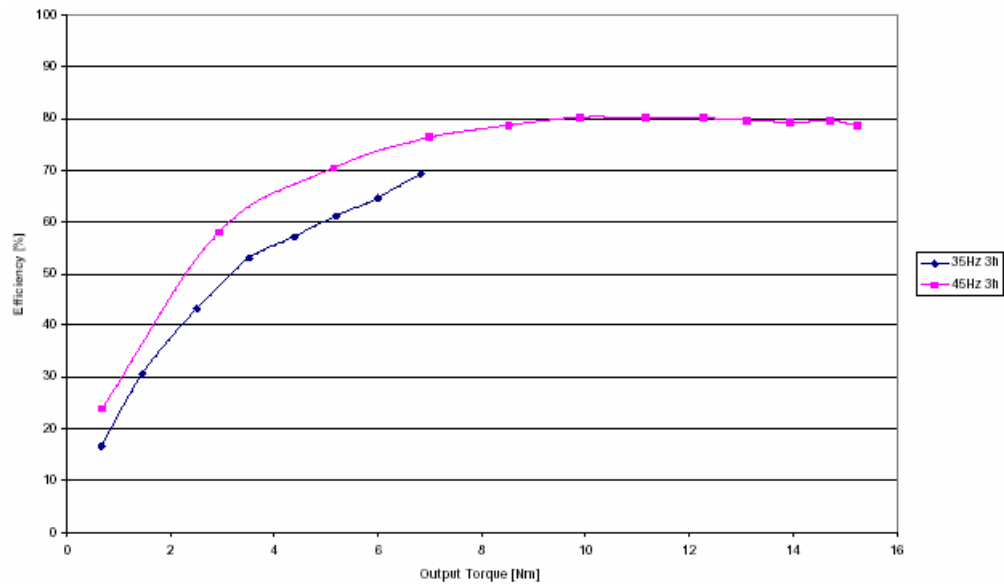


Figure 2.38 Six-phase machine efficiency at 45Hz. Comparison between the three-phase machine and the six-phase machine with and without third harmonic current injection.



Since the six-phase machine is designed based on the baseline three-phase machine, for 60Hz operation, the efficiency also increases with frequency for the case with injected third harmonic currents. This can be seen in Figure 2.39 where the efficiency of the six-phase machine, with third harmonic current injection, is plotted for 35 and 45Hz voltage power supply.



*Figure 2.39 Six-phase machine efficiency different frequencies with third harmonic current injection.*

For operation at 45Hz, the efficiency obtained experimentally was compared to the result from the steady-state equivalent circuit. Figure 2.40, Figure 2.41 show the comparison between the calculated and measured efficiency for the six phase machine. Since the iron loss and saturation effects are absent in the steady-state model, the calculated efficiency is higher than the experimental evaluation.

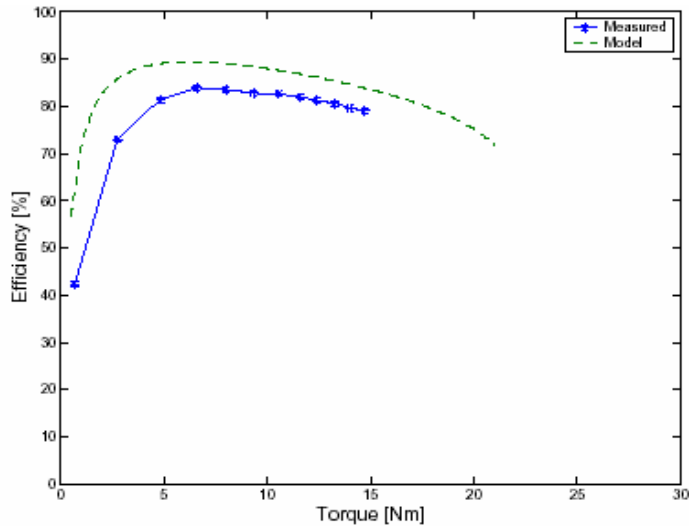


Figure 2.40 Calculated and measured efficiency for the six-phase machine without third harmonic current injection for 45Hz.

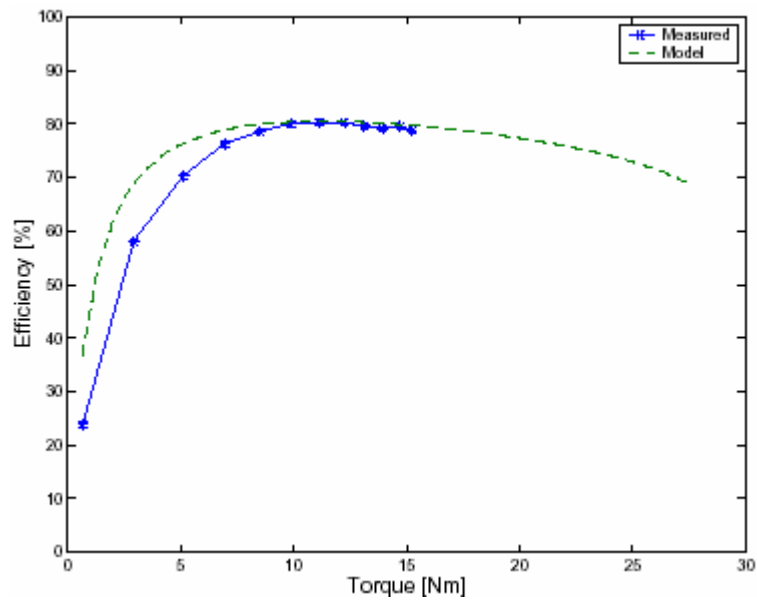


Figure 2.41 Calculated and measured efficiency for the six-phase machine with third harmonic current injection for 45Hz.

As mentioned before, the stator copper losses are the major cause for the decrease in the efficiency. For higher power level machines, the copper losses are expected to reduce increasing, therefore, the efficiency at lighter loads.

## **2.4 CONCLUSION**

To achieve higher power levels with limited range power converters, multi-phase systems are broadly used in industry. Additional torque production can be obtained in these systems if third harmonic currents are injected so to reshape the flux distribution in the machine and therefore obtain higher fundamental flux densities without extrapolating the flux limits and forcing the machine into saturation.

The research work in [1] proposes the use of a six-phase induction machine to gain these benefits. By constructing the machine with two three-phase groups phase shifted by thirty degrees, for the third harmonic currents, that are zero sequence currents in a standard three-phase machine, it is possible to create an additional rotating field that is in synchronism to the fundamental component. This results in, a reduction in the peak flux density.

By increasing the fundamental flux component to reestablish the air gap flux to its original peak value, an additional torque is then obtained. However, if applied to a standard three-phase machine, i.e. if the third harmonic currents are allowed to flow in that machine by connecting the neutral, pulsating torque will appear as a consequence of the interaction between the fundamental flux and the stationary third harmonic one.

It is analytically shown that an increase of up to 40% in the torque production can be expected with this technique when compared to a standard three-phase machine, for same peak flux distribution. To obtain the benefits, the winding function of the machine has to include third harmonic components. This is true for most of electrical machines due to the discrete construction of the windings that are distributed in finite number of slots. The best improvement would be obtained by using a concentrated winding machine since, for this case, the higher third

harmonic component in the winding function is obtained. However, distribution of the windings among a few slots contributes to the reduction of the unwanted harmonic components. Therefore, a trade off exists between the amplitude of the third harmonic winding distribution and the reduction of the unwanted harmonics.

The machine designed for the experimental evaluation was a distributed winding machine. This decision comes from the fact that it is necessary to establish a baseline for comparison, and, therefore the new machine is designed to have a similar winding function as the baseline machine. This is closer to the reality since it is necessary to distribute the coils in multiple slots to avoid large slot opening and depth.

The necessity of controlling the phase relation between fundamental and third harmonic flux components, is another fundamental issue in this application. If this relation is lost, a peaked flux density could be generated instead of the proposed flattened one. Magnetostatic finite element analysis was used to show the behavior of air gap and core flux with third harmonic currents.

It was shown that the injection of third harmonic currents increases the flux in the core but it is now more narrowly distributed. This indicates a possibility of compensated factors that would keep the core losses similar for the three-phase and six-phase cases. However experimental results demonstrate that for normal operating flux levels, iron and copper losses in the six-phase machine are comparable to the same size three-phase machine. Only when the flux levels are increased far beyond the rated values, the iron and copper losses become prohibitive. Copper losses, in per unit, reduces with the machine power rate and therefore, for large machines, the copper losses are expected to go down significantly.

The proposed system was tested experimentally to show the expected torque improvement. It was shown that for voltage fed systems the current sharing between the two three-phase groups could be uneven what could cause problems. Therefore the necessity of controlling the currents in the machine was put forward. The experimental results show that for same air gap peak flux density, the torque is

increased with the third harmonic current injection as a result of the increase in the fundamental component of current and flux. The experimental results validate the theoretical analysis and prove the improvement in the torque production as proposed in the mentioned research project.

However, in order to obtain the system overall efficiency correctly, in addition to experimental values, it is necessary to map the machine losses. Obtaining a mathematical model for these losses is an important tool in the machine design for correct calculation of losses of the machine. A model which was developed in another research thesis [18] for calculating the losses of induction machines requires the magnetic field distribution for calculations. In this study, the magnetic field distribution of a six-phase induction motor with third harmonic current injection is evaluated using a transient solution of a finite element software and the core losses of the motor is calculated by using a method that was evaluated in [18].

## **CHAPTER 3**

### **MACHINE LOSSES**

#### **3.1 INTRODUCTION**

The electrical motors have various types of losses. Some of these losses can be calculated using analytical methods. On the other hand, there exist no reliable methods to calculate the high frequency core losses of an induction motor analytically. The aim of this study is to calculate specifically the core losses of the motor explained in Chapter 2 by using the calculation method, which was presented by [18]. Since the calculation method is based on finite element solution, we need to create the finite element model of the motor.

In this chapter, losses of an induction motor will be briefly explained, and after an introduction of the finite element method, the process of creation of the finite element model of the motor will be presented.

#### **3.2 LOSSES OF INDUCTION MACHINES**

As the electrical motors started to find fast growing areas of application, calculation of their losses also began to present importance. Other factors to increase the significance of efficiency - and hence losses - are environmental pollution and saving primary energy resources.

In general there exist four types of losses in an induction motor [20].

### **3.2.1 Friction and windage losses:**

This kind of losses are due to the friction between the bearing and the rotor shaft. The load, peripheral speed of the shaft, the friction coefficient between the shaft and the bearing are examples of factors affecting the magnitude of these losses.

Peripheral speed of the rotor and construction characteristics of the motor like the core length and rotor diameter affect on the windage losses. These losses can only be determined by experiments.

### **3.2.2 Copper losses**

Two types may be mentioned,

a) Stator copper losses: These losses are due to the stator windings and may be calculated using the wire size and length of each phase winding. Total loss can be found by multiplying by the number of phases.

b) Rotor copper losses: These are due to the rotor windings. They are called rotor  $I^2R$  losses in squirrel cage rotor motors and can not be measured directly. By subtracting from the total copper loss which is determined by tests, these losses can be found.

### **3.2.3 Stray load losses**

These are defined as the portion of the total loss in a machine for the load conditions not accounted for by the sum of friction and windage, stator&rotor  $I^2R$  losses and core loss. In fact these are the eddy current losses caused by the increase and the pulsations in the air gap leakage fluxes, proximity effect and other minor causes. In various standards these losses are assumed to be approximately 0.5% of the rated output.

### **3.2.4 Core losses**

There are generally two types of core losses:

a) Fundamental frequency losses: These are supplied by the stator from the line and are assumed to exist only in stator teeth and core. That is because the frequency in

the rotor and hence the fundamental frequency loss is so low to take into account. The fundamental frequency losses are generally determined by using loss curves as in Figure 3.1. These curves are typical for the type of steel used in motor manufacturing.

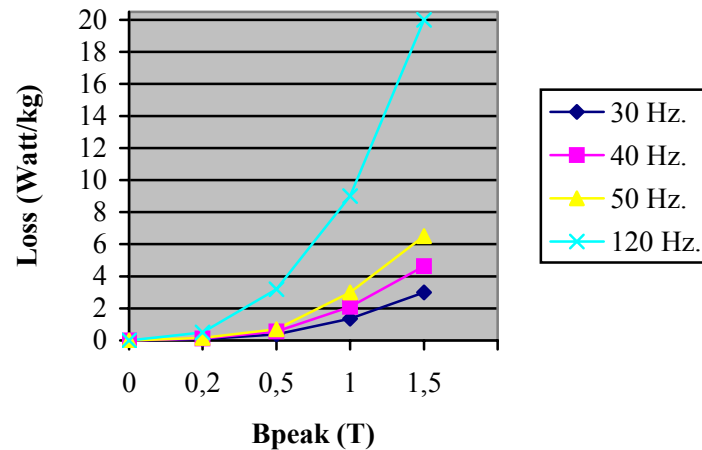


Figure 3.1 Fundamental frequency loss versus peak flux density curves for different frequencies. [21]

b) High Frequency losses: High frequency losses can be taken as an additional load since they are supplied by the mechanical power of rotor. These losses are due to the permeance variation, saturation, harmonics in the air gap field and the mmf. The most effective factor is the slotting. The high frequency losses can be determined by measuring at no load and subtracting the fundamental frequency losses, friction and windage losses and copper losses.

The task here is to be able to calculate the losses of the six-phase machine discussed in the previous chapters. If this can be done then it becomes possible to estimate the complete performance of the motor explained in Chapter 2. Hence better designs become possible. Alternatively it becomes possible to assess whether this type of motor is suitable for a given application.

The friction windage losses are usually accounted by using experimentally obtained data on the fan to be used for a given application. The calculation of copper losses



is straight forward. If the machine design details are available a 2D transient field solution with 3-dimensional effects would reveal the value of phase resistance and coil current. Therefore the Cu losses can be calculated. The remaining losses are the calculation of the core losses and stray load losses part of which is high frequency losses.

The fundamental frequency losses can be calculated from the field solution as described in section 4.2.1. There is no established solution for the calculation of high frequency losses. In this chapter, an attempt shall be made to develop a method for the estimation of fundamental and high frequency core losses. Accurate analytical calculation of the core losses is not possible. The approach developed here shall be based on the high frequency loss calculation method developed in [18]. This approach is based on finite element method. The following sections shall first discuss modeling of the motor for FE solution.

### **3.3 FINITE ELEMENT MODEL**

The finite element method is an analysis process by which thermal, mechanical and electromagnetic analysis can be performed. In this method, model of the subject device is divided into very small elements which are formed by three corners so called the nodes.

The finite element software allows the user to draw the geometry, create the mesh for the analysis, define the material properties and couple electrical circuits to the magnetic circuits. If the symmetry of the subject machine is appropriate, only a quarter of the machine can be modelled and solved. The solution process is easier for standard machines but in complex machines like the one in this thesis, it becomes more complex and time consuming to make an analysis.

The FE software uses the Maxwell equations in magnetic analyses. Three kinds of analyses can be performed using these programs:

a) Static magnetic analysis: Magnetic fields due to dc currents, permanent magnets are calculated. Time variant effects like eddy currents are not taken into account.

b) Harmonic magnetic analysis: All electrical and magnetic quantities are assumed to have a sinusoidal variation in this type of solution. The effects of sinusoidal currents or the voltage excitation effect in electromagnetic devices and moving conductors are calculated. Skin effects, power consumption due to eddy currents, torque, impedance and inductance are examples of these effects. Hysteresis effects are ignored.

c) Transient Magnetic Analysis: The time varying magnetic fields are calculated. The fields may be due to fluctuations in the current or the voltage, or external pulsed fields. Eddy currents, power consumption and induced magnetic forces due to these currents are examples of calculated quantities.

In this study, because the source has both fundamental and third harmonic components, the transient magnetic analysis had to be chosen. The analysis is done on a two-dimensional basis. The reason for that is three-dimensional solutions takes much more time and it presents quite a high complexity to create a three-dimensional model of a motor. Although a two-dimensional solution is chosen the solution time is still the main disadvantage of this type of analysis. The details of the solution process will be given in the next subsections.

### **3.3.1 Creation of the finite element model**

The motor in Chapter 2 is modelled by using Flux2D. The software is composed of different modules that are used for creation of different components of the finite element model. The drawing of the geometry, and then meshing the geometric model depending on the accuracy needed at different parts of the motor is done using the geometry module of the software. The material properties are defined to the program using the material module. On the other hand, the stator circuit is set up using the circuit module. Finally the boundary conditions are defined to the program and the electrical circuit is coupled to the physical model using the physical module. As the last step, the resulting file is solved using the solver module of the finite element software. The analysis of the results is done using the result module.

### 3.3.1.1 Drawing the geometry and the mesh

The model is created firstly by drawing of the motor geometry. The regions of the model are assigned as different parts of the motor like stator, rotor, etc. The possibility of drawing half or a quarter of the motor makes it easier to model. By this way the number of nodes and the elements are kept to a minimum and the time elapsed for the solution process decreases. In this study a quarter of the motor is drawn thanks to the symmetry conditions (Figure 3.2).

When creating the mesh, firstly an automatic mesh is generated using the program, then the mesh is restructured to supply the needs of this study by placing the sufficient but at the same time the least number of nodes. That is, the nodes which are placed automatically and generously by the program, are reduced to sufficient levels by the user. This is done by increasing the distances between the nodes. As going away from the air gap towards both to the shaft and to the outermost side of the stator core, the regions are meshed in a geometrically coarser manner. As can be seen in Figure 3.3, for example, the stator back core is divided into three subregions and meshed more coarsely since the accuracy of the values in this region is less significant than the ones in the regions closer to the air gap and the field distribution is smoother.

On the other hand; the regions, in which there is a need for more accurate results that will be used in the loss calculations, are meshed in a tighter manner. The rotor teeth for instance, are divided into three subregions according to the skin depths which will be calculated in Chapter 4 depending on the expected eddy current harmonics, and are meshed more tightly so that the eddy currents in the lamination are obtained with better precision.

Another significant part of the motor in electromagnetic problems, the air gap, is modeled as composed of three layers in order to get more accurate results. Hence more nodes are placed in the air gap region and more realistic measurements are obtained.

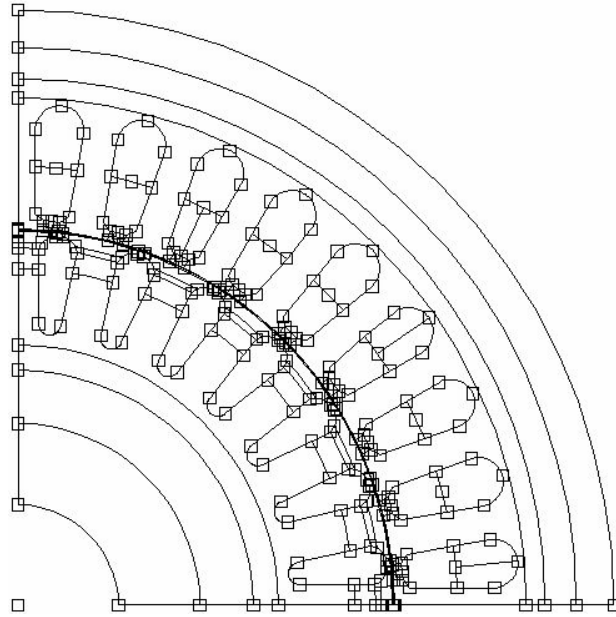


*Figure 3.2 The geometry drawn for the six phase machine.*

Regarding the meshing of the motor geometry, there exists a trade off between the accuracy of the results and the analysis time. The mesh used in this thesis has 17000 nodes and 8046 elements. The analysis takes a time period of about 25 hours to get the results of the 1.5<sup>th</sup> second of the motor operation.

The stator and rotor slots are also drawn and each of them is assigned as a separate region since these will be assigned the stator coils in the the electrical circuit in accordance with the winding arrangement shown in Figure 2.9. In Figure 3.3, the meshing of the stator and the rotor slots are displayed.

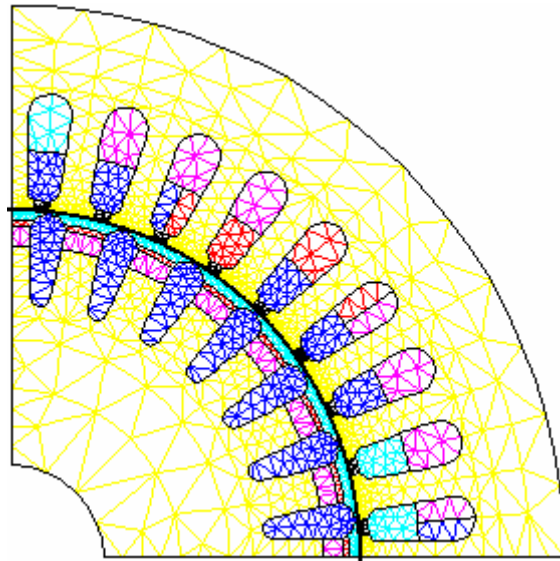


*Figure 3.3 The mesh created for the six phase machine.*

### **3.3.1.2 Boundary conditions**

The boundary conditions for the model is defined as in Figure 3.4. taking into account the symmetry conditions. Since a quarter of the motor is modelled, the boundary conditions have to be defined so that the software can complete the model to the whole motor when doing the calculations. These conditions are applied to the nodes which form the boundary regions of the model. In this study two types of boundary conditions are used in the analysis: Dirichlet, Anticyclic. According to Dirichlet condition, the vector potential at the inner boundary of the rotor and the outer boundary of the stator, is zero. The anticyclic condition allows the user to link two boundaries. According to the anticyclic condition the variable values on one boundary are of the opposite sign of the homologous nodes of the other boundary. That means, for example the flux values are of the opposite sign at the homologous nodes of the two sides of the quarter of the motor.

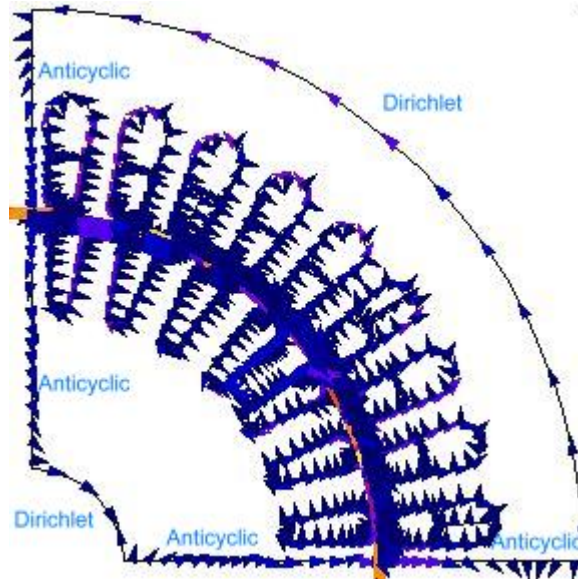


Figure 3.4 Boundary conditions

### 3.3.1.3 Defining the material properties

After the creation of the geometric model, the material properties are to be input. The B-H curve of the stator core and the rotor core, is defined to the program as in Figure 3.5.

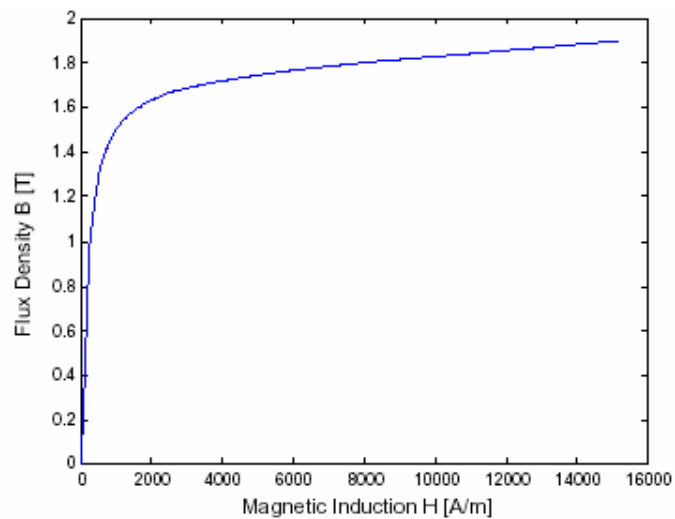


Figure 3.5 Iron BH curve used in the finite element analysis.

The subregions created in the rotor teeth in section 3.3.1.1, where the eddy currents are read from the program, are assumed to be composed of 97% iron and 3% isolation in order to obtain the magnitudes of the eddy currents in them. Hence the resistivity of the three subregions in the rotor teeth is taken as,

$$0.97 \times 9.7 \times 10^{-8} + 0.03 \times 2.2 \times 10^{-2} = 6 \times 10^{-4} \quad (3.1)$$

The rest of the core is assumed to have no resistivity. The reason for this is that assigning a resistivity to the entire core, elongates the convergence of the solution.

The properties of the stator windings and the rotor bars are also input. The resistivity of aluminium rotor bars and the copper windings are taken respectively as  $0.263 \times 10^{-7}$  Ohm x m. and  $0.172 \times 10^{-7}$  Ohm x m.

#### **3.3.1.4 Setting up the stator circuit**

The analysis performed by Flux 2D is a kind of the so called coupled analysis. The external circuit can be connected to the internal regions of conductors. For this purpose, the stator circuit is set up as in Figure 3.6. The six phase windings A, B, C, X, Y, Z, the fundamental and third harmonic current sources for each phase, end winding resistance and inductance (Table 3.1) are placed in the circuit for a quarter of the motor. The reason for using current sources instead of voltage sources, is explained in [1] as the necessity of controlling the phase relation between the fundamental and third harmonic currents. The values of the above parameters are input after being divided into the number of symmetrical parts of the motor. The rotor circuit is set up by the program itself. The end ring resistance and inductance are taken from the values of a similar induction machine and input to the program (Table 3.1) since there is no information in [1] on the parameters needed for the calculation of these values. The method to calculate the end winding and end ring parameters can be found in Appendix.

Table 3.1 Necessary calculated values for Flux2D

End winding resistance	0,172 Ohm
End winding inductance	0,136 mH
End ring resistance	$0,237 \times 10^{-5}$ Ohm
End ring inductance	$0,145 \times 10^{-4}$ mH

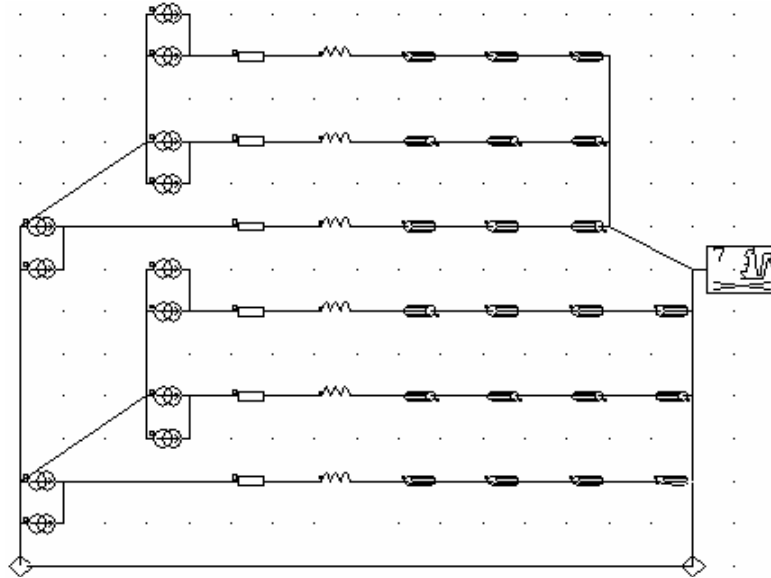


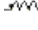




Figure 3.6 Stator circuit of the six phase machine.

-  Current source for fundamental and third harmonic components
-  End winding resistance
-  End winding inductance
-  Winding coil
-  Rotor circuit (including end ring resistance and inductance)

In accordance with [1], the phase currents are defined as,

$$I_A = I \cos\theta + I_3 \cos 3\theta \quad (3.2)$$

$$I_B = I \cos(\theta - 120) + I_3 \cos 3\theta \quad (3.3)$$

$$I_C = I \cos(\theta + 120) + I_3 \cos 3\theta \quad (3.4)$$

$$I_X = I \cos(\theta - 30) - I_3 \sin 3\theta \quad (3.5)$$

$$I_Y = I \cos(\theta - 150) - I_3 \sin 3\theta \quad (3.6)$$

$$I_Z = I \cos(\theta + 90) - I_3 \sin 3\theta \quad (3.7)$$

where  $I = 0.58$  A,  $I_3 = 0.4$  A, and,

$$\theta_{\text{elec.}} = \omega t = 2 \times \pi \times 40 \times t = 80\pi \times t \quad (3.8)$$



### 3.3.1.5 The solution process

After coupling the electrical circuit to the physical model using the physical module of the software, the finite element model becomes ready for solution. Before the solving process, the precision has to be determined. The default precision which is  $10^{-3}$ , is used for the analyses in this study. Higher precision rates extend the analysis time but provide no better results that are worth the longer time. A Pentium Centrino 1400 MHz computer is used for the analyses. An analysis with 17000 nodes is typically obtained in a time period of 25 hours to get the results for the 1.5 seconds of the machine operation and the resulting file occupied 3 gigabytes of hard disk space. The time step determines the time period between two successive solutions of the model, and is adjusted as 0.3 msec. With the 40 Hz. excitation in the solutions, 5000 time steps correspond to 1.5 sec.

### 3.3.2 Verification of the finite element model

In order to show the currents applied to the circuit are transferred to windings in a right manner, the instantaneous currents are calculated for an example time instant of 0.006 sec. and are compared with the current values in the windings read from Flux2D for the same time instant.

For  $t = 0.006$  sec.

$$\theta_{\text{elec.}} = 80 \times \pi \times 0.006 = 86.4^\circ \quad (3.9)$$

The period of the 40 Hz. current supply is  $T = 0.025$  sec. The same conditions occur also for the time instants,

$$t = 36 T + 0.006 = 0.906 \text{ sec. and,} \quad (3.10)$$

$$t = 42 T + 0.006 = 1.056 \text{ sec.} \quad (3.11)$$

On the other hand at 40 Hz. the rotor speed of the motor operating at no load condition is 1200 rpm. Hence the rotor completes a rotation of  $360^\circ$  in  $60/1200 = 0.05$  sec. Therefore, the rotor positions at  $t = 0.006$ ,  $t = 0.906$  and  $t = 1.056$  respectively are,

$$\theta_{\text{mech.}} = 0.006 \times 360 / 0.05 = 43.2^\circ \quad (3.12)$$

$$\theta_{\text{mech.}} = 0.906 \times 360 / 0.05 = 6523.2^\circ = 18 \text{ rotations} + 43.2^\circ \quad (3.13)$$

$$\theta_{\text{mech.}} = 1.056 \times 360 / 0.05 = 7603.2^\circ = 21 \text{ rotations} + 43.2^\circ \quad (3.14)$$

This information can be used to verify that the solution has converged. Indeed it is found that the currents and the rotor positions are the same at the three time instants. The phase currents calculated in accordance with Eq(3.2) to (3.7) at  $t = 1.056$  sec., and the current values read from Flux2D at  $t = 0.906$  sec. and  $t = 1.056$  sec. are presented in Table 3.2. Also, the mmf contributions of each slot is shown in the table. As can be seen from Table 3.2, the calculated phase currents are nearly the same with the values read from the program, and seem to have converged to their final values. It can be also concluded that the phase currents applied to the stator circuit, are transferred to the phase windings without any error.

In Figure 3.7, the mmf contribution of each slot calculated in Table 3.2 are plotted cumulatively. The mmf waveform presents a sinusoidal waveform.

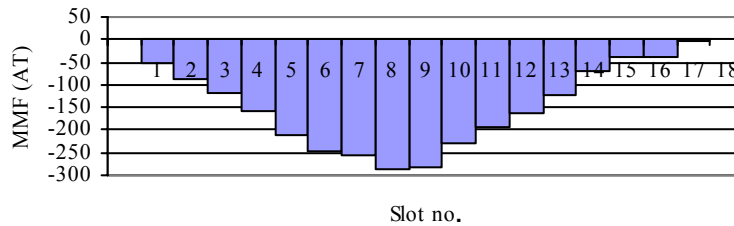
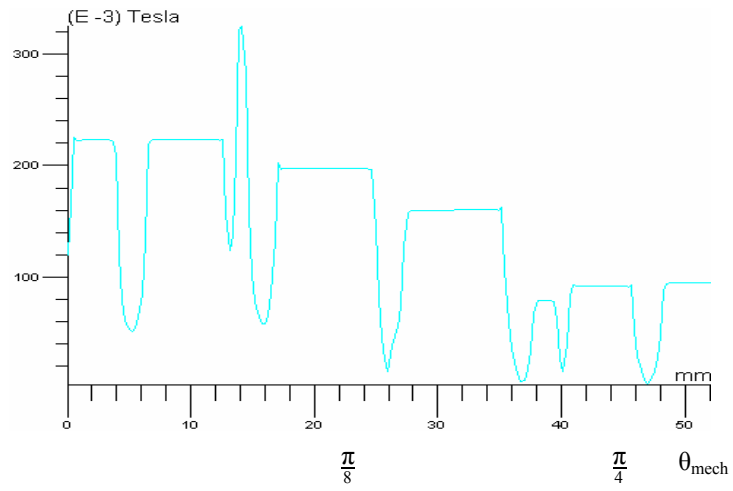


Figure 3.7 MMF Waveform created by the currents in Table 3.2

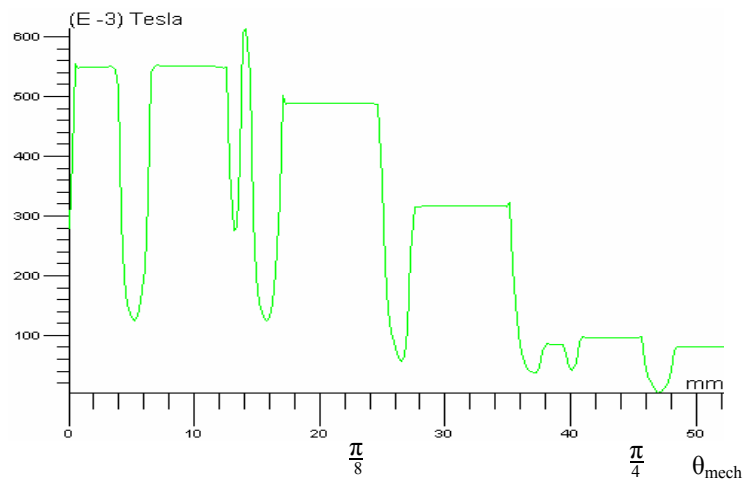
On the other hand, in order to decide on the convergence of the analysis, the air gap flux density is plotted for different time instants at which the rotor position is the same. In Figure 3.8 the air gap flux density waveforms for  $t=0.1473$  sec.,  $t=1.3473$  sec. and  $t=1.4973$  sec. can be found. Each notch in the waveform correspond to a stator slot opening. The air gap flux density seems not to have converged to its final waveform in Figure 3.8 (a). However, the waveforms and the maximum values of the curves in Figure 3.8 (b) and (c) are the same indicating convergence. When compared to the mmf waveform in Figure 3.7, it can be seen that the envelope of the flux density distribution in Figure 3.8 also presents a sinusoidal waveform matching the expectations.

Table 3.2 MMF contributions of slots for  $t=1.056$  sec.,  $w=80\pi$  rd/s.,  $n=1200$  rpm.

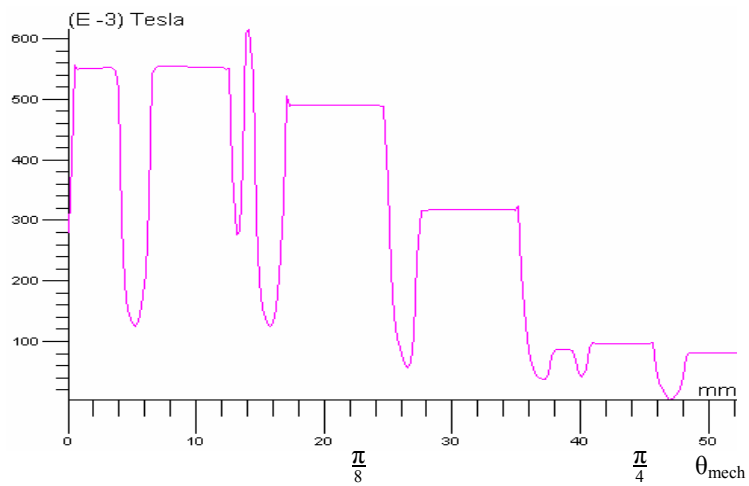
Slot No.	Wdg.	N	Instantaneous Current (A)			MMF Contribution (AT)	
			Calculated for $t = 1.056$ sec. Fund. + 3rd harm.	Read in Flux2D for $t= 0.906$ $t=1.056$			
1	X-	24	$0.3209 - (-0.393) = 0.7139$	0.713885	0.713886	-17.134	-50.934
	Z+	25	$-0.579 - (-0.393) = -0.186$	-0.1859	-0.1859	-4.65	
	C+	49	$-0.52 + (-0.07495) = -0.5949$	-0.5945	-0.5945	-29.1501	
2	Z+	49	$-0.579 - (-0.393) = -0.186$	-0.1859	-0.1859	-9.114	-38.264
	C+	49	$-0.52 + (-0.07495) = -0.5949$	-0.5945	-0.5945	-29.1501	
3	Z+	49	$-0.579 - (-0.393) = -0.186$	-0.1859	-0.1859	-9.114	-29.116
	B-	49	$0.4831 + (-0.07495) = 0.4082$	0.40812	0.40811	-20.002	
4	Z+	25	$-0.579 - (-0.393) = -0.186$	-0.1859	-0.1859	-4.65	-40.274
	Y-	24	$0.2579 - (-0.393) = 0.6509$	0.6508	0.6508	-15.6216	
	B-	49	$0.4831 + (-0.07495) = 0.4082$	0.40812	0.40811	-20.002	
5	Y-	49	$0.2579 - (-0.393) = 0.6509$	0.6508	0.6508	-31.894	-51.896
	B-	49	$0.4831 + (-0.07495) = 0.4082$	0.40812	0.40811	-20.002	
6	A+	49	$0.03642 + (-0.07495) = -0.03853$	-0.03854	-0.03854	-1.888	-33.782
	Y-	49	$0.2579 - (-0.393) = 0.6509$	0.6508	0.6508	-31.894	
7	A+	49	$0.03642 + (-0.07495) = -0.03853$	-0.03854	-0.03854	-1.888	-1.0262
	Y-	25	$0.2579 - (-0.393) = 0.6509$	0.6508	0.6508	-16.2725	
	X+	24	$0.3209 - (-0.393) = 0.7139$	0.713885	0.713886	17.134	
8	A+	49	$0.03642 + (-0.07495) = -0.03853$	-0.03854	-0.03854	-1.888	-33.093
	X+	49	$0.3209 - (-0.393) = 0.7139$	0.713885	0.713886	34.981	
9	C-	49	$-0.52 + (-0.07495) = 0.5949$	-0.5945	-0.5945	-29.15	5.831
	X+	49	$0.3209 - (-0.393) = 0.7139$	0.713885	0.713886	34.981	
10	X+	25	$0.3209 - (-0.393) = 0.7139$	0.713885	0.713886	17.848	51.648
	Z-	25	$-0.579 - (-0.393) = -0.186$	-0.1859	-0.1859	4.65	
	C-	49	$-0.52 + (-0.07495) = -0.5949$	-0.5945	-0.5945	29.1501	
11	Z-	49	$-0.579 - (-0.393) = -0.186$	-0.1859	-0.1859	9.114	38.264
	C-	49	$-0.52 + (-0.07495) = -0.5949$	-0.5945	-0.5945	29.1501	
12	Z-	49	$-0.579 - (-0.393) = -0.186$	-0.1859	-0.1859	9.114	29.116
	B+	49	$0.4831 + (-0.07495) = 0.4082$	0.40812	0.40811	20.002	
13	Z-	24	$-0.579 - (-0.393) = -0.186$	-0.1859	-0.1859	4.464	40.739
	Y+	25	$0.2579 - (-0.393) = 0.6509$	0.6508	0.6508	16.2725	
	B+	49	$0.4831 + (-0.07495) = 0.4082$	0.40812	0.40811	20.002	
14	Y+	49	$0.2579 - (-0.393) = 0.6509$	0.6508	0.6508	31.894	51.896
	B+	49	$0.4831 + (-0.07495) = 0.4082$	0.40812	0.40811	20.002	
15	A-	49	$0.03642 + (-0.07495) = -0.03853$	-0.03854	-0.03854	1.888	33.782
	Y+	49	$0.2579 - (-0.393) = 0.6509$	0.6508	0.6508	31.894	
16	A-	49	$0.03642 + (-0.07495) = -0.03853$	-0.03854	-0.03854	1.888	-0.3384
	Y+	24	$0.2579 - (-0.393) = 0.6509$	0.6508	0.6508	15.6216	
	X-	25	$0.3209 - (-0.393) = 0.7139$	0.713885	0.713886	-17.848	
17	A-	49	$0.03642 + (-0.07495) = -0.03853$	-0.03854	-0.03854	1.888	33.093
	X-	49	$0.3209 - (-0.393) = 0.7139$	0.713885	0.713886	-34.981	
18	C+	49	$-0.52 + (-0.07495) = 0.5949$	-0.5945	-0.5945	29.15	-5.831
	X-	49	$0.3209 - (-0.393) = 0.7139$	0.713885	0.713886	-34.981	



(a)



(b)



(c)

Figure 3.8 Bgap waveform for different time instants a)  $t=0.1473$  b)  $t=1.3473$  sec. c)  $t=1.4973$  sec.

However, despite the comparisons above there is no proof of the correctness of the finite element solution. One way to do this is to solve the model for various load conditions and compare the experimental results with the finite element model. The verification of the the correctness of the solution is left to another research study.

## **CHAPTER 4**

### **CORE LOSS CALCULATION**

#### **4.1 INTRODUCTION**

As mentioned earlier, the aim of this thesis is to calculate the core losses of the motor introduced in Chapter 2. However, since the analytical calculation of core losses presents unreliable results, a method which uses finite element method will be used to achieve this aim. Hence, after establishing the finite element model of the motor in the previous chapter, the calculation method of core losses evaluated in [18], will be applied to the subject motor in this chapter.

In order to establish a rational basis for comparison of the calculations in this thesis and the experimental results of [1], the motor is assumed to operate at no load. The reason for this is that, the magnetic losses of the motor is experimentally measured at no load condition in [1]. This means that we do not take into account the effects of the rotor currents. However, the method may be verified by doing the calculations for load conditions.

#### **4.2 CALCULATION OF LOSSES**

In this section, a method of calculation of core losses of an induction machine from FEM solutions will be explained. The fundamental frequency losses can be found by using the results of the finite element solution and the loss curves as explained in Chapter 3. On the other hand, for the high frequency losses a relatively difficult method has to be used because of the effect of lamination on eddy currents.

#### 4.2.1 Calculation of fundamental frequency losses of an induction motor

Fundamental frequency core losses are assumed to occur at the stator core and the stator teeth. This is because the frequency in the rotor is so low at normal operating speeds that the fundamental frequency losses in them can be neglected. This kind of core losses can be calculated using loss curves. These curves are provided by the machine or the material manufacturers. The loss curve in Figure 3.1 which is taken from [21], is used in this thesis.

In order to find the loss value of a stator element, the magnetic field density of that element should be known. The corresponding loss determined from the graph in Figure 3.1, should then be multiplied by the weight of the subject element. That is,

$$P_f = \sum_{i=1}^n P_i \times v_i \times d \quad (4.1)$$

where

$P_f$  : total fundamental frequency loss,  $P_i$  : fundamental frequency loss of an element

$v_i$  : volume of the element,  $d$  : density of the core material

#### 4.2.2 Calculation of high frequency losses of an induction motor

Because of the variations in the magnetic reluctance, the air gap flux density distribution presents a rippled waveform. In addition, the airgap field distribution varies with respect to time since the position of the mmf field with respect to the stator teeth varies, and this affects on the level of saturation at the teeth ends. This ripple moves on the rotor and induces eddy currents in the rotor surface and this results in surface losses in the stator.

High frequency losses are hard to calculate because of the complexity of the distribution of the flux density within a lamination and nonlinearity of the losses with the flux density. There are several calculation methods of high frequency losses. Some empirical curves were developed by Hanssen [18]. Heller's method constitute an important contribution to the calculation of high frequency losses [22]. Another calculation method proposed by Spooner and Kinnard, is based on a formula that was obtained after several loss measurements [23]. However none of these methods can provide reliable results.

Flux2D provides the eddy currents in the rotor teeth. However, these values are computed by the program ignoring the laminated core. In the actual machine the eddy currents are assumed to flow within the lamination since the lamination surfaces are electrically isolated. Here, we will use a method which is a modified version of the one used in [18] to include the effect of lamination.

The skin depths of each harmonic are calculated using the Eq.4.2 [20]

$$\delta_j = T_p \times f_s / \pi \times f_j \quad (4.2)$$

where,

$\delta_j$ : skin depth of  $j^{\text{th}}$  harmonic,  $T_p$ : stator pole pitch

$f_s$ : stator frequency,  $f_j$ : frequency of  $j^{\text{th}}$  harmonic

Consider a tooth pitch on the rotor side. The eddy current path in the solution of the field is in the axial direction. This is shown in Figure 4.1 in which the average rotor tooth pitch width for a certain length  $l_{av}$  in the axial direction at a certain skin depth is shown. In this figure,  $i_j$  is used for the current of one lamination flowing in the axial direction,  $e_j$  is used for the voltage of one lamination induced in the axial direction,  $l_{lam}$  is used for the thickness of the lamination. The induced emf causes this current to flow against resistance  $R_j$ , determined by the skin depth for the particular harmonic and the average width of the current path ( $l_{av}$ ) in the radial direction.

$$R_j = \frac{\rho_{lam} l_c}{A} = \frac{\rho_{lam} l_c}{\delta_j \times l_{av}} \quad (4.3)$$

where,  $R_j$ : the resistance of one rotor tooth at the skin depth of  $j^{\text{th}}$  harmonic the finite element analysis assumes.

$\rho_{lam}$ : resistivity of the lamination,  $l_c$ : core length.

$A$ : cross-section of one rotor tooth in one lamination under the skin depth of  $j^{\text{th}}$  harmonic.

$\delta_j$ : the skin depth of  $j^{\text{th}}$  harmonic,  $l_{av}$ : average current path width



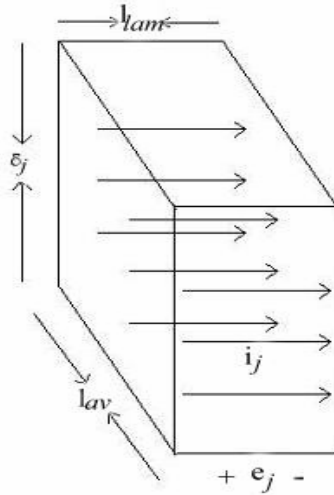


Figure 4.1 The current path the finite element analysis assumes in a rotor tooth pitch

If the induced emf in the axial direction has an average magnitude  $e_j$ , for the portion of the rotor considered, the average current flowing in the cross section is as,

$$i_j = \frac{e_j}{R_j} = \frac{e_j \times \delta_j \times l_{av}}{\rho_{lam} \times l_c} \quad (4.4)$$

where,

$i_j$ : the current flowing in the axial direction.

$e_j$ : average magnitude of the the emf drop in the axial direction.

In the calculations that follow, the eddy currents are assumed to flow within the lamination. This naturally reduces the magnitude of eddy currents since any current must be due to the induced emf in the axial direction. This subsection discusses how the calculated losses from the FE software can be modified to take into account the effect of laminations.

Let us now assume that, in fact the eddy currents are confined to a lamination and current circulate within the lamination over a rotor tooth pitch as shown in Figure 4.2. In this case, the currents circulate due to the emf  $e_i$ , induced due to the  $i^{\text{th}}$  harmonic field in the axial direction. The thickness of the lamination ( $l_{lam} = 0.5$  mm.) therefore determines the magnitude of  $e_i$ . The current path in this case is also

considerably elongated as shown in Figure 4.2. Since the thickness of the lamination is much shorter than the tooth pitch, the resistance of the eddy current path may be assumed to be  $2l_{av}$ . Also, the center of the lamination region may be assumed to carry no currents (the emf gets too small). As seen in Figure 4.2, the current path width varies depending on the skin depth. Since taking into account the skin depths of all of the harmonics makes the problem more complex, an averaging has to be made for the current path width and skin depth values.

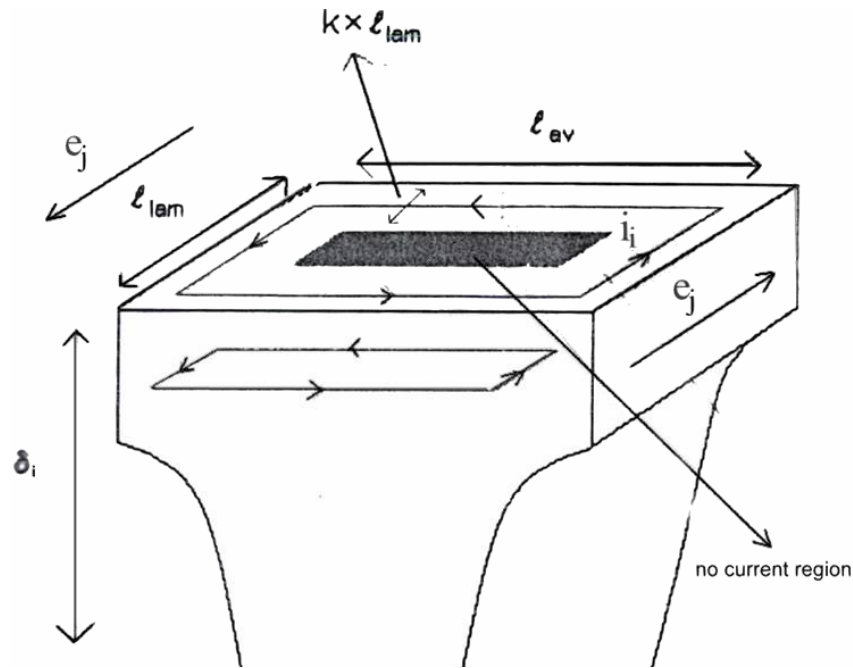


Figure 4.2 The current path considering the laminations

Therefore, the resistance of the circulating eddy current path for the  $i^{\text{th}}$  harmonic is,

$$R_i = \frac{\rho_{lam} l}{A} = \frac{2 \times \rho_{lam} l_{av}}{\delta_i \times l_{lam} \times k} \quad (4.5)$$

where,

A : cross-sectional area of the circulating eddy current path in one lamination of one skin depth region.

k : coefficient

$\delta_i$  : radial height of each skin depth in the rotor teeth.

The eddy current loss therefore in the considered portion of the rotor tooth is given by Eq.4.6 for the  $i^{\text{th}}$  harmonic.

$$P_i = e_i \times i_i = e_i^2 / R_i = (2 \times e_j)^2 / R_i = (2 \times i_j \times R_j)^2 / R_i \quad (4.6)$$

$$P_i = i_j^2 \times [2 \times \rho \times l_c^2 \times l_{\text{lam}} \times k / (\delta_i \times l_{\text{av}}^3)] \quad (4.7)$$

Then, the total high frequency loss of an induction motor is obtained by doing the above calculations for each harmonic component in every rotor tooth in the model and then using the formula below,

$$P_{\text{total}} = 4 \times t \times \sum_{i=2}^n P_i \quad (4.8)$$

where  $P_i$  is the eddy current loss of a harmonic in a quarter of the motor in one lamination and  $t$  is the number of laminations. The factor 4 is used since a quarter of the motor is modelled.

### 4.2.3 Implementation of the calculation method of fundamental frequency core losses

By using Flux2D, one stator tooth pitch is divided vertically into two and horizontally into ten regions as in Figure 4.3. The reason for not calculating the loss for every mesh element is that the program doesn't provide us with the volume and the flux density of each mesh element. Therefore the stator tooth pitch is divided into regions, the volumes of which are easy to calculate.



Figure 4.3 The regions assumed to exist in one tooth pitch of the stator core

Then the corresponding weight values are found by using  $7850 \text{ kg/m}^3$  as density of iron. The flux density of the points at the center of gravity of each region is read from the program along one cycle of the 40 Hz current source. 43 samples are read from the program along a period of the 40 Hz. source, which is 25 msec. That is, a sample is taken nearly every 0.6 msec.

The read flux density values are input to Matlab Simulink and the magnitudes of the spectrum of every region is evaluated. The fundamental and the third harmonic frequency peak flux density values are taken and the corresponding watt/kg values in the loss curve of Figure 3.1 are multiplied by the weight of each region in the stator tooth pitch. The loss of one tooth pitch is found by summing the loss of all regions. Then the total fundamental frequency loss is calculated by multiplying the loss of one tooth pitch by 36, which is the number of stator slots. The results of the fundamental frequency loss calculations will be elaborated on in detail in the next chapter. In Table 5.1, the fundamental and third harmonic components of the flux density in each region can be seen.

#### **4.2.4 Implementation of the calculation method of high frequency core losses**

In this section, by using the method explained in section 4.2.2, the high frequency core losses of the subject motor are calculated. The calculation procedure started actually while creating the finite element model of the motor. The rotor teeth are splitted into 3 regions according to the skin depths of 5<sup>th</sup>, 11<sup>th</sup>, 17<sup>th</sup> as shown in Figure 4.4. This was essential to avoid creating an excessive number of FE elements and possibly causing instability in the solution, since some of the element mesh sizes would have been very small values.

The reason behind the choice of the size of these 3 regions is explained below. According to [24] the harmonics expected to exist in the rotor are found by the equations below,

The air gap harmonics of the order  $n = 6m + 1$  rotate in the same direction with the fundamental.

The air gap harmonics of the order  $n = 6m - 1$  rotate in the opposite direction with the fundamental.

where  $m$  is an integer.

According to the rules above; 5<sup>th</sup>, 7<sup>th</sup>, 11<sup>th</sup>, 13<sup>th</sup>, 17<sup>th</sup>, 19<sup>th</sup>, 23<sup>rd</sup>, 25<sup>th</sup> air gap harmonics are expected to induce currents in the rotor core of the test motor;

On the other hand, the stator slot harmonics are also estimated to occur in the rotor. The order of the stator slot harmonics can be calculated as [18]:

$$n = (N_s \times n_r) / (60 \times f_s) \quad (4.9)$$

where,

$n$ : order of the expected stator slot harmonic,  $N_s$  : number of stator slots = 36,

$n_r$  : rotor speed = 1200 rpm.,  $f_s$  : source frequency

For the test motor there are two source frequencies at the same time: 40 Hz. and 120 Hz. because of the third harmonic current injection. Therefore; 6<sup>th</sup> and 18<sup>th</sup> harmonics are expected to exist in the rotor core caused by the fundamental and the third harmonic sources respectively.

In Table 4.3, the skin depths calculated using Eq.(4.2) for the expected harmonics are presented. By taking into account the approximation of the skin depths to each other as seen in Table 4.3., an averaging is done for the skin depths and hence the three skin depth regions are created based on the skin depths for;

5<sup>th</sup> harmonic, used also for 3<sup>rd</sup>, 6<sup>th</sup> and 7<sup>th</sup> harmonics.

11<sup>th</sup> harmonic, used also for 9<sup>th</sup> and 13<sup>th</sup> harmonics.

17<sup>th</sup> harmonic. used also for 15<sup>th</sup>, 18<sup>th</sup> and 19<sup>th</sup> harmonics. (Figure 4.4)

In fact more accurate results could be obtained if the rotor teeth were splitted according to all harmonics. However, this elongates the computation time of the program and increases the complexity of the problem but it is not worth to face with these difficulties for too accurate results.

Table 4.1 Calculated skin depths of the harmonics, and the skin depth values used in the loss calculations.

Harmonic no.	f (Hz)	Actual Skin Depth (mm)	Used Skin Depth (mm)
3	120	10	6
5	200	6	
6	240	5	
7	280	4.286	2.727
9	360	3.333	
11	440	2.727	
13	520	2.308	
15	600	2	1.765
17	680	1.765	
18	720	1.67	
19	760	1.579	

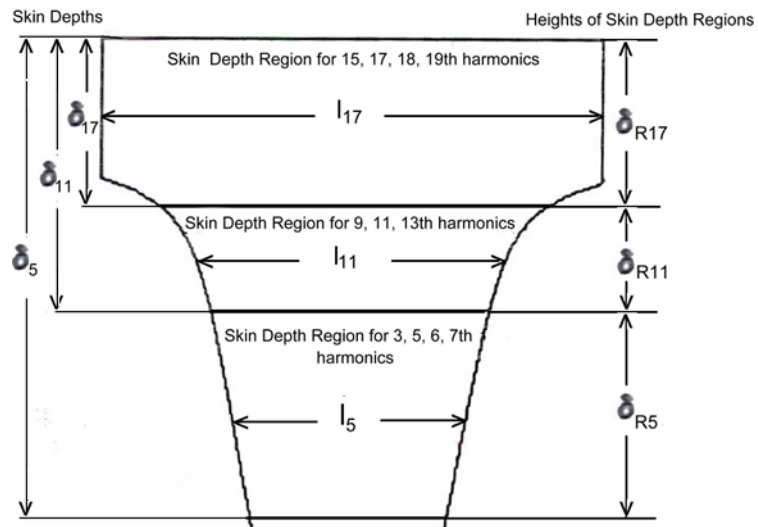


Figure 4.4 Skin depth regions and average current path width values in a rotor tooth

The eddy current values of the three skin depth regions at the rotor teeth are read from Flux2D, and the harmonic components of the currents ( $i_j$ ) are evaluated along a period of the 40 Hz supply also in the same program. The magnitudes of the harmonic components are transferred to the Excel table in Tabel 5.2 and the loss contribution of each harmonic is calculated for 7 rotor teeth according to Eq. (4.7). Here, the second term of Eq.(4.7) is named as the skin depth region coefficient as in Eq.(4.10) and three coefficients are calculated for the three skin depth regions as in Table 4.2.

$$\eta_{Ri} = [2 \times \rho \times l_c^2 \times l_{lam} \times k / (\delta_i \times l_{av}^3)] \quad (4.10)$$

where,

$$\rho = 6 \times 10^{-4} \text{ Ohm} \times \text{m}$$

$$l_c = 65.5 \text{ mm}$$

$$l_{lam} = 0.5 \text{ mm.}$$

$$k = 0.3$$

*Table 4.2 The calculated skin depth region coefficients*

$\eta_{R5}$	0,943
$\eta_{R11}$	2,568
$\eta_{R17}$	0,50684

Figure 4.4 also shows the  $l_{av}$  values which are taken as the width at the middle point of each skin depth region. The skin depths are found in accordance with Eq.(4.2). Then the height of each skin depth region ( $\delta_{Ri}$ ) is substituted for the term  $\delta_i$  in Eq.(4.10) as calculated in Table 4.3.

*Table 4.3 Skin depth regions and their  $l_{av}$  and  $\delta_{Ri}$  values.*

<b>Skin Depth Region</b>	<b><math>l_{av}</math></b>	<b><math>\delta_{Ri}</math></b>
<b>R5</b>	$l_5 = 6.62 \text{ mm}$	$\delta_5 - \delta_{11} = 3.27 \text{ mm.}$
<b>R11</b>	$l_{11} = 7.12 \text{ mm}$	$\delta_{11} - \delta_{17} = 0.965 \text{ mm.}$
<b>R17</b>	$l_{17} = 10 \text{ mm}$	$\delta_{17} = 1.765 \text{ mm.}$

Next, the high frequency loss of one rotor tooth of the motor is calculated by multiplying the loss of one lamination by the number of laminations which is,

$$\begin{aligned} t &= \text{rotor stack length} / \text{lamination thickness} \\ &= 65.5 \text{ mm} / 0.5 \text{ mm} = 131 \end{aligned} \quad (4.11)$$

And finally, the total high frequency of 28 rotor teeth is calculated by multiplying the loss of seven rotor teeth by 4 according to according to Eq.(4.8). The results of the loss calculation will be elaborated in the next chapter in detail.



## **CHAPTER 5**

### **RESULTS AND CONCLUSIONS**

#### **5.1 INTRODUCTION**

As stated before, the aim of this thesis is to calculate the core losses of the motor introduced in Chapter 2. However, since the analytical calculation of core losses presents unreliable results, a method which uses finite element solutions is used to achieve this aim. Hence, after establishing the finite element model of the motor in Chapter 3, the calculation method of core losses developed in [18], is applied to the test motor described in Chapter 4.

In this chapter the results of the loss calculations in Chapter 4 will be elaborated on and compared with the experimental results of [1]. Then the discussions and final conclusions on this thesis and suggestions for future work will be provided.

#### **5.2 THE RESULTS OF THE FUNDAMENTAL FREQUENCY CORE LOSS CALCULATIONS**

In this thesis, the fundamental frequency loss of the motor is calculated using the values read from the loss curves in Figure 3.1. By using Flux 2D, one stator tooth pitch is divided vertically into two and horizontally into ten regions as in Figure 4.3. By this way the problem is relatively simplified. Therefore the stator tooth pitch is divided into coarser regions, the volumes of which are easy to calculate.

Taking  $7850 \text{ kg/m}^3$  as density of iron, the weight values of each region is found. The flux density of the points at the center of gravity of each region is read from the program along one cycle of the 40 Hz current source (25 msec.). 43 samples are read from the program along a period of 25 msec. The smaller number of samples

are found not to be sufficient for obtaining the harmonic spectrum of the flux density.

In Figures 5.1, 5.2, 5.3 and 5.4, the flux density magnitudes at four example pairs of regions in the first half and the second half of the tooth pitch (Figure 4.3), are displayed in graphs along a period of 25 msec. These values are read from the software by writing down a macro for the program to make a recursive analysis.

After obtaining 43 flux density values at every region of a tooth pitch as in the Figures 5.1 to 5.4., the fundamental and third harmonic flux density components of every region are obtained using the “fft” function of Matlab Simulink and. Then the watt/kg values that correspond to the magnitudes of the fundamental and the third harmonic components of the flux density, using the the loss curve of Figure 3.1.

The corresponding watt/kg values are multiplied by the weight of each region and the fundamental frequency core loss values are found. The loss of one tooth pitch is calculated by summing the loss of all regions after finding them as mentioned above. Then the total fundamental frequency loss is calculated by multiplying the loss of one tooth pitch by 36, which is the number of stator slots. In Table 5.1, the fundamental and third harmonic components of the flux density and their loss contributions in each region can be seen.

Referring to Figure 3.1 and Eq. (4.1), the fundamental frequency losses of the motor turn out to be at the level of 13 watts. (Table 5.1)

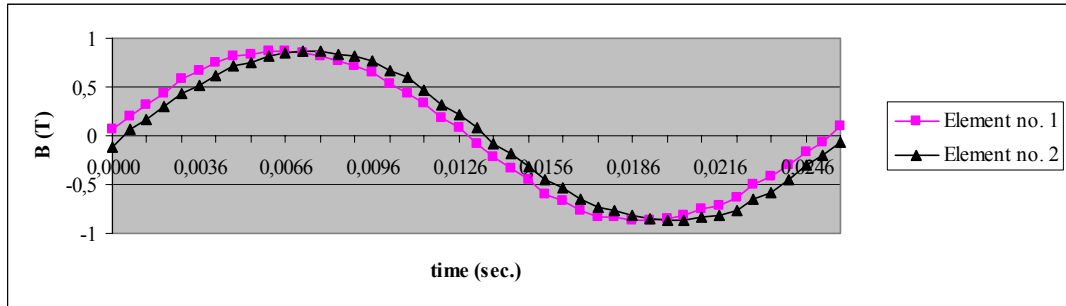


Figure 5.1 Flux density of the regions at the outermost part of a stator tooth pitch

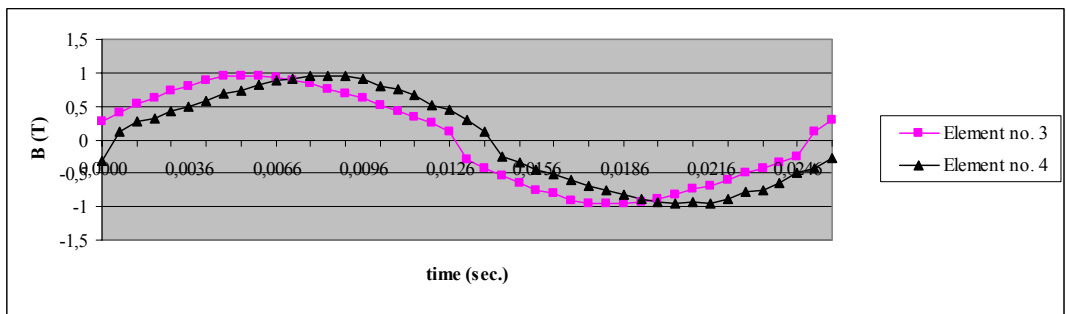


Figure 5.2 Flux density of regions at the slot ends in a stator tooth pitch.

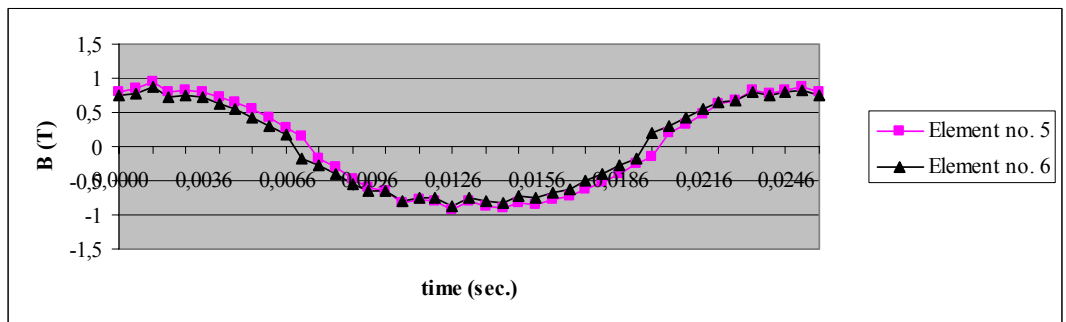


Figure 5.3 Flux density of the regions in the middle of the tooth in a stator tooth pitch

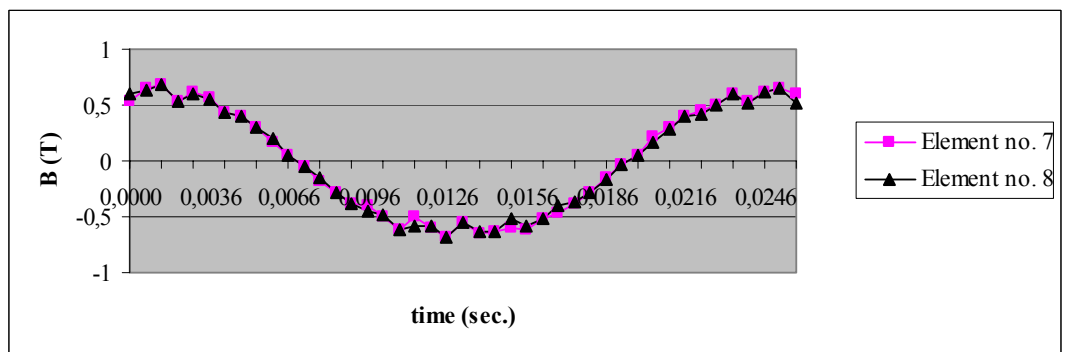


Figure 5.4 Flux density of the regions at the tooth tip in a stator tooth pitch

In Table 5.1, it can be seen that the flux density magnitudes in the regions at the first and second half of the tooth pitch are quite similar to each other. This verifies that the number of horizontal regions is more or less sufficient for quite a reliable calculation except for the tooth tips. The low level of flux density at the tooth tips, points out the insufficient number of horizontal regions at this part of the tooth pitch. However, when the tooth tips were splitted into more horizontal regions, the volume and so the weight of the regions would decrease. This decrease is considered to keep the calculated loss values at the same level as for now. Concerning the vertical division of the stator tooth pitch, although it is certainly clear that; the more the number of regions, the better the accuracy of the calculations; splitting the tooth pitch into 10 vertical regions is considered a simplified and a sufficient choice for the requirements of this study.

Table 5.1 Microsoft Excel table used to calculate the fundamental frequency losses

						First half of the Tooth Pitch						Second half of the Tooth Pitch						Tooth Pitch Loss (W)		
R1	R2	Width (o)	Volume (mm3)	Weight (kg)		B1 <sub>peak</sub> (T)	B3 <sub>peak</sub> (T)	W/kg 1	W/kg g 3	Loss1 (W)	Loss3 (W)	B1 <sub>peak</sub> (T)	B3 <sub>peak</sub> (T)	W/kg 1	W/kg 3	Loss1 (W)	Loss3 (W)			
<b>Stator Core</b>																				
95	89	5	3394.34	0.026646		0.86306	0.01414	1.77	0.02	0.04716	0.00053	0.86606	0.01403	1.77	0.02	0.04716	0.00053	0.09539114		
89	84	5	2659.515	0.020877		0.92004	0.04964	1.98	0.1	0.04134	0.00209	0.93072	0.02189	2.02	0.04	0.04217	0.00084	0.08643156		
84	81	5	1521.919	0.011947		0.96205	0.04764	2.07	0.1	0.02473	0.00119	0.96258	0.0385	2.06	0.06	0.02461	0.00072	0.0512529		
81	79	5	983.8667	0.007723		0.9091	0.07542	1.93	0.15	0.01491	0.00116	0.89975	0.06986	1.9	0.14	0.01467	0.00108	0.03182022		
79	73	2	1121.608	0.008805		0.95397	0.10448	2.06	0.2	0.01814	0.00176	0.88971	0.10311	1.87	0.2	0.01646	0.00176	0.03812402		
73	68	2	867.0325	0.006806		0.93868	0.08807	2.04	0.18	0.01388	0.00123	0.93853	0.08787	2.04	0.18	0.01388	0.00123	0.03021955		
68	64	2	649.352	0.005097		0.93707	0.08648	2.04	0.18	0.0104	0.00092	0.93682	0.08613	2.04	0.18	0.0104	0.00092	0.02263251		
64	62.5	2	233.3609	0.001832		0.9209	0.08108	1.98	0.16	0.00363	0.00029	0.90754	0.07626	1.92	0.17	0.00352	0.00031	0.00774886		
62.5	61.5	3.1	236.374	0.001856		0.8412	0.06972	1.7	0.14	0.00315	0.00026	0.81971	0.06263	0.7	0.1	0.0013	0.00019	0.00489861		
61.5	60	3.1	347.4125	0.002727		0.67423	0.05692	0.65	0.1	0.00177	0.00027	0.66575	0.05117	0.64	0.1	0.00175	0.00027	0.00406351		
<b>Total</b>										0.17911	0.0097					0.17593	0.00784	<b>0.37258289</b>		

Total Fundamental Loss of 36 Tooth Pitches	<b>13,413</b>	<b>Watt</b>
--	---------------	-------------

### 5.3 THE RESULTS OF THE HIGH FREQUENCY CORE LOSS CALCULATIONS

The high frequency loss calculations are done according to section 4.2.4. The eddy currents in the skin depth regions and their harmonic contents are evaluated using the finite element software. Example plots of the eddy currents and their harmonic contents are given in Figure 5.5, 5.6 and 5.7. for the three skin depth regions of the 4<sup>th</sup> rotor tooth.

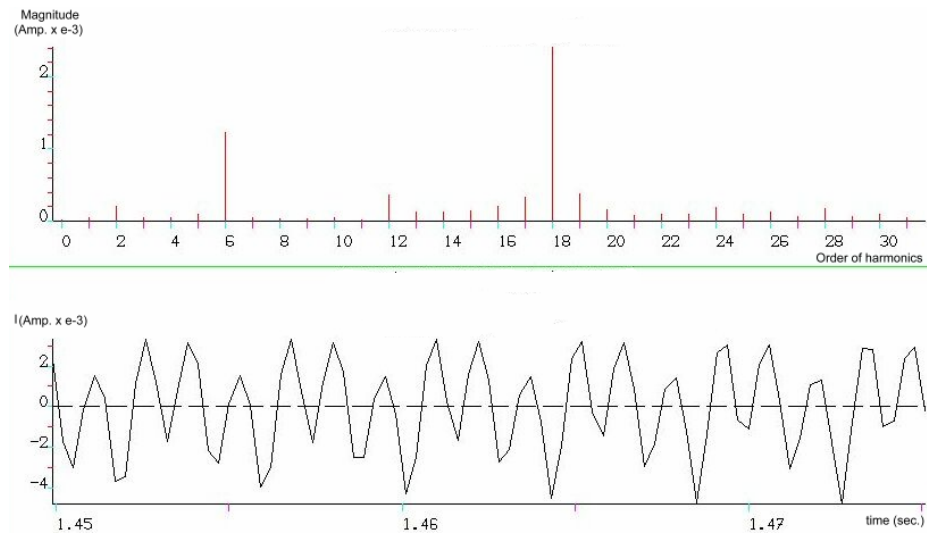


Figure 5.5 Time variation and harmonic content of eddy currents in region R5 of the 4<sup>th</sup> rotor tooth

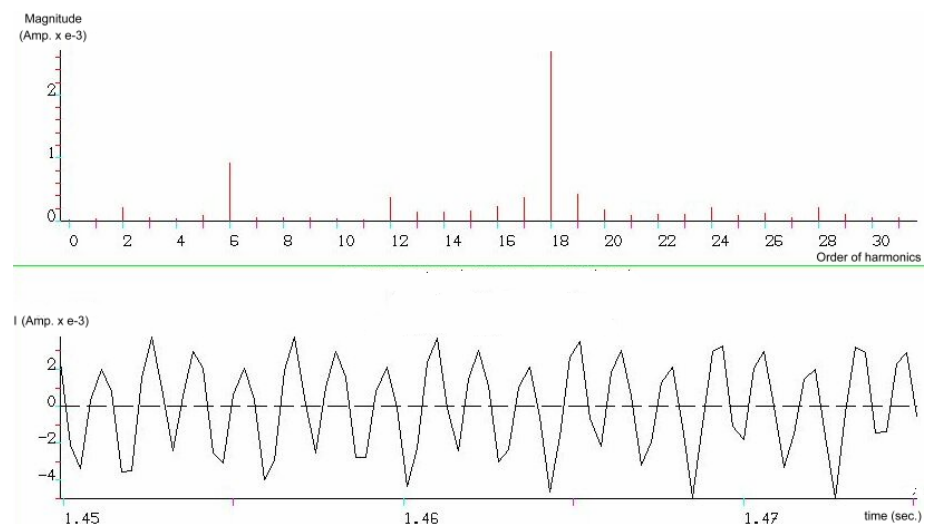
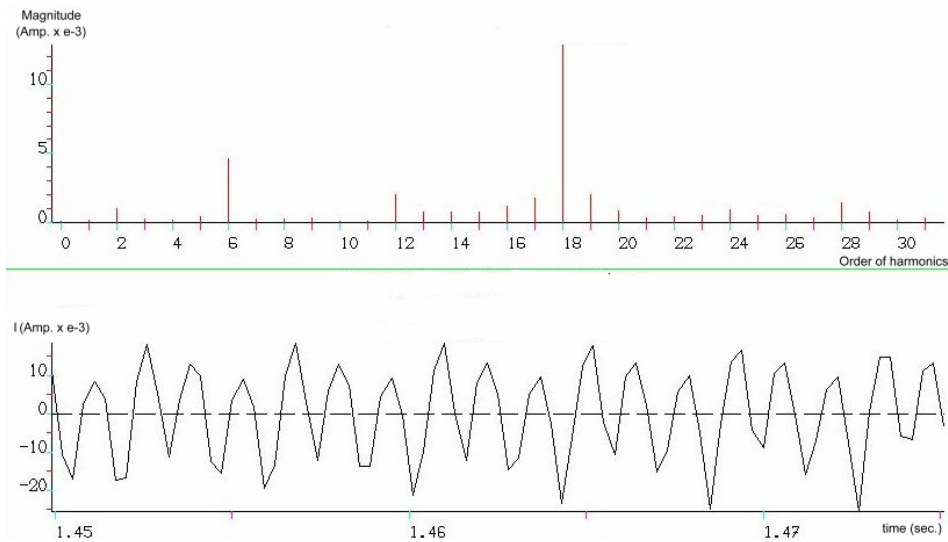


Figure 5.6 Time variation and harmonic content of eddy currents in region R11 of the 4<sup>th</sup> rotor tooth



*Figure 5.7 Time variation and harmonic content of eddy currents in region R17 of the 4<sup>th</sup> rotor tooth*

As can be seen in the above figures, the dominant harmonics are found to be 6<sup>th</sup> and 18<sup>th</sup> harmonics in the rotor teeth. These are obviously due to the stator slotting as can be calculated from Eq. 4.9. The loss calculations are made for two options. When the high frequency loss is calculated taking into account only the dominant harmonics, the result comes out to be 0.715 Watt. If we take all of the harmonics present in the laminated core, we get the high frequency loss of the motor as 0.8 Watt. The dominant harmonics induce 90% of the total high frequency losses.

The reason for the small high frequency loss value is considered to be the low level of flux density in the air gap. The mean value of the air gap flux density is calculated to be 0.303 T. In commercial motors this value is in the order of 0.5 - 0.6 T. This points out that the motor is operated much under its capacity. Another reason could be the operating slip. Since the motor was operated at no load during the core loss measurements in [1], the finite element model of the motor is also operated at no load in order to establish a rational basis for comparison of the experimental and finite element solution results. Microsoft Excel Table used to calculate the high frequency losses with the effects of the dominant harmonics are added, can be found in Table 5.2.

As mentioned in Chapter 3, the rotor teeth are divided into three horizontal parts depending on the skin depths in Table 4.3. Here an important point should be stated. The harmonics should mainly exist in the core beginning from the surface of a rotor tooth till the skin depth calculated using Eq.(4.2). For instance, the skin depth of 5<sup>th</sup> harmonic is 6 mm. This means that the 5<sup>th</sup> harmonic currents should exist at the points till 6 mm. deep in the core with respect to the air gap. Similarly the 17<sup>th</sup> harmonic currents are expected to exist mainly until 1.765 mm. deep in the core from the air gap. However, the 17<sup>th</sup> harmonic currents should have smaller magnitudes in other skin depth regions.(Figure 4.4)

When we look at Table 5.2., we can see that the rule mentioned above is valid for the harmonic currents. For example, the 6<sup>th</sup> harmonic currents exist in all skin depth regions at certain levels. On the other hand, the 18<sup>th</sup> harmonic currents have their greatest value in their own skin depth region and exist at very low levels in other regions. The magnitude of 18<sup>th</sup> harmonic currents in the skin depth region of 5<sup>th</sup> harmonic, are very smaller than the 5<sup>th</sup> harmonics.

By analyzing Table 5.2, it can be figured out that 79.4% of the loss contribution of 18<sup>th</sup> harmonic currents, occur at region R17 which forms the skin depth of 17<sup>th</sup> harmonics. This numerical example verifies both the loss calculations and the rule which claims that each harmonic induces losses mainly at its own skin depth.



Table 5.2 Microsoft Excel table used to calculate the high frequency losses.

Rotor Teeth	Skin Depth Regions	Harmonic Currents and Loss Contributions				Total Loss of One Lamination (W)
		6		18		
		$i_i$ (A)	$P_i$ (W)	$i_i$ (A)	$P_i$ (W)	
1 (Half)	R 5	0,00064070	0,00000310	0,00117806	0,00001047	0,00001422
	R 11	0,00049745	0,00000508	0,00142650	0,00004180	0,00004863
	R 17	0,00245512	0,00002444	0,00845845	0,00029010	0,00032301
2	R 5	0,00099079	0,00000093	0,00211509	0,00000422	0,00000526
	R 11	0,00072872	0,00000136	0,00265822	0,00001815	0,00001994
	R 17	0,00389134	0,00000767	0,01355781	0,00009316	0,00010372
3	R 5	0,00097079	0,00000089	0,00193577	0,00000353	0,00000454
	R 11	0,00079525	0,00000162	0,00264418	0,00001795	0,00001996
	R 17	0,00440219	0,00000982	0,01367676	0,00009481	0,00010730
4	R 5	0,00122488	0,00000141	0,00240896	0,00000547	0,00000701
	R 11	0,00092045	0,00000218	0,00270417	0,00001878	0,00002132
	R 17	0,00460355	0,00001074	0,01283531	0,00008350	0,00009621
5	R 5	0,00201286	0,00000382	0,00325738	0,00001001	0,00001538
	R 11	0,00142170	0,00000519	0,00273101	0,00001915	0,00002709
	R 17	0,00610267	0,00001888	0,01086585	0,00005984	0,00008883
6	R 5	0,00160405	0,00000243	0,00281734	0,00000748	0,00001019
	R 11	0,00105970	0,00000288	0,00237889	0,00001453	0,00001787
	R 17	0,00437362	0,00000970	0,00975968	0,00004828	0,00005937
7	R 5	0,00198257	0,00000371	0,00327298	0,00001010	0,00001537
	R 11	0,00136179	0,00000476	0,00273393	0,00001919	0,00002668
	R 17	0,00577296	0,00001689	0,01081721	0,00005931	0,00008578
8 (Half)	R 5	0,00054311	0,00000223	0,00115009	0,00000998	0,00001272
	R 11	0,00043702	0,00000392	0,00131658	0,00003561	0,00004121
	R 17	0,00231152	0,00002166	0,00740610	0,00022240	0,00025636
Loss contributions of harmonics			0,00016532		0,00119783	0,00142797

$\eta_{RS}$ Coefficient	$\eta_{R11}$ Coefficient	$\eta_{R17}$ Coefficient
0,943	2,568	0,50684

$$P_{lam} = t x \Sigma P_i = 0,178 \text{ Watt} \quad \text{Total loss of } (65,5 \text{ mm} / 0,5 \text{ mm} = 131) \text{ laminations of a quarter of the motor}$$

$$P_{total} = 4 x t x \Sigma P_i = 0,715 \text{ Watt} \quad \text{Total loss of 28 rotor slots}$$

$$P_i = i_j^2 x [2 x \rho x l_c^2 x l_{lam} x k / (\delta_i x l_{av}^3)]$$

$$\eta_{Ri} \text{ coefficient} = [2 x \rho x l_c^2 x l_{lam} x k / (\delta_i x l_{av}^3)]$$

## 5.4 COMPARISON WITH THE EXPERIMENTAL RESULTS

In [1], the magnetic losses of the six phase machine with third harmonic current injection at 40 Hz. are measured as 13 Watts at a peak air gap flux density of 0.55 T as seen in Figure 2.32. According to [1], the measurement procedure of the magnetic losses of the motor is as follows: The machine was driven mechanically at synchronous speed and the input power was measured. Magnetic power losses were obtained by subtracting the stator copper losses from the measured power. This value is considered as the sum of fundamental frequency losses and high frequency losses since the friction and windage losses were supplied by the power applied to the shaft.

The results of the core loss calculations presented in the previous sections in this thesis and the experimental loss measurements in [1] are compared to each other in Table 5.3. The comparison shows that the loss model applied to the motor predicts the losses very accurately.

*Table 5.3 Comparison of the measured and calculated core losses*

	<b>Fundamental Freq.</b>	<b>High Freq.</b>	<b>Total</b>
<b>Measured in [1]</b>	-	-	13 Watt
<b>Calculated in this thesis</b>	13.4 Watt	0.8 Watt	14.2 Watt

An important point here is that, the measurements on the test motor were done at no load condition in [1]. While creating the finite element model in this study, the motor is naturally operated the same conditions for comparison with the experimental results. This means that in the simulations and tests above the rotor currents do not exist. The accuracy of the loss calculations may not be the same under load conditions. Furthermore, the available test results were obtained with a current source. Therefore none of the electrical measurements nor the mechanical output torque (torque = 0 for no load) could be compared with the FE solution results. The method may be verified by doing the FE computations for several operating conditions under load and comparing with experimental results (currents, torque output etc.).

## 5.5 KEY FINDINGS AND RECOMMENDATIONS

Calculation of the losses of electrical motors using analytical methods while they are being designed, is hard to achieve. The best way to do this is the production of a model motor and test it to see if the objective performance criteria are achieved or not. However, this method can cost not only too much money but also time, which is a scarce resource for production and marketing. Finite Element Software products open a way to calculate the losses without production of the physical models of electrical motors. By using these computer aided design tools, designers can achieve better performance results in shorter periods of time.

On the other hand, FE software, present some difficulties which are of course can not be compared to the difficulties above. Examples of the problems faced during the modelling of the machines are; the long computation time for complex machines and insufficiently user friendly program interfaces.

Regarding the subject of this thesis for instance; the software does not allow the user to inject third harmonic currents in magnetodynamic analysis. Therefore the user has only one choice which is the time consuming transient analysis. Software products of this type should be further developed and made easier to use.

In addition, parameters like the k coefficient, lamination thickness, the number of laminations, resistivity of the lamination etc. play an important role in the accuracy of the results. The k coefficient is taken as 0.3 taking into account the results of [18] and [19]. However the value of k may be a function of the frequency.

Since the material properties of the motor, core losses of which are calculated in this study, are not known precisely, the calculations may not reflect the real motor. Since it was not possible to obtain the loss curve of the motor from [1], a typical loss curve from [21] is used in the calculations.

## 5.6 AREAS FOR FURTHER RESEARCH

In this study, the core loss calculation method evaluated in [18] is applied in modified form to a 6 phase motor with 3<sup>rd</sup> harmonic injection introduced in [1]. It is shown in this work that the high frequency losses can be calculated with good accuracy using the approach here. However this research work is done within the framework of a MS research study and is by no means complete. It is thought that the following investigations are needed to increase reliability of the results obtained

- The modelled motor may be solved for several operating conditions at different frequencies under load and compared with measurements under the same conditions to really verify the calculation method.
- High frequency core losses of the motor can be calculated for a normal winding and can be compared with the case with 3<sup>rd</sup> harmonic injection via FE simulation. This would clarify whether the losses increase or not. Of course having measurements on an actual motor for this condition would also be very useful.
- Measurements can be done on the test motor with increased air gap flux density to find out the effect of this on losses and motor performance and to determine whether the design in hand is optimal. The fact that this frame size is normally capable of providing 5.5 kW output suggests that the motor is poorly designed and therefore unnecessarily large in size with very small high frequency losses.
- The efficiency of the motor may also be evaluated when fed from a voltage source, by calculating the core losses and copper losses using 2D harmonic field solution with 3D effects. In this case superposition of harmonic solutions for the fundamental and 3<sup>rd</sup> harmonic frequencies would be needed. Of course this would first require verification of the validity of the superposition required here.
- The value of  $k$  may be studied further especially regarding frequency dependency.
- Another issue to work on is whether making the loss calculations on a small number of regions (instead of each mesh element) is causing any serious errors.

## REFERENCES

- [1] Lyra, R. O. C., "Torque density improvement in a six-phase induction motor with third harmonic current injection," PhD thesis, University of Wisconsin, 2002.
- [2] Munoz, A. R., Lipo, T. A. "Dual stator winding induction machine drive," IEEE Transactions on Industry Applications, vol. 36, pp. 1369 – 1379, Sept 2000.
- [3] Ojo, O., Davidson, I. E. "Pwm - vsi inverter-assisted stand-alone dual stator winding induction generator," IEEE Transactions on Industry Applications, vol. 36, pp. 1604 – 1611, Nov 2000.
- [4] Gopakumar, K., Ranganathan, T., Bhat, S. R. "Split-phase induction motor operation from pwm voltage source inverter," IEEE Transactions on Industry Applications, vol. 29, pp. 927– 932, Sept 1993.
- [5] Bakhshai, A. R., Joos, G., Jin, H. "Space vector pwm control of a split-phase induction machine using the vector classification technique," Proceedings of Applied Power Electronics Conference and Exposition, 1998, vol. 2, pp. 802 – 808, Feb 1998.
- [6] Nelson, R. H., Krause, P. C. "Induction machine analysis for arbitrary displacement between multiple windings," IEEE Transactions on Power Apparatus and Systems, vol. 93, pp. 841 – 848, May 1974.
- [7] Lipo, T. A. "A d-q model for six phase induction machines," Proceedings of the International Conference on Electrical Machines, Athens,, pp. 860 – 867, Sept 1980.
- [8] Andresen, E., Bieniek, K., "On the performance of inverter fed induction motors with six phases," Proceedings of the International Conference on Electrical Machines, Athens, pp. 909 – 917, Jan 1980.
- [9] Vander Duijn, N. P., Gordon, B. M., McMahon, R. A. "Multiphase induction motors for integrated drives," Proceedings of the 9th International Conference on Electrical Machines and, pp. 6 – 11, Jan 1999.

- [10] Abbas, M. A., Christen, R., Jahns, T. M. "Six-phase voltage source inverter driven induction motor," IEEE Transactions on Industry Applications, vol. 20, pp. 1251 – 1259, Sept 1984.
- [11] Fu, J. and Lipo, T. A. "Disturbance free operation of a multiphase current regulated motor drive," IEEE Transactions on Industry Applications, vol. 30, pp. 1267 – 1274, Sept 1994.
- [12] Novotny, D. W., Lipo, T. A., Vector Control and Dynamics of AC Drives. New York: Clarendon Press - Oxford, 1996.
- [13] Lipo, T. A., Introduction to AC Machine Design. Madison - WI: University of Wisconsin, 1996.
- [14] Lipo, T. A. "Flux sensing and control of static ac drives by the use of flux coils," IEEE Transactions on Magnetics, vol. MAG-13, pp. –, Sept 1997.
- [15] Miranda, M. S., Lyra, R., Silva, S. R. "An alternative isolated wind electric pumping system using induction machines," IEEE Transaction on Energy Conversion, vol. 14, pp. 1611 – 1616, Dec 1999.
- [16] Zhao, Y. Lipo, T. A., "Space vector pwm control of dual three-phase induction machine using vector space decomposition," IEEE Transactions on Industry Applications, vol. 31, pp. 1100 – 1109, Sept 1995.
- [17] Ertan, H.B., Electrical Machine Design Lecture Notes. Ankara: Middle East Technical University, 1991.
- [18] Pirgaip, M., "Computation of core losses in three-phase smooth rotor induction motors using finite element method," Master's thesis, Middle East Technical University, September 1998.
- [19] Avenoglu, B. "İndüksiyon motorlarında yüksek frekans kayıplarının ve motor parametrelerinin hesaplanması," Master's thesis, Hacettepe University, 2001
- [20] Lipo, T.A., Electromagnetic design course notes, Madison, 1990.
- [21] Roters, H.C. Electromagnetic devices, John Wiley & Sons Ltd., 1941
- [22] Heller, B., Hamata, V., Harmonic field effects in induction machines, Elsevier Scientific Publishing Co., New York, 1977
- [23] Veinott, C. Theory and design of small induction motors, McGraw-Hill Book Co., Inc., New York, 1959.
- [24] Say, M.G., The performance and design of alternating current machines, Pitman Paperbacks, 1958.

## APPENDIX

### CALCULATION OF PARAMETERS NEEDED AS INPUT FOR FLUX2D SOLUTIONS

#### 1. Calculation of End Winding Resistance

$$R_{et} = (8 \rho l_{ew} N_{tsp} N_{spp}) / (\pi N_b N_f d_w^2) = 0.687 \text{ Ohm} \quad l_{ew} = \frac{\pi(D_{al} + 2 h_{ss}) + 2 h_{ss}}{2p}$$

$\rho$  : wire resistivity =  $1.72 \cdot 10^{-8}$  Ohm $\cdot$ m.       $l_{ew}$  : end wdg. length = 0.166 m.  
 $N_{tsp}$  : number of turns per slot per phase = 49       $N_{spp}$ : no. of slots/pole/phase = 6  
 $N_b$  : number of coils parallel per phase = 3       $N_f$ : no. of wires in series per turn = 2  
 $d_w$  : wire diameter = 0.00072 m.       $p$  : number of pole pairs = 2  
 $D_{al}$ : stator inner diameter = 0.12 m.       $h_{ss}$  : stator slot height = 0.02 m.

#### 2. Calculation of End Winding Inductance

$$L_{ew} = \frac{\mu_o}{18p} (N_{ss} \times N_{tsp} / N_b)^2 P = 0.54 \text{ mH.} \quad l_{ap} = \frac{\pi(D_{al} + 2 h_{ss})}{2p} = 0.11 \text{ m.}$$

$$P = 0.47 l_{ew} - 0.3 l_{ap} = 0.04502$$

$N_{ss}$ : number of stator slots = 36       $\mu_o$  : permeability of air =  $4\pi \times 10^{-7}$   
 $\omega$  : source pulsation =  $80 \times \pi$  rd/sec.

### 3. Calculation of End Ring Resistance

$$R_{er} = \frac{\rho \pi p}{N_r e_{eq} h} (D_r - D_i) \times (D_r^{2p} + D_i^{2p}) / (D_r^{2p} - D_i^{2p})$$

$N_r$ : number of rotor bars                       $\rho$ : end ring resistivity  
 $D_r$ : end ring equivalent diameter       $D_i$ : end ring inner diameter  
 $e_{eq}$ : end ring equivalent thickness       $h$ : end ring height

### 4. Calculation of End Ring Inductance

$$L_{er} = \frac{\pi \mu_0}{N_r} (D_e - h_{eq}) \times \lambda_{er} \qquad \lambda_{er} = 0.365 \text{ Ln} \left[ \frac{3\pi \times (D_e - h_{eq})}{4 (h_{eq} + e_{eq})} \right]$$

$$D_e = D_i + h$$

$D_e$  : end ring outer diameter                       $h_{eq}$  : end ring equivalent height  
 $e_{eq}$  : end ring equivalent thickness.